Perturbation de CO2 dans les aquifères : cinétique des réactions et comportement des métaux

Jean Rillard

HAL Id: tel-01176961
https://tel.archives-ouvertes.fr/tel-01176961

Submitted on 16 Jul 2015

THESE DE L'UNIVERSITE DE LYON

Délivrée par

L'UNIVERSITE CLAUDE BERNARD LYON 1

ECOLE DOCTORALE

Evolution Ecosystèmes Microbiologie Modélisation

DIPLOME DE DOCTORAT

(arrêté du 7 août 2006)

par

M Jean RILLARD

TITRE :

CO_2 perturbation in aquifers: reaction kinetics and metals behavior

JURY :
M. Luc AQUILINA-(Rapporteur)   Université Rennes 1
Mme Anne-Marie AUCOUR- (Examinateur)   Université Claude Bernard Lyon 1
M. Philippe GOMBERT-(Examinateur)   INERIS
M. Pierre HANTZPERGUE-(Examinateur)   Université Claude Bernard Lyon 1
M. Yousif KHARAKA-(Examinateur)   United States Geological Survey
Mme Hélène PAUWELS-(Rapporteur)   Bureau de Recherche Géologique et Minière
M. Pierre TOULHOAT-(Examinateur)   Université Claude Bernard Lyon1/INERIS
M. Pierpaolo ZUDDAS-(Directeur de Thèse)   Université Pierre et Marie Curie

This PhD has been realized in partnership between :

 (*)

(*) Financial support

Remerciements

La partie "remerciements" n'est pas la plus simple à écrire. Tout d'abord parce que c'est la partie par laquelle les lecteurs commencent le manuscrit, mais surtout parce qu'elle résume une thèse sur le plan humain. C'est à mon sens ce qui pourrait représenter le mieux mes trois années passées sur ce projet. Je définirais ma thèse avant tout comme une aventure humaine, composée de rencontres, de partage, de découverte, de bons moments, mais aussi de difficultés, de doutes, de déceptions et de leçons d'humilité. Je dois dire que je n'ai pas vu le temps passer, les difficultés auront été nombreuses et les enseignements très riches. J'ai dû frayer mon petit bonhomme de chemin entre les mondes tortueux de la science, des relations humaines et de la réalité des expériences de terrain. Cela n'aura pas été simple de composer avec les différents intérêts mis en jeu, d'accepter et de faire accepter d'être parfois dans la contradiction pour pouvoir avancer. J'en retiendrais beaucoup de choses, à commencer par une certaine leçon d'humilité et de philosophie. Toutefois, même si le cheminement n'aura pas été aussi linéaire que je l'aurai souhaité, j'ai le sentiment d'être arrivé au bout de ce que je voulais faire, ce qui est le plus important.

Pour commencer les remerciements, je souhaiterais adresser ma gratitude aux membres du jury de ma thèse, pour avoir accepté d'évaluer mon travail. En particulier je remercie les rapporteurs Hélène Pauwels et Luc Aquilina pour le temps qu'ils m'ont accordé et leurs nombreux commentaires et observations qui ont contribué à améliorer ce manuscrit. Je souhaite également remercier Anne Marie Aucour pour ses remarques et corrections. I would sincerly thanks Yousif Kharaka for his interest on my work, interesting advises, exchanges, comments, and "english corrections"... Je remercie également mes encadrants à commencer par mon directeur de thèse Pierpaolo Zuddas. Merci de m'avoir ouvert l'esprit vers des aspects scientifiques qui m'étaient inconnus au début de ma thèse et de m'avoir fait confiance malgré les différends que nous avons pu avoir par moments. Je souhaite également remercier mon second encadrant Philippe Gombert pour son aide, en particulier sur la préparation des travaux de terrain, pour son soutien, et pour sa disponibilité malgré son emploi du temps parfois chargé. Je remercie Pierre Toulhoat pour sa confiance et pour avoir partagé avec moi sa grande expérience de la géochimie de terrain. Je souhaite remercier de tout cœur Patrick Vuillemenot et Pierre Nogier, pour l'investissement passionné avec lequel ils ont pris part à l'expérience de terrain, et sans qui cela n'aurait jamais pu se faire. Cela aura été un réel plaisir de travailler avec vous! Un grand merci à Alfonso Segura, "mon stagiaire Erasmus" pour son aide très précieuse pour les mesures de terrain. Grâce à lui, une bonne partie des résultats ont pu être collectés. Merci également aux personnes de l'INERIS qui ont participé directement ou indirectement au projet lors d'échanges pendant les réunions d'avancements, en particulier Mehdi Ghoreychi et Christophe Didier. Merci également à Regis Farret, pour les nombreuses discussions que nous avons pu avoir, ses

3

Summary:

The aim of this thesis was to investigate hydrogeochemical perturbation induced by CO_2 in aquifers. In a first step, we used chemical data from natural CO_2-rich hydrothermal water. We studied variation of fluid chemical composition as a function of CO_2 content in order to evaluate reactivity of minerals composing the initial reservoir. Fluid chemical analyses showed decrease in pH, and systematic enrichment in alkalinity and major cations correlated to increase in CO_2 content. Chemical reaction was studied by kinetic approach to estimate variation of mineral reactive surface area as function of CO_2 perturbation. Results showed that mineral reactive surface area could varied by two to four orders of magnitude as a function of CO_2 perturbation.

In a second step a field experiment consisting on injection of water saturated with CO_2 in aquifer was performed following a single well push-pull test protocol. Analysis of groundwater composition before and after injection allowed to study the impact of CO_2 perturbation on water-rock interaction processes. A particular focus was made on dissolved metals behavior. Results showed a decrease in pH (from 7.3 to 5.7), involved with enrichment in alkalinity by a factor two, and a weak increase of nearly 30% in bivalent cations Ca^{2+} and Mg^{2+}. The production of alkalinity, Ca^{2+} and Mg^{2+} was correlated to dolomite dissolution. Further, we observed an enrichment of approximately one order of magnitude for dissolved metals (Fe, Mn, Zn) and by a factor two for As. Saturation index calculation showed that dissolution of metals hydroxide such as ferrihydrite was correlated to iron and other metals release. A method based mass transfer calculation allowed us to evaluate the effect of transport and mixing on measured elements concentration and to estimate the rate of metals release by kinetic approach. Results indicated that dissolution of metals oxides obeyed to a complex order reaction.

This work highlighted that for long term safety of CO_2 storage site, physico-chemical properties of formation water and reservoir rock must be evaluate precisely. Geochemical model used to evaluate CO_2 perturbation have to performed with constrain on source term (i.e. chemical reactions, mineral reactive surface area) to predict the evolution of water-rock equilibrium and to prevent the risk of metals remobilization.

Contents

6

Introduction

Carbon capture and sequestration (CCS) technology is one prominent and feasible approach to help mitigate impacts from increasing rates of CO_2 release from emission point sources. The technology, in its most simplistic description, involves the capture of CO_2 from an industrial source, such as a coal-fired power plant, compression and transport of CO_2 to an injection site, and finally its sequestration to a deep underground geologic formation for long-term storage. Sedimentary basins in general and deep saline aquifers in particular, are being investigated as possible repositories for large amounts of anthropogenic CO_2 that must be sequestered to stabilize atmospheric CO_2 concentrations (Bachu 2003; White et al. 2003). These basins are attractive for CO_2 storage, because they have huge potential capacity, estimated globally at up to 11,000 Gt of CO_2, and advantageous locations close to major CO_2 sources (Holloway 1997; Benson and Cook 2005). Although, in the long geologic time scale the sequestered bulk CO_2 is unlikely to escape because of various trapping mechanisms, such as solution, physical, and mineral trapping, slow leakage of buoyant CO_2 or CO_2 saturated brine even under favorable storage conditions may occur (Karamalidis et al 2013, Kharaka et al 2010).

In this context, the study of CO_2 perturbation in natural systems has numerous implications in both fundamental and applied research. The understanding of chemical species behavior over CO_2-water-rock interaction process appears as a key parameter for applications such as Carbon Capture and Storage (CCS), geothermic, waste water management, groundwater pollution and remediation. Perturbations caused by natural or artificial CO_2 may modify the natural water-rock equilibrium occurring in deep geological reservoirs and subsurface aquifers. An important question concerns the possible mobilization of dissolved metal species resulting from the water acidification by CO_2 perturbation as encountered in certain natural CO_2-rich fluids in geothermal fields. The behavior of chemical elements over CO_2-water-rock interactions is dependent on acido-basic, redox and mineral-water equilibrium processes, operating in various proportions, over different time and space scales.

This thesis is focused on hydrogeochemicals modifications induced by the CO_2 perturbation in aquifers, with special focus on water-rock equilibrium, reaction kinetics, and their on field conditions, with particular emphasis on metal species remobilisation.

This work includes two major parts:

The first part is devoted to the study of natural CO_2 rich water from geothermal field of Galicia (Spain). In this study, time scale of CO_2-water-rock reaction is unknown but considered as resulting from long term (>1000 years) process. Similarly, the space scale corresponds to a large domain of natural geothermal field (about 100km^2). For such space and time scales, the CO_2-water-rock process

was considered as mainly controlled by chemical reactivity and thermodynamic processes, where transport and fluid mixing effects can be considered negligible as a first approximation. Under these conditions we studied the mineral reactivity in response to natural CO_2 perturbation using a kinetic approach that allowed to estimate the variation of reactive surface area of minerals.

In the second part we performed a field injection of water-CO_2 mixture in a subsurface aquifer. A push-pull test protocol was used to evaluate the impact of CO_2 perturbation in an "equilibrated system". Here we focused on the behavior of trace metals. Under these conditions, the impact of CO_2 perturbation was investigated over a time scale of several days, and space scale of a small subsurface aquifer. In this case, the effect of transport and mixing processes had to be evaluated, and we proposed an estimation of mineral reactivity and fate and transport of chemical elements induced by the CO_2 perturbation.

1. Hydrogeochemical perturbation by CO_2 in a natural system: application and concept

In this section is presented a general description of CO_2-water-rock interaction processes, in term of application, environmental issues, mechanism, equilibrium model and kinetic of reaction.

1.1. CO_2 geological storage: general concept

One of the key issue in understanding CO_2-water-rock interaction process concern the Carbon Capture and Storage (CCS). The concept of CCS was proposed as a potential response to the climate change in the early 2000s. This idea was proposed to meet the commitments undertaken in 1997 in the Kyoto Protocol for reducing anthropogenic emission into the atmosphere. Carbon-dioxide sequestration, in addition to energy conservation and increased use of renewable and lower-carbon, intensity fuels, is now considered an important component of the portfolio of options for reducing greenhouse gas emissions to stabilize atmospheric levels of these gases and global temperatures at acceptable values that would not severely impact global economic growth (Benson and Cook 2005 ; Holloway et al. 2007 ; IPCC 2007 ; Lackner 2010 ; Oelkers and Cole 2008 ; Schrag 2009 ; Sundquist et al. 2009). Since the early 2000s, a lot of projects were conducted in both applied and fundamental research to develop this approach.

The general concept is the capture of CO_2 directly from anthropogenic sources and disposing of it deep into the ground for geologically significant period of time (i.e. >1000 years)(Bachu 2002). The objectives of this technique is to reach a storage capacity of several billion of tones of CO_2 to significantly mitigate the amount of CO_2 into the atmosphere.

An important argument to move forward such a project is the fact that technology for deep injection of gas, oil, CO_2 and industrial liquid waste is already well developed and widely practiced. Sedimentary basins in general, and deep saline aquifers in particular, are being investigated as possible repositories for large volumes of anthropogenic CO_2 that must be sequestered to mitigate global warming and related climate changes (Hitchon 1996 ; Benson and Cole 2008 ; Kharaka et al. 2006, 2009). Deep saline aquifer have important distribution all around the globe. Further, water formation in deep aquifer are designed as 'brine' characterized by high mineralization and salinity, and therefore are not usable for water resources.

Four main CO_2-trapping mechanisms are considered: 'structural' ,'residual', 'solution' and 'mineral'.(Bachu 2002, Kharaka and Cole 2011). Reservoir capacity and integrity are strongly dependent on the trapping mechanism. Dissolved CO_2 is likely to react with the reservoir and cap rocks, causing dissolution, precipitation and transformation of minerals, and changing the porosity, permeability and capacity of the reservoir, as well as impacting the extent of CO_2 and brine leakage that, as noted by Kharaka et al. (2006, 2009) and Benson and Cole (2008) could contaminate underground sources of drinking water. Reservoir capacity, performance and integrity are strongly affected by the four possible CO_2 trapping mechanisms (Benson and Cook 2005 ; Friedmann 2007 ;

Benson and Cole 2008): (1) 'structural and stratigraphic trapping' , where the injected CO_2 is stored as a supercritical and buoyant fluid below a cap rock or adjacent to an impermeable barrier; (2) 'residual trapping' of CO_2 by capillary forces in the pores of reservoir rocks away from the supercritical plume; (3) 'solution trapping' , where the CO_2 is dissolved in formation water forming aqueous species such as $H_2CO_{3\_}$, HCO_3^-, and CO_3^{2-}; and (4) 'mineral trapping' , with the CO_2 precipitated as calcite, magnesite, siderite and dawsonite (Gunter et al. 1993 ; Palandri et al. 2005 ; Bénézeth et al. 2007, 2009 ; Oelkers et al. 2008). Therefore the potential of deep aquifer CO_2 sequestration can be considered through 3 different phases such as free CO_2 into the pore space, $CO_{2(aq)}$ dissolved into the aqueous phase and CO_2 converted into the rock matrix.

Those three different processes occur at different time and space scale, and are strongly dependent on the reservoir properties, i.e. mineral composition, porosity/permeability, temperature, pressure, and fluids chemical compositions.

Deep saline aquifers in sedimentary basin considered for CO_2 sequestration are usually situated between 800 and 4000m depth, and previous studies have showed that from 800m depth, CO_2 would be present under the form of supercritical fluid (Bachu 2002). Considerable uncertainties and scientific gaps, however, exist in understanding CO_2-water/brine-mineral interactions at reservoir conditions, because supercritical CO_2 is buoyant, displaces huge volumes of formation water, and becomes reactive when dissolved in the formation water (Kharaka et al. 2009 ; Haszeldine 2009). The bulk of CO_2 will be stored initially as a supercritical fluid, with some rapidly dissolving in formation water, but mineral and additional solution - trapping will be slower, yet more permanent. The supercritical state is defined for a fluid by his critical point (critical point is 31,1°C and 7,38 MPa for CO_2), where distinct liquid and gas phases do not exist. The supercritical state for a fluid and physico-chemical interaction with host rock are very complex to define.

Geochemical studies are essential for providing improved understanding of CO_2-water/brine-mineral interactions, which strongly affect storage injectivity and security. In is this work, we focus on the consequences of CO_2 perturbation on water-rock interaction processes, in relation with CO_2 geological storage. In particular, we are interested on the part of CO_2 which actually dissolve into the aqueous phase ($CO_2 \rightarrow CO_{2(aq)}$), and which interact with reservoir rock, defined as CO_2-water-rock system, and implication for long term environmental issues.

1.2. Feedback from natural and artificial CO_2 perturbation in natural system and potential environmental issues

1.2.1. Safety of CO_2 geological sequestration sites

Due to the high cost and technical issues of CO_2 injection experiment in deep geological formation, very few results and feedbacks from field experiments are available to date. To partially fill up this gap, a lot of experiments have been performed in laboratory, and by numerical approach. Furthermore certain natural hydrothermals waters can present naturally high concentration in CO_2, and can be used as potential natural analogs to understand the long term CO_2-water-rock interaction processes.

The safety of CO_2 geological storage site must be established on case by case basis (Bachu 2002). One of the major risk concerns the potential for CO_2 upward migration and escape into other aquifer or any other geological formations during or immediately after injection. This could happen mainly through existing natural or induced open fault, regardless of the means of sequestration. Other risks exist as a long term prospective, with lateral migration of CO_2 in aquifer, with potential for crossing existing formation flow, where carbon dioxide could reach aquifers. This phenomena can happen immediately after injection or as a long term issue, depending on site characteristics. In both long term and short term, CO_2 may contaminate mineral and water and may even reach the surface. The assessment of sequestration site safety needs to be done on the basis of better understanding in situ physico-chemical processes associated with CO_2 injection and storage, improving numerical modeling of CO_2 fate, and detailed knowledge of relevant site characterization. The safety evaluation will probably reduce further the site selection for CO_2 geological sequestration. For these reasons, the understanding of CO_2-water-rock interaction processes in both long and short term, and at reservoir scale to sedimentary basin scale are very important. To evaluate these risks requires a detailed geologic site characterization, and an improved understanding of formation properties and how the injected CO_2 spreads and interacts with the rock matrix and reservoir fluids (Bachu 2003; Friedmann 2007). Geologic formations typically consist of layers of rock with different porosities, thicknesses, and brine and mineral compositions. All of these factors, together with the presence of faults and fracture systems, affect the suitability of the formation as a site for CO_2 sequestration. Porosity and thickness determine the storage capacity of the formation, and chemical composition determines the interaction of CO_2 with the minerals in place. Also, an impervious cap rock and absence of high-permeability faults are necessary to prevent the sequestered buoyant CO_2 from migrating to the surface. Finally, if the geological section consists of a series of aquifers, it is necessary to ensure that CO_2 stored in a saline formation does not migrate to a potable aquifer.

1.2.2. Potential impact for water resources

Special issue concerning the potential environmental impact of CCS is the consequence of water contamination by CO_2 leakage. A particular experiment performed in Frio, where results were published in 2006 and 2009 by Kharaka et al, showed a potential consequence of CO_2 injection on formation water chemistry. This experiment constitutes one of the first feedback concerning the potential environmental impact of CCS.

This experiment was performed to investigate the potential for the geologic storage of CO_2 in deep saline aquifers. A volume of 1600 tones of CO_2 was injected under supercritical state at 1500m depth into a 2-4m thick sandstone section of the Frio Formation, a regional brine and oil reservoir. Fluid chemistry was analyzed continuously before, during and after CO_2 injection by sampling grouwater in an observation well situated approximately 30m downward the injection well. This sandstone formation is characterized by a mineral composition mainly constituted by quartz and feldspar, with minor amounts of illite, smectite and calcite. Main hydraulic barrier to CO_2 leakage are constituted by thick marine shale beds.

Chemical analyses of water samples obtained from well prior to injection showed that the Frio brine is Na-Ca-Cl type water, with a very high salinity of 93000± 3000 mg/L of total dissolved solid (TDS). Major chemical changes were observed as the CO_2 reached the observation well, including a sharp drop in pH (from 6,5 to 5,7) and pronounce increase in alkalinity, from 100 to 3000 mg/L (i.e. $1,6 \ 10^{-3}$ mol/L to $4,9 \ 10^{-2}$ mol/L) as bicarbonate.

Additionally, laboratory determinations showed major increases in dissolved Fe (from 30 to 1100 mg/L) and Mn (from 2 to 10 mg/L), and marked increase in the concentration of Ca. The most dramatic changes in chemistry occurred at CO_2 breakthrough (Fig.1.3).
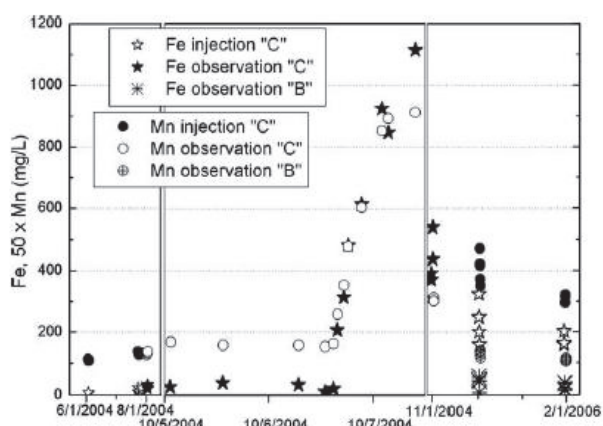
Fig.1.3: Concentrations of Fe and Mn in Frio brine from June 2004 to April 2005. Note sharp increase in metal content during 6 October 2004 at time of CO2 breakthrough (source Kharaka et al 2006)

Organic matter, measured by Dissolved Organic Carbon (DOC), obtained during CO_2 injection increased moderately from 1 to 5-6 mg/L.

Isotopic tracer such as $\delta^{18}O$, $\delta^{13}C$, rare gas He, Ar were used to trace the CO_2 plume, and confirmed that previous large increase of dissolved elements (HCO_3^-, Fe, Mn, Ca, and DOC) were correlated to CO_2 plume breakthrough.

Geochemical model simulations identified rapid dissolution of minerals, such as calcite and iron oxi-hydroxides caused by low pH brine (Karaka et al 2009). This dissolution could have important environmental implications with regard to creating pathways in the rock seals and well cements that could facilitate leakage of CO_2 and brine. Further metal oxi-hydroxide minerals are known to have potentially large amount of trace metals such as Pb, As, Cd, Zn, U (etc.) as surface sorbed or cosorbed species.

Kharaka and co-workers concluded that deep saline aquifers and depleted petroleum fields in sedimentary basins provide advantageous locations close to major CO_2 sources and huge potential capacity for the storage of large amounts of CO_2. However, maintaining reservoir integrity that limits CO_2 leakage to very low levels is essential to the success of injection operations. Preventing brine migration into overlying drinking water supplies is also important, because dissolution of minerals would potentially mobilize Fe, Mn, and other metals, in addition to the chemicals of the ambient brine. Therefore feedback of this experience showed potential consequence for water resources, with the fate of potentially toxic elements, especially metal species resulting from complex behavior involved with CO_2-fluids-minerals interaction.

Geochemical results from Frio tests proved powerful in: (i) tracking the successful injection of CO_2 ; (ii) detecting CO_2 in the overlying sandstone; (iii) showing mobilization of metals and organics, and major changes in chemical and isotopic compositions of brine. Modelling and Fe isotopes indicate dissolution of calcite and Fe - oxyhydroxides, and well-pipe corrosion.

Geochemical changes, including pH-lowering, alkalinity increases and metals mobilization, were also observed in shallow groundwater following CO_2 injection at the zero-emission research and technology (ZERT) site, Montana (Kharaka and Cole 2011).

1.2.3. Feedback from natural analogues

The use of natural CO_2 - bearing geologic systems as proxies for understanding the behaviour of CO_2 in the subsurface has gained considerable momentum in recent years as various developing countries wrestle with the issue of storage of anthropogenic CO_2 in geological formations (e.g. Pearce et al. 2003 ; Lewicki et al. 2007 ; Fessenden et al. 2009 ; Wilkinson et al. 2009; Angelone et al. 2005 Pauwels et al 2007; Czernichowski-Lauriol 2003). The study of these natural analogue systems can provide valuable insights into: (i) potential leakage or migration pathways and CO_2 fluxes to the shallow subsurface, (ii) long - term consequences of CO_2- water - rock interactions on reservoir rocks and cap rock seals, (iii) relative contribution by various storage mechanisms to the security of CO_2 storage for time frames in excess of those currently available to us via existing CO_2 injection demonstration tests, and (iv) the robustness of computer modelling of water - rock interactions to predict behavior well beyond the limits of either bench - scale or field tests. One distinct advantage natural analogues provide is a snap-shot or long-lived systems that contained large amounts of CO_2. A major difference, however, with proposed injection scenarios associated with stationary point sources of CO_2 (i.e. power plants) is that the injection rates in the industrial systems will be much greater than what we typically predict for natural settings.

Further, one of the main issue when studying natural CO_2 hydrothermal source results on identifying and estimating the origin source of CO_2. To partially filled up this gap, isotopic data such as $\delta^{13}C$ or noble gas (He, Ne, Ar, Kr and Xe) can be used to categorise source the origin of CO_2 (Gilfillan et al 2008, 2009). Compounding this issue is the fact that isotopic compositions of CO_2 can be altered by a number of different reaction pathways such as dissolution into brine or oil, and reaction with host rock particularly carbonates. Furthermore, it is unlikely that just one source of CO_2 will dominate any given geologic system, so the challenge is to deploy a set of multiple geochemical tools to sort out the various potential sources.

Water-rock interactions in CO_2 rich geothermal fluids result from complex phenomena, involving pH, temperature, mixing, dynamic of dissolved carbonates, speciation phenomena, redox control, and mineral dissolution/precipitation.

In particular, certain geothermal CO_2 rich waters are known to contain significant concentrations in metals species. Further, precious metals ore deposits (Au, U, Mo, Cu, Rare earth elements) are often involved with hydrothermal alteration caused by geothermal fluids (Chenevoy and Piboule 2007). These fluids were extansively studied as a part of research projects concerning radioactive waste geological storage and geothermal prospection (Criaud and Fouillac 1989; Sanjuan et al. 1988; Michard and Beaucaire 1993; Beaucaire et al. 1987; Cidu and Bahaj 2000). Therefore, CO_2 geothermal rich fluids have been studying as natural analogs for long term CO_2-water-rock interaction.

Some studies showed an interesting focus on long term CO_2-water-rock interaction processes and metal species behavior (Keating et al 2010, Criaud and Fouillac 1986, Beaucaire et al. 1987).

1.3. CO$_2$-water-rock interaction process

1.3.1. CO$_2$-water-rock equilibrium and kinetic of reaction

Reactions occurring during perturbation of water-rock system by CO$_2$ are mainly acido basic reactions (Michard 2002). Carbon dioxide dissolution in water produces carbonic acid species. This reaction is dependent on pressure, temperature and initial chemical composition of the aqueous species. The CO$_2$(g)-water equilibrium can be calculated by the Henry's law :.

$$CO_{2(aq)} = \alpha \ pCO_2 \qquad (1.3.1)$$
$$\alpha \ pCO_2 = H_2CO_3 \qquad (1.3.2)$$

Where α is the Henry's constant, which depends on pressure and temperature of the system. Subsurface and deep aquifer are characterized by low water/rock ratio, and by fluid in equilibrium with mineral composing the host rock.

Injection of CO$_2$ of any form into the pore water of a reservoir leads to 'solubility trapping'. The solubility depends on several factors, most notably pressure, temperature and brine salinity (Spycher et al. 2003 ; Lagneau et al. 2005 ; Rosenbauer et al. 2005 ; Koschel et al. 2006 ; Raistruck et al. 2006). The chemical equilibria associated with the dissolution of CO$_2$ in formation brine are expressed in equations *(1.3.3)-(1.3.5)*:

$$CO_2 + H_2O \leftrightarrow H_2CO_3 \qquad (1.3.3)$$
$$H_2CO_3 \leftrightarrow HCO_3^- + H^+ \qquad (1.3.4)$$
$$HCO_3^- \leftrightarrow CO_3^{2-} + H^+ \qquad (1.3.5)$$
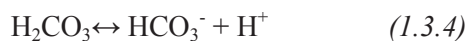
At pH values lower than approximately 6, carbonic acid (H$_2$CO$_3$) is the dominant carbonate species, with bicarbonate (HCO$_3^-$) and carbonate (CO$_3^{2-}$) becoming dominant in brine at intermediate and high pH values respectively. At the onset of injection, the fluid in the vicinity of the well is quite acidic, leading to increased reactivity with the host minerals.

Under these conditions, "equilibrium conditions" can be estimated by thermodynamic calculation. In such a system, we have to determinine in which conditions the water composition is fixed by reaction with minerals, and which are the main parameters that determine water composition. Chemical elements can be designed as mobile or controlled (Michard 2002, Stumm and Morgan 1996, Brantley et 2008). An element is designed as mobile when the maximum concentration of an element that can be extracted by dissolution is inferior to equilibrium concentration with neo-formed phase. A chemical

element is designed as controlled when his concentration is controlled by precipitation by one or several phases.

To describe multi-mineral complex system, thermodynamic equilibrium can be used by calculating saturation with respect to one or several minerals phases. Or, as an inverse approach, determine the mineral phase in equilibrium with water composition.

For example, in natural water, major cations resulting from water-rock interaction are Ca^{2+}, Mg^{2+}, Na^+, K^+, major anions are CO_3^{2-}, HCO_3^-, Cl^-, SO_4^{2-}. These species result from water-rock interaction and are major constituents of natural water. Other major constituents of minerals such as Fe, Al and Si are usually controlled by the low solubility of neo-formed phases such as metals oxides, quartz or clay mineral such as kaolinites. They are present in relatively low concentration in neutral pH range of natural waters. pH perturbation by CO_2 intrusion can significantly influence solubility of Al, Fe, Si, and other majors species, and modified their concentration in solution (Michard 2002, Stumm and Morgan 1996). By these examples we can see that water-rock reactions are complex to model and predict.

Several computer codes have been developed to calculate mineral-fluid equilibrium. These are can be used to calculate free ionic species and speciations, saturation degrees (of solid and gaseous phases), masse transfers and kinetics of reaction. However, the quality of geochemical equilibrium model results are obviously strongly dependent on the quality of input chemical data and on the representativeness of used thermodynamic database. Several geochemical computer code are available. PhreeqC code (Packrust and Appelo 1999)was used as a part of this work. Several database are available, some of them are commonly used such as *phreeqc.dat, wateq4f.dat* or *mineteq.v4.dat* database. However, thermodynamic constant are constantly updated, especially concerning trace metals elements..

1.3.2. Kinetics of reaction

Modeling water-mineral reactions is difficult since rocks are multi-minerals systems. Generally, rate laws, including kinetics and thermodynamic constrains are determined semi-empirically, including both laboratory experiments and theoretical aspects. Most of those laws were developed and described by A. Lasaga, P. Aagaard and H.G. Helgeson and their coworkers, during 1970 to late 90s. Their approach consisted on defining rate of mineral dissolution as a function of mineral saturation state or reaction chemical affinity (Helgeson et al. 1984, 1970, 1969, Aagard 1982, Lasaga A.1981,1986).

For a **simple reaction** occuring at constant volume and temperature:

$$A+B \rightarrow AB \qquad (1.3.6)$$

19

Where A and B are reactive species and AB the product. is occurring, The rate of consumption of reactive A is defined at any time of the reaction:

$$r_A = -\frac{d[A]}{dt} \qquad (1.3.7)$$

On the other hand, the rate of production of AB is defined by:

$$r_C = \frac{d[AB]}{dt} \qquad (1.3.8)$$

At any time of the reaction $r_A = r_{AB}$, and can be calculated. A useful concept of *reaction advancement* introduced by T. DeDonder in 1920 can be used. This concept is defined by

$$\zeta = \frac{n_i^0 - n_i}{v_i} \qquad (1.3.9)$$

Where n_i^0 is the initial number of moles of a reactant or product, n_i is the moles at time t, and v_i is the stoichiometric coefficient for that species in the written reaction. ζ is expressed in mole. The reaction advancement ζ is a time independent variable. Therefore, each chemical reaction can be viewed independently of time scale. This parameter can be helpful to describe a system where absolute time of chemical reaction cannot be quantified properly, as in the case of natural systems. This concept can be also used to study the evolution of a system perturbated by CO_2.

Therefore, the rate of reaction r, is defining per unit of volume of the studied system as follow:

$$r = \frac{1}{V}\frac{d\zeta}{dt} \qquad (1.3.10)$$

Thus for a given species i, rate of reaction can be defined by:

$$r = \frac{1}{Vv_i}\frac{dn_i}{dt} \qquad (1.3.11)$$

Analysis of reaction rates is usually estimated as a first approach as a function of chemical composition of the studied system (including gaz, fluid and solid composition). For the reaction *(1.3.6)*, the rate equation might be written as:

$$r = k([A]^{\alpha} [B]^{\beta} [AB]^{\sigma}) \qquad (1.3.12)$$

The exponents α, β and σ are partial orders of reaction with respect to A, B, and AB and the sum of all of the partial orders is the overall order of reaction. For phenomenological treatments of reaction kinetics, these orders are empirical and need not be integral values. Note also that no simple relationship need exist between the stoichiometry of an equation and the order of the reaction. In fact, the kinetics of many geochemical systems are only treated with a phenomenological approach where equations such as Eq. *(1.3.12)* are treated simply as fitting equations (Lasaga 1998, Brantley 2008). It is important to note that in contrast with thermodynamic equations, rate of reactions are defined using molar concentration rather than activity, in order to be consistent with physical dimension of the system. In the case of mineral dissolution into aqueous solution, rate of dissolution k is explained in mole·m^{-2}·sec^{-1}, where m^{-2} corresponds to the reactive surface area of minerals.

Considering a single mineral dissolution reaction into aqueous solution, the maximum rate of the reaction is a function of the reactive surface area of mineral and the chemical reaction affinity. The general rate equation can be written for the flux (r) of a given reactant mineral as (Aagard and Helgeson, 1982):

$$r = \frac{1}{S}\frac{dn}{dt} = \frac{1}{S}\frac{d\zeta}{dt} = k\left[1 - \exp\left(-\frac{A}{\sigma RT}\right)\right] \qquad (1.3.13)$$

Where r stands for the rate of dissolution per m^2 of effective mineral surface area, defined in moles·m^{-2}·time^{-1}, t is time in seconds, ζ designates the reaction advancement for the process (DeDonder, 1920, Helgeson, 1979) in moles, S refers to the effective surface area of the reactant mineral (which corresponds to the total area of active(reactant) sites exposed to the aqueous phase) in m^2, n stands for the number of moles of the reactant mineral in the system, R designates the gas constant in cal mole K^{-1}, T represents temperature in Kelvin, A stands for the chemical affinity of the overall reaction in Cal mole^{-1}, σ refers to the average stoichiometric number, and k denotes the rate constant for the process in moles·m^{-2}·sec^{-1}.

In a complex system, where concentration are controlled by an association of different minerals, the kinetic rate of dissolution can be calculated by a series of mass balance equation involving the rate of relevant mineral phase.

For a given system containing N_{tot} species and N_r reactions can be expressed as (Marini et al 2000, Steefel and Mc Quarrie 1996) :

$$I \cdot \frac{dn}{dt} = \nu \cdot R \qquad (1.3.14)$$

Where **I** stands for the identity matrix (dimension $N_{tot} \times N_{tot}$), **n** refers to the vector of solute concentration (length N_{tot}), n is the stoichiometric reaction matrix (dimension $N_{tot} \times N_r$), t stands for time, and **R** refers to the reaction rate vector (length Nr; comprising both equilibrium and kinetically-controlled reactions). If all reactions are described with kinetic rate laws, the system of differential equations can be solved in time-mode, or in reaction advancement mode by substituting for the experimentally determined rate laws in the reaction vector **R** (Marini et al 2000, Sciuto and Ottonello 1995). However, the application to practical cases and field experimental conditions, is often hindered by the lack of knowledge of the actual surface area of minerals that participate to fluid reactivity and chemical composition.

Therefore the estimation of Reactive Surface Area (RSA) of minerals can be estimated to evaluate the reactivity of individual minerals in multimineral-water interaction system (Marini et al 2000, Sciewlevski and Zuddas 2010).

1.3.3. The mineral reactive surface area

As previously mentioned, one of the key input parameter to take into account for modeling and predict evolution of water-rock interaction is the estimation of the surface area which actually interacts with fluids. Over the past 30 years, silicate and carbonate mineral dissolution rates have been thoroughly investigated through both laboratory experiments and field scales studies (White and Brantley, 1995; Brantley et al., 2008). The studies produced significantly different results, depending on whether the estimates were made under laboratory conditions or in the field. One of the reasons is that under controlled experimental conditions the surface area cannot be readily reconciled with the contact surface between minerals and the percolating waters in soils and rocks usually estimated by porosity. Moreover, the dissolution process is not homogeneous and the reactive surface area, i.e. the portion of the mineral surface area exposed to the aqueous solution and actively participating in the reaction, may be significantly different from the total surface area (Helgeson et al., 1984). Given that fluid-mineral

interactions occur primarily at selected sites of the available mineral surface area (Xu et al., 2005; Brantley et al., 2008 Gaus et al., 2008), many authors recognize that the reactive surface area in heterogeneous reactions involving simultaneous dissolution of several minerals is difficult to quantify (Hochella and Banfield, 1995; White and Brantley, 1995; Oelkers, 1996; Lichtner, 1996, 1998). The mineral surface area can be estimated, under experimental conditions, assuming particles have smooth and regular surfaces and a uniform geometry or by the isotherm adsorption of inert gases like N_2 or Ar (i.e.B.E.T method). Indeed numerous parameters can influence the mineral surface reactivity, such as sorption-desorption, surface complexation, neo-formed phase precipitation etc. Therefore, surface of mineral is defined by their geometric surface, corresponding to the total mineral surface in contact with water, and the reactive surface area designs the mineral surface portion which actually interact with the water and participate to the water chemical composition. Geochemical study on water-rock interaction process showed that there is no clear correlation between geometric surface area and reactive surface area of minerals (Brantley et al. 2008).

Further, for multi-mineral systems, since only part of the mineral surface is involved in the reaction (e.g., Xu et al., 2007), during kinetic reactions, the specific surface area increases or decreases as the morphology of mineral changes (Velbel, 1984, 1986, Sciechlewski and Zuddas 2010). This can result in an uncertainty of the modeled results of up to several orders of magnitude. Moreover, it is generally considered that the total available surface area is between one and three orders of magnitude larger than the actual reactive surface area (Gaus et al., 2005; Xu et al., 2007) with variations of several orders of magnitude during the overall reaction time.

1.4. Perspectives and main focus

In the light of previous development, the aims of thesis are:

- Evaluating the reactivity of mineral under CO_2 perturbation in natural system, over a long term perspective (>1000years), within a large space scale. A field kinetic approach was used to estimate the reactive surface area of mineral using chemical data of thermal water perturbated by CO_2 from geothermal origin in Galicia (Spain).

- Performing a field experiment of injection of water saturated in CO_2 in subsurface aquifer following a push-pull test protocol. Similarly to previous part, the aim of this experiment was applying a field kinetic approach where time and space scale is limited (within few days) and can be estimated at reservoir scale. The aim of this second part was to evaluate the impact of CO_2 perturbation on groundwater chemical composition, with special focus on trace metals behavior, reactivity of minerals and major influence parameter (pH, redox, and speciation).

2. Kinetic approach to estimate the mineral reactivity in response to CO_2 perturbation

In this part is presented an evaluation of the reactivity of mineral in response to CO_2 perturbation. This model was based on studying data of a natural geothermal CO_2 rich water. The long term evolution of CO_2-water-rock system was estimated by the variation of water composition. This chapter is presented under the form of scientific publication, in preparation for submission to a journal of geochemistry

Kinetic approach to study difference of mineral reactivity in response to natural CO_2 perturbation

Jean Rillard[1,2] and Pierpaolo Zuddas[1,3]

[1]Département Sciences de la Terre "Terre Planète Environnement", UMR 5276, Université Claude Bernard Lyon1. 2, rue Dubois, F69622 Villeurbanne Cedex, France.

[2] INERIS, Institut National de l'Environnement industriel et des Risques, Parc Technologique Alata, F60550 Verneuille en Halate, France

[3]Université Pierre and Marie Curie Paris-Sorbonne, ISTEP, 4 place Jussieu, F75005 Paris, France

ABSTRACT:

Evaluating the reactivity of minerals in response to CO_2 perturbation is one of the major challenges facing both fundamental and applied geoscience today. The fluid reactivity process is a function of the net rate of mineral dissolution and precipitation that in turn regulates the fluid composition of the Earth's crust.

To study the effect of CO_2 perturbation, we estimated ratio of reactive surface area (RSA) of main minerals composing the Galician (Spain) geothermal field using the chemical composition of fluids as input data. We implemented an original methodology to quantify ratio of mineral RSA in the field taking into account that the chemical composition of fluids evolves over time notably by incorporating reservoir properties. Our methodology is based on reconstructing the fluid composition according to a perturbation progress schema that uses the degree of advancement of the mass-transfer process. In our methodology, RSA is quantified by a ratio between the different main minerals, normalized to the most abundant minerals (Albite). A transposed reaction rate that introduces experimental kinetic rate constants.

We found that over the entire reaction process the kinetic rate of mineral dissolution remained constant whereas the ratio of RSA(Albite)/RSA(Biotite) varied by 1–3 orders of magnitude; while ratio of Albite/K-feldspar remain quite constant, explaining the changes observed in CO_2 partial pressure and

fluid pH. Values obtained for the mineral surface area differ significantly according to the calculation methodology employed. We found that ratio of reactive surface area are 1 to 3 order of magnitude different from ratio calculated by modal mineral composition. Based on our findings, we propose that when modeling CO_2 mineralization in natural water-rock systems, the current geo-mechanical method is insufficient to account for the evolution of the fluid chemical composition. To accurately predict the ultimate mineralization capacity of any given natural reservoir and to estimate the presence of extraneous chemical elements entering the fluid composition, it is essential to take a geochemical approach and to evaluate the evolution of the RSA itself. Our approach offers a reliable geochemical methodology for estimating the evolution of mineral RSA ratio in natural water-rock interaction systems where fluids have long residence time.

1. <u>Introduction</u>

Fluid – rock interaction controls many environmental and geological processes occurring at the Earth's surface. The quantification of these processes is important in most treatments of global element cycles, notably carbon dynamics (Berner, 1983) and in the challenging areas of geothermal resource evaluation and CO_2 geological storage. The amount of CO_2 reacting and potentially mineralized through rock reactivity (Keating et al 2010) is mainly dependent on the rate of mineral dissolution and precipitation that regulates the fluid composition in the upper-crust. To understand the mechanisms by which minerals dissolve, dissolution rates have been extensively studied in laboratory settings (White and Brantley 2003; Brantley et al; 2008); however, the comparison of laboratory derived rates to field scale studies is difficult due to the fact that most laboratory-derived rates are significantly different than field derived rates (White and Brantley, 2003; Navarre-Sitchler and Brantley, 2007, Noiriel et al 2009). Given the complexity of evaluating reactive transport processes (Malmström 2000, White et al 2003), studies generally apply mass balance isotopic concepts like the water-rock ratio; whereas fluid flow and T-xCO2 equilibrium are rarely evaluated in a kinetic framework under natural conditions.

It is the mineral's reacting surface area (RSA), i.e. the real surface in contact with the interacting fluids, which controls the dissolution rate of silicate and carbonate. This parameter is very difficult to estimate given that all mineral surface sites do not react identically (Brantley et al 2008). Major discrepancies are generally observed between dissolution rates estimated under different conditions because surface area under controlled experimental conditions in the laboratory cannot be readily reconciled with the contact surface between minerals and percolating fluids in soils and rocks. When modeling natural situations, RSA is generally assumed to be constant or is deduced by measuring physical properties such as porosity and permeability. Factors including tectonics (Stallard, 1992; Riebe et al. 2004; West et al. 2005), the composition of reacting fluids (Burch et al. 1993) as well as possible biological activity (Lucas, 2001) vary from the laboratory to the field. In the case of long-term natural fluid-rock systems, the specific reactive surface area of minerals also depends on mineral composition variability, abundance, morphology, and the size of the minerals as well as the fluid's spatial flux distribution. RSA is extremely difficult to determine in natural systems given their heterogeneous nature and there is no simple relationship between what constitutes the 'reactive' surface of the minerals and how this may relate to the physical surface area of weathering rock (White et al 1990; Velbel 1993, Malmström et al 2000, Ganor et al 2005, Maher 2010). It has been argued that laboratory and field rates can be reconciled by using integrated methods (Sverdrup and Warfvinge, 1995) or with methods able to integrate the change of scale (Navarre-Stichler and Brantley (2007).

In this work, we attempt to estimate reactivity of minerals in response to natural CO2 perturbation, taking into account variations in the mineral reactive surface, by quantifying ratio of minerals RSA using chemical fluid composition as input data. We developed an original methodology for quantifying this variable in a natural context and assumed that the evolution of chemical fluids is the signal response to the water-rock interaction as it intrinsically incorporates timescale and reservoir properties (porosity, permeability, water/rock ratio, and dimension). We used data from the Galician geothermal field because of its relatively homogenous geological setting and fluid evolution with a wide range of pCO_2 partial pressure at emergence (Michard and Beaucaire 1993).

2. Rock system and sampling

2.1. Rock system

The Spanish Galician geothermal zone covers an area of at least 100 km^2. It is characterized by two Variscan granites generated by an anatexis process (Capdevilla et al 1973) with two series: the first is alkaline composed of leuco-granites containing feldspars, biotite and muscovite with pegmatite, tourmaline and greisens; the second, younger and of deeper origin, is calco-alkaline with a similar mineralogical association. Present-day hydrothermal activity is related to the presence of several Alpine Orogeny faults, mainly oriented NNE-SSW, that are responsible for contact between alkaline and calco-alkaline granites. Galician granites have very low porosity with hydrological circulation along the main fractures (Delgado-Outeiriño et al. 2009, Marques et al. 2010).

Petrographic observations indicate the presence of a pervasive (diffuse) alteration event that affects the entire granitic batholite. This process, typically found in Western European granites, is responsible for the alteration of biotite and plagioclase creating secondary chlorite and sericite, respectively. In our zone of investigation however, microcline remains unaltered. Marques et al. (2010) observed a vein alteration stage along major fracture zones and documented the presence of secondary quartz and clay minerals. The uniform distribution and mineralogy of the alteration assemblage shows a dominant facies characterized by biotite suggesting small variations in the fluid/rock mass ratio and temperature. Based on petrographical modal abundances, the main mineralogical paragenesis is constituted by silicate minerals in the following proportions: quartz 35%, K-feldspar 20% albite 35%, biotite 10% and muscovite 1%. Accessory minerals like calcite and clays, mainly kaolinite, generally fill secondary porosities in the rock fractures (Michard and Beaucaire 1993), calcite proportion was estimated at 0,1%.

3. <u>Fluid Chemistry</u>

The Galician geothermal field is characterized by $Na-HCO_3$ waters, with an emergence temperature ranging from 15° to 57°C, pH varying from 9.5 to 5.8 and ionic salinity from 6 to 78 mmol/kg (Table 1). We did not observe a clear correlation between temperature and chemical composition, while we did find a slight inverse linear relationship between ionic salinity and pH. The fluid saturation state (S.I.), estimated by PhreeqC geochemical code (Parkhust and Appelo, 1999) using wateq4f.dat thermodynamic database (Dzombak and Morel, 1990), reveals saturation with respect to kaolinite and quartz. This indicates that all major cation activity (Ca^{2+}, Mg^{2+}, Na^+, K^+) is controlled by the dissolution of granite parent minerals while silica and aluminum activity is controlled by the solubility of neogenic mineral phases. The deep fluid temperature estimated using silica geothermometers (Helgeson 1978, Fouillac and Michard 1981) falls within an average temperature of 110±10°C for all the sampling points.

The pCO_2 partial pressure at equilibrium was estimated from alkalinity and pH using PhreeqC software. Fig. 1 shows that pCO_2 partial pressure increases linearly from 1 to 10^5 Pa as the sum of major cations increases from 10^{-5} to 10^{-2} mol/L, and Alkalinity from $2·10^{-3}$ to $1·10^{-2}$ mol/L. Therefore the hydrothermal field of Galicia was described as following: a high pH=9,8 poorly mineralized water in equilibrium with granite, perturbated by different amount of CO_2 from hydrothermal origin (see Fig.2) . The increase of CO_2 perturbation induce a dissolution of mineral, therefore an increase in major cations concentration (Ca^{2+}, Mg^{2+}, Na^+, K^+) and Alkalinity, related to decrease of pH water. We can see that molar concentration of cations and alkalinity are perfectly correlated. The Galician geothermal system can be viewed as granitic rock system with different fluid circulation and CO_2 content, and therefore different fluid reactivity. The geothermal field of Galicia can be viewed as an equilibrated water with granitic rocks, perturbated by different CO_2 circulation, see Fig 2. At the emergence, fluid are characterized by different pCO_2 signature, resulting from different exposure to hydrothermal CO_2 perturbation. This perturbation can be quantify by pH, cations concentrations, alkalinity and pCO_2 calculation. This differential composition in cations and pCO_2 of each sampled fluids was used to quantify the perturbation of water-rock equilibrium by CO_2. The dissolution of Al-silicates and carbonates is induced by CO_2 content and involved acidification increasing fluid reactivity. The pCO_2 partial pressure at equilibrium was estimated from alkalinity and pH using PhreeqC software. Fig. 1 shows that pCO_2 partial pressure increases linearly from 1 to 10^5 Pa as the sum of major cations increases from 10^{-5} to 10^{-2} mol/L; indicating that the Galician geothermal field can be described as a continuous process between two end-members: one with low pCO_2, low mineralization and high pH and the other with high pCO_2, high mineralization and low pH. As previously shown, the compositional trend of spring

30

waters is indeed continuous in terms of solute molalities. The overall fluid-rock interaction process can be estimated by a continuous rock perturbation (dissolution of Al-silicates and carbonates) mainly driven by the variation increase in pCO_2.
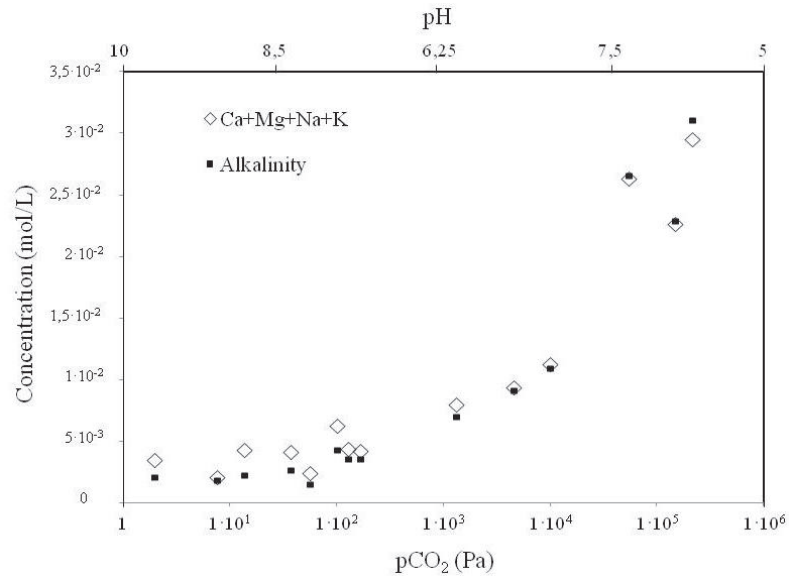

Fig. 1: Sum of major cation concentration (Na^+, Ca^{2+}, K^+ and Mg^{2+}) of geothermal fluid, and alkalinity plotted as a function of pH and pCO_2
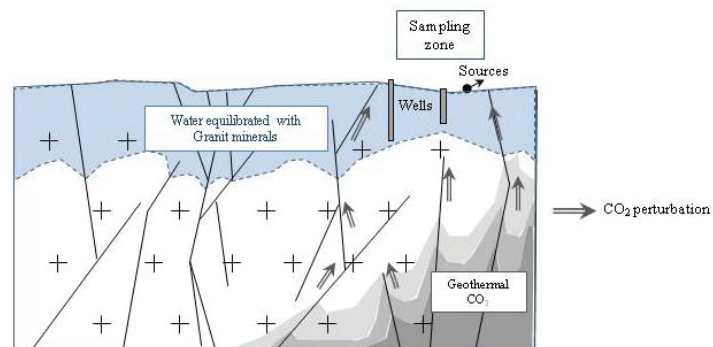

Fig. 2: Simplified geological cross section of Galician geothermal field, where CO_2 rises with deep water equilibrated granitic rocks, along faults and forms springs with different a CO_2 content.

Table 1:

Sampling point	Temperature	pH	Ca²⁺	Mg²⁺	Na⁺	K⁺	Li⁺	Cl⁻	SO₄²⁻	Alk.**	H₄SiO₄
	°C		$mmol \cdot l^{-1}$	$mmol \cdot l^{-1}$	$mmol \cdot l^{-1}$	$mmol \cdot l^{-1}$	$mmol \cdot l^{-1}$	$mmol \cdot l^{-1}$	$mmol \cdot l^{-1}$	$mmol \cdot l^{-1}$	$mmol \cdot l^{-1}$
Guitiriz	15	9.83	0.045	0.00036	3.45	0.0177	0.115	0.00081	0.11	2.1	0.72
Cuntis	57.2	9.02	0.037	0.00014	4.27	0.0726	0.0184	0.00192	0.25	2.27	1.51
Partovia	22.3	9.19	0.068	0.00096	2.07	0.023	0.027	0.00025	0.1	1.87	0.6
Prexigueiro	50	8.67	0.076	0.00237	4.06	0.086	0.118	0.00067	0.26	2.75	1.4
Canedo	69	8.13	0.074	0.0047	4.13	0.081	0.084	0.00043	0.09	3.6	1.27
Tintero	46	8.25	0.094	0.00546	4.28	0.081	0.088	0.00038	0.08	3.64	1.13
Reyes	45.8	8.2	0.216	0.0087	9.49	0.154	0.156	0.00685	0.06	2.5	0.9
Brea	22.4	8.43	0.1	0.00495	6.05	0.163	0.039	0.00098	0.11	4.37	1.62
Lugo	42.8	8.16	0.24	0.0153	6.21	0.133	0.122	0.00114	0.81	2.91	1.27
Tui	44.3	8.12	0.272	0.012	9.24	0.227	0.116	0.00666	0.48	1.96	1.53
Beran	27	8.25	0.166	0.0184	2.25	0.027	0.027	0.00039	0.14	1.59	0.76
Mondariz S	19.5	8.25	0.102	0.00815	4.37	0.078	0.165	0.0004	1.17	3.91	0.79
Layas	46	7.53	0.134	0.0134	7.71	0.153	0.144	0.00063	0.06	7.06	1.09
Burgas	66.5	7.1	0.3	0.0292	8.86	0.222	0.186	0.00068	0.03	9.14	0.27
Molgas	46.5	6.84	0.29	0.089	10.7	0.243	0.24	0.0004	0.01	10.94	1.1
Requeixo	20.5	6.49	0.48	0.221	24.8	0.835	0.425	0.00096	0.003	26.63	0.42
Mondariz G	16.4	5.99	1.38	2.14	18.1	1.04	0.425	0.0028	0.02	22.9	1.02
Cabreiroa	18	5.96	0.58	0.731	26.9	1.34	0.534	0.00106	0.04	31.1	0.98

*Data are from Michard and Beaucaire (1993) with permission

**Alk=Alkalinity

4. **Geochimical model**

4.1 Mathematical formulation

The Galician geothermal field shows evidence of simultaneous mineral dissolution and precipitation. In this section we present a theoretical methodology for evaluating ratio between main mineral RSA.

The rate of mineral dissolution reaction 'R', corresponding to the amount of matter released to the fluid per unit of reaction time, can be expressed by the following equation (Marini et al 2000):

$$R_i = S_i \cdot \overline{R_i} \qquad (1)$$

Where: R is the "*in-situ*" rate of dissolution (in mole per unit of time) representing the mineral dissolution rate under Galician field conditions, $\overline{R}$ is an absolute rate of dissolution expressed in mole·m^{-2}·sec^{-1} usually estimated by laboratory experiments and representing the maximum dissolution rate per unit of mineral area, while S is the reactive surface area (m^2), all evaluated for the ith mineral phase. In a multi-mineral system, fluid-rock reactions can be described by a series of mass balance equations for each of the relevant mineral phases in relation to the reaction rate. The rate of dissolution can be expressed by a system containing N$_{tot}$ species and N$_r$ reactions by (Steefel et al. 1998):

$$\frac{dn}{dt} = v \cdot R \qquad (2)$$

Where **n** is molar concentration, v is the stochiometric coefficient and R is the *in situ* rate. This equation system can be solved introducing the perturbation progress mode φ, where no time scale provision is needed (Suarez and Wood, 1996; Marini et 2000; Scislewski and Zuddas, 2010). Bearing in mind that the perturbation of the system from equilibrium state can be viewed from a starting point 0 to ending point 1, operating variables become a specific function of the advancement of the perturbation φ (Prigogine, 1955. Helgeson et al. 1968, 1969) resolved in a time-independent space. Considering temperature, pressure, volume and perturbation progress φ of each specific reaction as an independent variable, the system can be easily solved by (Sciuto and Ottonello 1995a, b):

$$n_{j,end} - n_{j,start} = \int_{\varphi=0}^{\varphi=1} \left(\sum_i \frac{\partial n_{i,j}}{\partial \varphi} \right) d\varphi \quad (3)$$

$$\text{With} : 0 \leq \varphi \leq 1 \qquad (3a)$$

Where n$_{j,i}$ stands for the molality of the jth aqueous solute in the ith reaction, φ represents the overall perturbation progress. Therefore we can define φ$_j$ is the individual perturbation progress related to the jth sampled fluids. Perturbation progress can be estimated using the evolution of the normalized progressive major cation concentration observed in the field by the relation:

$$\varphi = n_{Na+} + n_{K+} + n_{Mg2+} + n_{Ca2+} \qquad (4)$$

The variable φ can be calculated for each water samples. Therefore, water samples with low φ values represent low perturbation by CO_2, and higher φ values represent high perturbated waters. Each individual φ_j values can be divided by the higher value of φ in order to get a system normalized $0 \leq \varphi_j \leq 1$, where φ_j is very close or equal to 0, it represents non perturbated fluid in equilibrium with rock, and $\varphi_{i,h}=1$ represents the higher perturbated fluid into the system. Since the variation in concentration of Eqn 2 is known in the compositional space $0 \leq \varphi \leq 1$, the system is now solved for R (the problem is inversed) and Eqn. 2, in the reaction progress mode, becomes:

$$\frac{dn}{d\varphi} = v \cdot R_\varphi \tag{5}$$

Therefore R_φ can be transposed in equation (2) and defined as:

$$R_{\varphi i,h} = S_i \cdot \overline{R_i} \left(\frac{dt}{d\varphi} \right) \tag{6}$$

Where R is the *in-situ* dissolution rate, S_i is the reactive surface area of the ith minerals, $\overline{R}$ is a kinetic function of the reaction affinity and dissolution constants depending on pH, temperature and chemical composition. If R and $\overline{R}$ are calculated independently as a function of the perturbation advancement φ, the reactive surface area S can be also determined a function of the perturbation advancement φ (Eqn.6). It is important to note that the term S_i is expressed in square meters per kilogram of water (m^2/kg_w) in contact with the given mineral surface.

However, since the time t, representing the actual time scale of reaction, cannot be directly quantify into a natural system For example, the age of non perturbed water in equilibrium with granitic reservoir rock can be different from the age of the CO_2 perturbation. Therefore, the function (dt/dφ) cannot determined properly. In other words that the evolution of φ as a function of time cannot be determined properly (DeDonder 1920, Prigogine 1955). However, this system can be considered as irreversible, therefore the derivative ratio dt/dφ is a strictly increasing function:

$$\frac{dt}{d\varphi} \geq 0 \tag{7}$$

As corollary R_φ and therefore S_i cannot be quantified as absolute value. Therefore variation of mineral reactive surface area can be quantified in term of ratio between the different minerals involved in CO_2-water-rock interaction. The variation of reactive surface area can be evaluated using the term *M* defining as:

$$M = \left(\frac{(dt/d\varphi)S(MineralX)}{(dt/d\varphi)S(MineralY)} \right)$$

(8)

Where S is the reactive surface area of mineral X, in the rock. Therefore (dt/dφ) function can be simplified, and the ratio between mineral X and Y can be determined.

4.2 <u>In situ mineral-dissolution rate calculation</u>

The main source of sodium, potassium and magnesium can be attributed to albite, K-feldspar and biotite respectively, while calcium comes from calcite dissolution (Helgeson, Garrels and MacKenzie, 1969). Although calcite is a minor granite mineral, calcite's ubiquity and rapid dissolution rate justify this hypothesis (White et al. 1999). Therefore, individual *in-situ* mineral dissolution rates can be calculated by:

$$\frac{d(Ca^{2+})}{d\varphi} = R_{Calcite}$$

(9-1)

$$\frac{d(K^{+})}{d\varphi} = R_{KFeld}$$

(9-2)

$$\frac{d(Na^{+})}{d\varphi} = R_{Albite}$$

(9-3)

$$\frac{d(Mg^{2+})}{d\varphi} = 3R_{Biotite}$$

(9-4)

In-situ rate R were calculated thanks to the partial derivative of molar concentration of each cations as a function of the perturbation progress φ. Polynomial curve fitting by last square criterion was used to calculate polynomial expressions relating molar concentrations of cations to the overall perturbation process φ(see Fig.3). Therefore, partial derivative of each individual polynomial expression was used to calculate rate of reaction R.
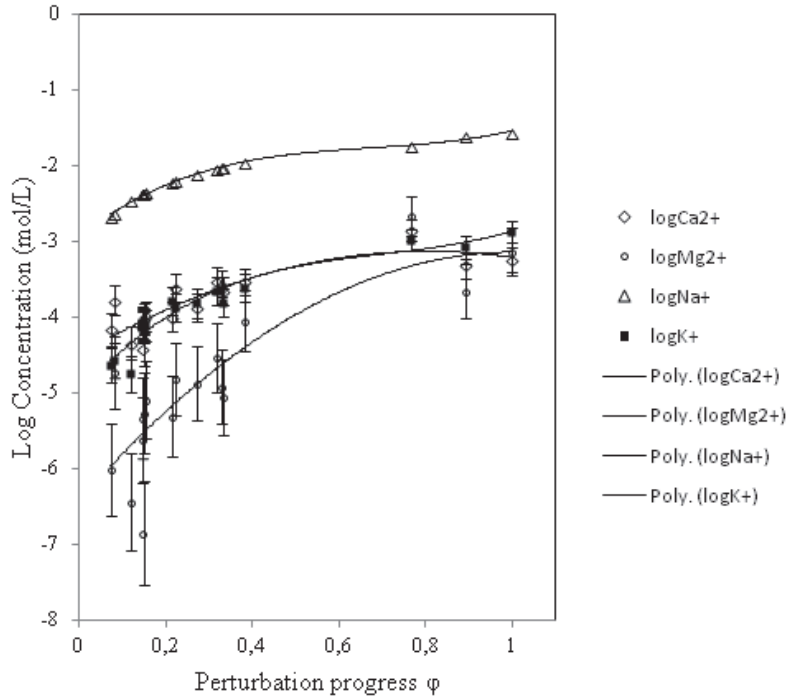
Fig.3: Molar concentrations of cations versus perturbation progress φ. Curves represent polynomial feet of molar concentration as function of perturbation progress φ

Chemical reactions controlling chemical fluids compositions of Galician geothermal field and used for our calculation are listed in Table 2.

$CaCO_3 + H^+ \leftrightarrow Ca^{2+} + HCO_3^-$	(1)
$NaAlSi_3O_8 + 8 H_2O \leftrightarrow Na^+ + Al(OH)_4^- + 3 H_4SiO_4$	(2)
$KAlSi_3O_8 + 8 H_2O \leftrightarrow K^+ + Al(OH)_4^- + 3 H_4SiO_4$	(3)
$K(Mg)_3(AlSi_3O_{10})(OH)_2 + 10H^+ \leftrightarrow K^+ + 3Mg^{2+} + Al^{3+} + 3SiO_{2(aq)} + 6H_2O$	(4)
$SiO2 \leftrightarrow SiO_{2(aq)}$	(5)
$Al_2Si_2O_5(OH)_4 + 6H^+ \leftrightarrow 6H^+ + 6\ SiO_{2(aq)} + 4H_2O$	(6)
$CaAl_2Si_2O_8 + 8H^+ \leftrightarrow Ca^{++} + 2Al^{3+} + 2SiO_{2\ (aq)} + 4H_2O$	(7)
$KAl_3Si_3O_{10}(OH)_2 + 10H^+ \leftrightarrow K^+ + 3Al^{3+} + 3SiO_{2(aq)} + 6H_2O$	(8)
$HCO_3^- \leftrightarrow H^+ + CO_3^{2-}$	(9)
$H_2CO_3 \leftrightarrow H^+ + HCO_3^-$	(10)
$H_2O \leftrightarrow H^+ + OH^-$	(11)
$H_2O + CO_2\ (g) \leftrightarrow H_2CO_3$	(12)

Table2: List of chemical reaction controlling the chemical composition of the geothermal field of Galicia

4.3 Reaction kinetics

The kinetic behavior of mineral phases has often been described in terms of forward (dissolution) affinity of reaction (Aagard and Helgeson, 1982):

36

$$\overline{R} = k\left[1 - \pmb{exp}\left(\frac{A}{RT}\right)\right] \tag{10}$$

Where k is the dissolution rate constant, and A is the thermodynamic affinity of the reaction equal to:

$$A = -RT\ln\left(\frac{Q}{K}\right) \tag{11}$$

Where Q is the ion activity product and K is the mineral solubility constant.

Based on available experimental data, the dissolution rate constant k of most silicates is conveniently expressed as a semilogarithmic function of the system pH (Helgeson 1984, Alekseyev 1997. Marini et al. 2000):

$$\log k = \log k_0 + b_i (pH-pH_0) \tag{12}$$

where $\log k_0$ is the value of logk at pH = pH_0 and b_i is the slope of the linear function in the logk vs pH plot (values of log k_0, b_i and pH_0 adopted in this study are listed in Table 3 and 4). The rate constants for calcite dissolution, estimated by Plummer et al. 1978; Busenberg and Plummer, 1982 and Chou et al. 1989, are reported in Table 4 and Table 5. We found that the rate of albite, K-feldspar, biotite and calcite dissolution does not change significantly over the advancement of the reaction (see Fig. 3) shows that the calcite dissolution rate is 6 orders of magnitude higher than the rate of silicate dissolution in agreement with the known rapid dissolution rate of carbonate compared to silicate minerals (White et al 1993, 1998, 2000; Marini et al 2000; Brantley et al 1992; Zhu et al 2005; Busenberg and Plummer 1986; Arvidson 2004).

Table 3: Values adopted for the parameter log $k^0_{+, i}$, b_i and pH_0 used in the kinetic rate law, where log $k^0_{+, i}$ is in mol·m^{-2}·sec^{-1}.

Phase	Component	log $k^0_{+,i}$	b_i	pH_0	Ref
Albite	$NaAlSi_3O_8$	-16.75	0.3	6.00	a
K-feldspar	$KAlSi_3O_8$	-17.00	0.3	6.00	a
Biotite[1]	$K(Mg,Fe)_3(AlSi_3O_{10})(OH)_2$	-17.00	0.25	6.00	b

(a)Marini et al (2000)
(b)Nagy et al (1995)
[1]Values were defined for muscovite, but the biotite pH as dependence is similar considered to that observed for muscovite.

Table 4: Values adopted for the rate constant needed to calculate the absolute rate of dissolution of Calcite (in mol·m^{-2}·sec^{-1})

Phase	Component	k_1	k_2	k_3	k_4	Ref
Calcite	$CaCO_3$	8.9×10^{-5}	5.0×10^{-8}	6.5×10^{-11}	1.9×10^{-2}	a

[a] Chou et al. (1989).

Reaction rate of calcite is calculated by: $\overline{R}_{CaCO3} = k_1[H^+] + k_2[H_2CO_3] + k_3[H_2O] - k_4[Ca^{2+}][CO_3^{2-}]$
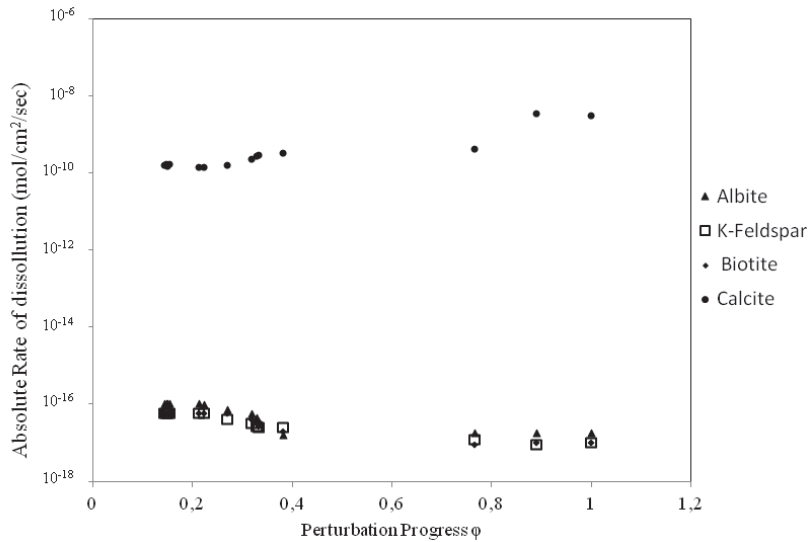
Fig.4: Absolute rate of dissolution in mole/m^2/sec calculated for Albite, K-Feldspar, Biotite and Calcite plotted vs. the perturbation progress φ

5. Results

Calculated in situ rate of dissolution R, absolute rate of dissolution $\overline{R}$, and (dt/dφ)S values are listed in table 5. We estimated the reactivity of minerals by the ratio of RSA. As previously mentioned, RSA cannot be considered as absolute value since the function (dt/dφ) cannot be determined properly. However ratio can be calculated and used to quantify variations between reactive surface area of minerals. The ratio of minerals has been normalized to the most abundant mineral Albite (35% of the modal rock composition) (see Fig 5). The ratio RSA(K-Feldspar)/RSA(Albite) shows variation between 0.032 to 0.164, which corresponds to a variation by less than one order of magnitude. The ratio RSA(Biotite)/RSA(Albite) shows variation by 4 orders of magnitudes, from $3 \cdot 10^{-4}$ to 2,03. Ratio RSA(Calcite)/RSA(Albite) shows values about 10 order of magnitude lower than ratio calculated for alumino-silicate minerals, ranging from $3,5 \cdot 10^{-10}$ to $8,9 \cdot 10^{-9}$. The lower ratio for calcite RSA comparing to alumino-silicate minerals may be related to the fact that fluids are occasionally close to equilibrium with respect to calcite and only a minimal amount of calcite can therefore be dissolved. Only an increase in pCO2 effectively generates a decrease in the calcite saturation index. However, it is important to note that calcite can be considered as a disseminated mineral controlling the Ca^{2+} activity and that plagioclase dissolution may contribute to calcium flux (White et 1999). Our calcite

RSA values may therefore be subject to a greater margin of uncertainty than our findings for other silicate minerals.

For both alumino silicate ratio, i.e. RSA(K-Feldspar)/RSA(Albite) and RSA(Biotite)/RSA(Albite), maximum values is observed for maximum perturbation advancement φ values 0.7 and 1 respectively. Ratio of RSA estimated for K-feldspar and Albite shows a similar trend, with a no significant variation over the entire CO_2-water-rock process. Feldspar dissolution mechanisms are strongly dependent on mineral composition, the chemistry of interacting fluids (Chardon et al 2006). Our results suggest that K-Feldspar and Albite have a comparable behavior in response to CO_2 perturbation and involved variation of fluids chemical composition.

Our results show a higher variation in biotite RSA throughout the entire CO_2-water-rock interaction process comparing to Albite. The determining role played by biotite in the global granite hydrothermal alteration process was earlier proposed by Edmunds et al (1985) in their study of the Cornwell Carnemellis granite. Malmström (1997), on the other hand, posited that biotite dissolution may be inhibited by neogenic iron oxy-hydroxide surface coatings resulting from the iron redox reactivity. Since our kinetics approach indicated that biotite RSA increased continuously comparing to other minerals, the formation of surface coatings does not significantly influence the amount of available reactive surface at the scale of our study. Biotite appears to be the most reactive granite mineral and therefore the primary mineral controlling CO_2 neutralization in agreement with the lower activation energy of biotite compared to the other silicate minerals (feldspars). Our study shows the significant biotite contribution in the long term and a large scale evolution of crust-water interaction and quantifies previous estimations based on Sr isotopic ratios (Seimbille et al. 1997; Li et al 2007).
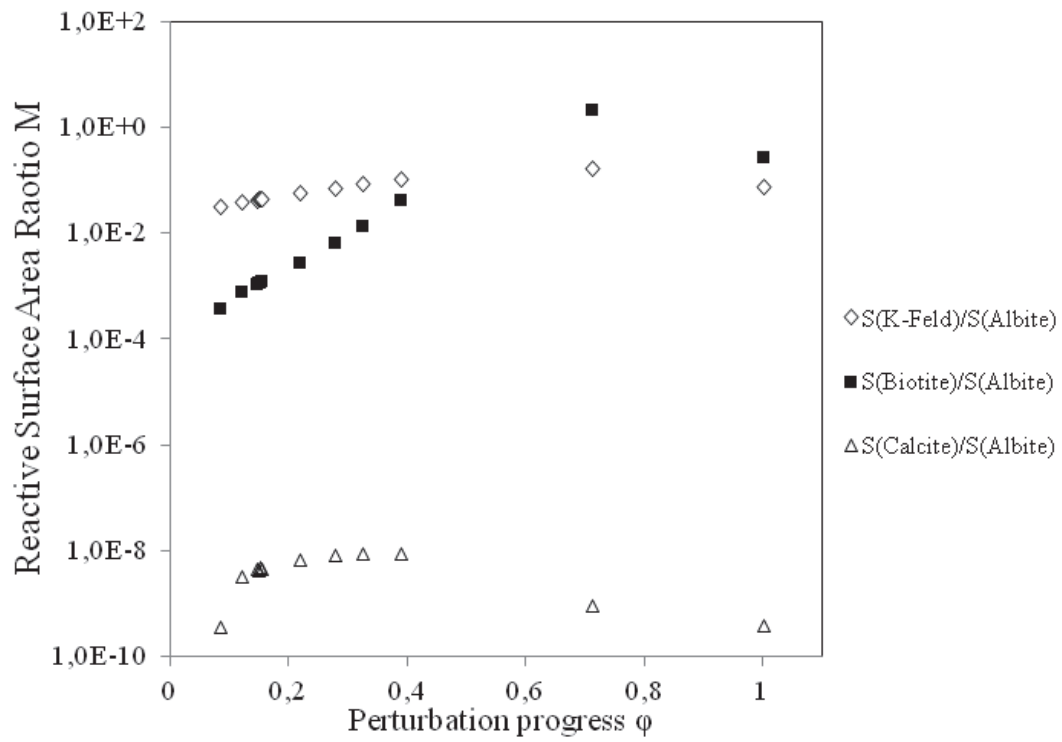
Fig. 5: Mineral reactive surface ratio (dimensionless) S(K-Feld)/S(Albite); S(Biotite)/S(Albite);
S(Calcite)/S(Albite) plotted versus perturbation progress φ

Table 5: *In situ* rate of dissolution R, absolute rate of dissolution $\overline{R}$, for relevant mineral considered involved with the chemical composition of the fluids, computed at various values fractional advancement of the reaction process ζ. Reactive surface , S, area of relevant mineral involved with the fluid chemical composition.

| | Albite | | | K-feldspar | | | Biotite | | | Calcite | | |
| | $\log R$ | $Log\,\overline{R}$ | $(dt/d\varphi)\log S$ | $\log R$ | $\log\,\overline{R}$ | $(dt/d\varphi)\log S$ | $\log R$ | $\log\,\overline{R}$ | $(dt/d\varphi)\log S$ | $Log\,R$ | $\log\,\overline{R}$ | $(dt/d\varphi)\log S$ |
$0<\zeta<1$	mol·time^{-1}	mol·cm^{-2}·sec^{-1}	m²·kg$_w$$^{-1}$	mol·time^{-1}	mol·cm^{-2}·sec^{-1}	m²·kg$_w$$^{-1}$	mol·time^{-1}	mol·cm^{-2}·sec^{-1}	m²·kg$_w$$^{-1}$	mol·time^{-1}	mol·cm^{-2}·sec^{-1}	m²·kg$_w$$^{-1}$
0.0847	-1.714	-15.827	10.111	-3.466	-16.077	8.611	-5.407	-16.077	6.67	-5.08	-9.745	0.665
0.1219	-1.646	-15.914	10.27	-3.324	-16.165	8.841	-5.013	-16.165	7.152	-4.009	-9.796	1.787
0.1465	-1.607	-15.971	10.364	-3.24	-16.225	8.985	-4.83	-16.223	7.393	-3.801	-9.804	2.004
0.1487	-1.606	-15.975	10.371	-3.233	-16.228	8.996	-4.815	-16.228	7.413	-3.785	-9.775	1.989
0.1520	-1.6	-15.983	10.384	-3.223	-16.238	9.017	-4.79	-16.236	7.444	-3.764	-9.812	2.049
0.1546	-1.597	-15.991	10.393	-3.214	-16.241	9.025	-4.775	-16.24	7.467	-3.747	-9.783	2.033
0.2190	-1.533	-16.131	10.597	-3.036	-16.385	9.35	-4.351	-16.385	8.033	-3.426	-9.851	2.425
0.2775	-1.511	-16.247	10.736	-2.914	-16.499	9.583	-3.963	-16.5	8.537	-3.2	-9.842	2.643
0.3255	-1.517	-16.337	10.821	-2.845	-16.587	9.744	-3.635	-16.587	8.953	-3.031	-9.799	2.769
0.3898	-1.553	-16.449	10.895	-2.783	-16.699	9.916	-3.19	-16.708	9.519	-2.821	-9.644	2.822
0.7120	-1.824	-16.796	10.971	-2.86	-17.045	10.185	-1.764	-17.045	11.279	-2.554	-8.469	1.914
1	-1.148	-16.747	11.6	-2.529	-16.996	10.468	-1.971	-16.996	11.025	-2.315	-8.5	2.185

6. Discussion

Results given by our model showed that pCO_2 variation greatly influence reactivity of minerals. We can see that comparative reactivity of minerals can be significantly different. However, the representativeness of calculated ratio S may be limited by the fact that minerals constituting the hydrothermal reservoir are not pure phases but a mixture of various end members. Plagioclases are not pure albite and micas are not pure biotite. The activity term of Eqn. 9 must therefore be corrected to derive a new chemical affinity. Based on existing experimental data on single-mineral dissolution experiments (Brantley et al 2008), we assumed that the parametric constant, log ki of plagioclase and alkali feldspar (Eqn.10) varies linearly with the mineral chemistry. This compositional effect on the mineral reaction kinetics should theoretically produce effects on the term $(dt/d\phi)S$ used to calculate ratio of RSA.

Ratio of RSA are calculated thanks to $dt/d\phi$ term, expressed in terms of the non-dimensional reaction progress ζ and we lack the time $\rightarrow\zeta$ conversion of Eqn (6). This does not affect the bulk evolution of the fluids nor the ratios between different RSA, but only their absolute values.

The result of our calculation suggests that RSA of mineral in response to CO_2 perturbation is not a constant parameter, as usually considered in classical geochemical model. Results showed that a variation of RSA between two minerals can be from 2 to 4 of magnitude in response to the same CO_2 perturbation.

The ratio RSA(Calcite)/RSA(Albite) is extremely low, suggesting that contribution of Calcite is negligible comparing to alumino-silicate contribution, this is in agreement with rock composition considering that local geology is mainly composed by granite, therefore calcite is present as accessory mineral. However dissolved calcium in weathering process of granitoïd rock is considered as largely regulated by disseminated calcite reactivity (White et al 1999).Chemical composition of fluids showed that concentration of Ca is very low comparing to Na. Therefore calcite minerals are present under the form of disseminated trace minerals, which correspond to ratio RSA(Calcite)/RSA(Albite) ranging between 10^{-10} to 10^{-9} in our case. Results suggest that for higher CO_2 perturbation, dissolution of disseminated calcite is negligible comparing to dissolution of albite. Further, we can see that RSA(K-Feldspar)/RSA(Albite) remains quite constant comparing to RSA(Biotite)/RSA(Albite). This suggests that behavior of Albite and K-Feldspar are quite similar over the entire perturbation progress. On the other hand, RSA ratio varies by several of magnitude for Biotite/Albite ratio, resulting suggest that biotite has a different reactivity in response to CO_2 perturbation.

In this model, sampled water have geothermal origin, characterized by long residence time (>1000 years). However, this model consider that dominant process participating to chemical composition are thermodynamic process and that transport process (diffusion, dispersion, advection) have negligible effect on fluid composition. This is the case for fluid having long residence time in reservoir (Maher et

al 2010). Therefore this model appears as adapted for modeling hydrological system containing long fluid residence time, which is potentially the case in geothermal reservoir, or in potential CO_2 geological storage site, but cannot generalized for system with effect of groundwater flow circulation on fluids chemical composition.

7. <u>Conclusion:</u>

Our study shows that when modeling CO_2 perturbation in natural water-rock systems, the current geo-mechanical method is insufficient to account for the evolution of the fluid chemical composition over a long residence time. Our kinetic approach uses the fluid's measured chemical composition to estimate variations of mineral reactivity over the CO_2-water-rock interaction process in the field. To accurately predict the ultimate mineralization capacity of any given natural reservoir and to estimate the presence of extraneous chemical elements entering the fluid composition, it is essential to take a geochemical approach and to evaluate the evolution of the RSA itself. It shows that the parent mineral's RSA is not a constant parameter, contrary to what is generally assumed in current modeling. Our findings indicate that CO_2 perturbation in granite hydrothermal fields is mainly driven by silicate minerals, whereas neo formed-calcite dissolution contributes only negligibly to the global budget. The kinetic approach used in this study offers a reliable geochemical methodology for estimating the evolution of mineral reactivity, taking into account ratio of RSA of different minerals in natural water-rock interaction systems. We believe that our methodology could serve as a useful and reliable tool when evaluating potential geological reservoir sites for CO_2 storage, not only for estimating storage capacity but also in identifying potential geo-chemical risks resulting from the sustained release of toxic metals.

43

References:

Alekseyev V.A., Medvedeva L.S., Prisyagina N.L., Meshalkin S.S., Baladin A.I.,1997. Change in dissolution rates of alkali feldspars as a result of secondary mineral precipitation and approach equilibrium. Geochim. Cosmochim. Acta 61, 1125-1142

Arvidson R.S., Beig. M.S., Lüttge. A., 2004. Single-crystal plagioclase feldspar dissolution rates measured by vertical scanning interferometry. Am. Mineral. 89, 51–56.

Bandstra J.Z.. Brantley S.L., 2008. Surface evolution of dissolving minerals investigated with a kinetic Ising model. Geochim. Cosmochim. Acta 78, 2587-2600

Banwart S.A.. Gustafsson E.. Laaksharju M., 1999. Hydrological and reactive processes during rapid recharge to fracture zones: the Äspo large scale redox esperiment. App. Geoch. 14, 873-892

Berner R.A., Lasaga A.C., Garrels R.M., 1983. The carbonate-silicate geochemical cycles and its effect on the atmospheric carbon dioxide over the past 100 million years. Am. J. Sci. 283, 641-683

Brantley S.L.. Kubicki J. D.. White A. F., 2008. Kinetics of Water-Rock Interaction. Springer 852p.

Burch T.E., Nagy K.L., Lasaga A.C., 1993. Free energy dependence of albite dissolution kinetics at 80°C and pH 8.8, Chem. Geol. 105, 137-162

Busenberg E.. Plummer L.N., 1986.The solubility of $BaCO_3(cr)$ (witherite) in CO_2-H_2O solutions between 0 and 90°C. evaluation of the association constants of $BaHCO_3^+(aq)$ and $BaCO_3^0(aq)$ between 5 and 80°C and a preliminary evaluation of the thermodynamic properties of $Ba^{2+}(aq)$. Geochim. Cosmochim. Acta 50, 2225-2233

Cidu R. Bahaj S.,2000. Geochemistry of thermal waters from Morocco. Geothermics 29, 407-430

Capdevilla R., Corretge Q., Floor P., 1973. Les granitoïdes varisques de la Meseta Ibérique. Bull. Soc. Geol. Fr. 15, 209-22

Chou L. and Wollast R., 1984. Study of the weathering of albite at room temperature and pressure with a fluidized bed reactor. Geochim. Cosmochim. Acta 48, 2205–2217.

Chou L., Garrels R. M., and Wollast R., 1989. Comparative study of the kinetics and mechanisms of dissolution of carbonate minerals. Chem. Geol. 78, 269–282.

Delgado-Outeiriño I., Araujo-Nespereira P., Cid-Fernández J.A., Mejuto J.C., Martínez-Carballo E., Simal-Gándara J., 2009. Behaviour of thermal waters through granite rocks based on residence time and inorganic pattern. Journal of Hydrology 373, 329–336

Dzombak D. A., Morel F. M. M., 1990. Surface Complexation Modeling. Hydrous Ferric Oxide. Wiley-Interscience, NewYork. 393p

Edmunds W.M., Kay R.L.F., McCartney R.A., 1985. Origin of saline groundwaters in the Carnmenellis Granite (Cornwall. England): Natural processes and reaction during Hot Dry Rock reservoir circulation. Chem. Geol. 49, 287-301

Fouillac C. et Michard G., 1981. Sodium/Lithium ratio in water applied to geothermometry of geothermal reservoirs. Geothermics 10, 55-70

Ganor J., Roueff E., Erel Y., Blum J.D., 2005. The dissolution kinetics of a granite and its minerals-implications for comparison between laboratory and field dissolution rates. Geochim. Cosmochim. Acta 70, 3883-3904.

Helgeson H.C., Garrels R.M., Mac Kenzie F.T., 1969. Evaluation of irreversible reactions in geochemical processes involving minerals and aqueous solutions II. Applications. Geochim. Cosmochim. Acta 33, 455-481

Helgeson H. C., Brown T. H., Nigrini A., Jones T. A., 1970. Calculation of mass transfer in geochemical processes involving aqueous solutions. Geochim. Cosmochim. Acta 34, 569–592.

Helgeson H. C., Delany J. M., Nesbitt H. W., Bird D. K.,1978. Summary and critique of the thermodynamic properties of rockforming minerals. Am. J. Sci. 229p

Helgeson H. C., Murphy W. M., Aagaard P.,1984. Thermodynamic and kinetic constraints on reaction rates among minerals and aqueous solutions. II. Rate constants. effective surface area. and the hydrolysis of feldspar. Geochim. Cosmochim. Acta 48,2405–2432.

Holdren Jr. G.R., Berner R.A.,1979. Mechanism of feldspar weathering: I. Experimental studies. Geochim. Cosmochim. Acta 43, 1161–1171.

Keating E.H., Fessenden J., Kanjorski N., Koning D.J., Pawar R., 2010. The impact of CO_2 on shallow groundwater chemistry: observations at a natural analog site and implications for carbon sequestration. Environ. Earth Sci. 60, 521-536

Krumbein W., Monk G., 1942. Permeability as a function of the size of unconsolidated sands. AIME Petrol. Trans. 151, 153-163

Lasaga A. C. and Blum A. E.,1986. Surface chemistry, etch pits and mineral-water reactions, Geochim. Cosmochim. Acta 50, 2363–2379.

Li G., Chen J., Ji J., Liu L., Yang J., Sheng X., 2007. Global cooling forced increase in marine strontium isotopic ratios: Importance of mica weathering and a kinetic approach. Earth Planet. Sci. Lett. 254, 303–312

Lichtner P. C., 1985. Continuum model for simultaneous chemical reaction and mass transport in hydrothermal system. Geochim Cosmochim. Acta 49, 779-800

Lucas Y., 2001. The role of plants in controlling rates and producs of weathering: importance weathering: importance of biological pumping. Ann. Rev. Earth Plan. Sci. 29, 135-163

Maher K., 2010 The dependence of chemical weathering rates on fluid residence time. Earth Plan. Sci. Lett. 294, 101-110

Malmström M., Banwart S., 1997. Biotite dissolution at 25 °C: the pH dependence of dissolution rate and stoichiometry. Geochim. Cosmochim. Acta 61, 2779–2799

Malmström M., Destuni G., Banwart S.A., Strömberg B.H.E, 2000. Resolving the Scale-Dependence of Mineral Weathering Rates . Env. Sci. Tech. 34,. 1375-1378

Marini L., Ottonello G., Canepa M., Cipolli F., 2000. Water–rock interaction in the Bisagno valley (Genoa. Italy): application of an inverse approach to model spring water chemistry. Geochim. Cosmochim. Acta 64, 2617–2635

Marques J. M., Matias M J., Basto M.J., Carreira P.M., Aires-Barros L.A., Goff F. E. 2010, Hydrothermal alteration of Hercynian granites. its significance to the evolution of geothermal systems in granitic rocks. Geothermics 39,152–160

Michard G., Grimaud D., D'Amore F., Fancelli R. 1989. Influence of mobile ion concentrations on the chemical composition of geothermal waters in granitic areas. Example of hot springs from Piemonte (Italy). Geothermics 18, 729-741

Michard G., Beaucaire C., 1993. Les eaux thermals du granite de Galice (Espagne): des eaux Carbogazeuse aux eaux Alcalines. Chem. Geol. 110, 345-360

Morse J. W., Arvidson R. S., 2002. The dissolution kinetics of major sedimentary carbonate minerals. Earth Sci. Rev. 58, 51-84

Nagy K. L., 1995. Dissolution and precipitation kinetics of sheet silicates. Rev. Mineral. 31,173–233.

Navarre-Sitchler A., Brantley S., 2007. Basalt weathering across scales. Earth Planet. Sci. Lett. 261, 321-334

Noiriel C., Luquot L., Madé B., Raimbault L., Gouze P., Van Der Lee J., 2009. Changes in reactive surface area during limestone dissolution: An experimental and modelling study. Chem. Geol. 265, 160-170

Ottonello G., 1997. Principles of Geochemistry. Columbia University Press. New York 894p.

Parkhust D. L., Appelo C.A.J., 1999. User's Guide to Phreeqc (version 2) – A Computer Program for Speciation. Batch-Reaction. One-Dimensional Transport. and Inverse Geochemical Calculations. U.S. Department of the Interior/ U.S. Geological Survey. Denver. Colorado.

Prigogine I., 1968. Introduction to Thermodynamics of Irreversible Processes. 2nd edition. Interscience Publishers. New York.147p

Riebe C.S., Kirchner J.W., Finkel R.C., 2004. Erosional and climatic effects on long-term chemical weathering rates in granitic landscapes spanning diverse climate regimes. Earth Plan. Sci. Lett. 224, 547-562

Sciuto P. F., Ottonello G., 1995a. Water-rock interaction on Zabargad Island (Red Sea) – a case study: I. Application of the concept of local equilibrium. Geochim. Cosmochim. Acta 59, 2187–2206.

Sciuto P. F., Ottonello G. 1995b. Water-rock interaction on Zabargad Island (Red Sea) – a case study: II. From local equilibrium to irreversible exchanges. Geochim. Cosmochim. Acta 59, 2207–2213.

Scislewski A.. Zuddas P., 2010. Estimation of reactive mineral surface area during water–rock interaction using fluid chemical data .Geochim. Cosmochim. Acta 74, 6996–7007

Stallard R.F., 1992. Tectonic Processes, Continental Freeboard, and the Rate-controlling Step for Continental Denudation. Int. Geoph. 50, 93-121

Steefel C. I. and MacQuarrie K. T. B., 1996. Approaches to modeling of reactive transport in porous media. Reviews in Mineralogy. Mineralogical Society of America. Washington D.C. 34. 83–129.

Steefel C.I. DePaolo D.J.. Lichtner P.C, 2005. Reactive transport modeling: An essential tool and a new research approach for the Earth science. Earth Planet. Sci. Lett. 240, 539-558

Stumm W., Morgan J. J., 1996. Aquatic Chemistry. Chemical Equilibrium and Rates in Natural Waters. John Wiley and Sons. New York.1022 p.

Suarez D.L., Woods J.D., 1996. Short- and long-term weathering rates of a feldspar fraction isolated from an arid zone soil. Chem. Geol. 132,143-150

Tarantola A., Valette B., 1982. Generalized non linear problems solved using the least squares criterion. Rev. Geoph. Sp. Phy. 20, 219-232

Velbel M.A.,1993. Constancy of silicate mineral weathering-rate ratios between natural and experimental weathering- implications for hydrologic control of differences in absolutes rates. Chem. Geol. 105, 89-99

White A. F., Peterson M. L.,1990. Role of reactive surface area characterization in geochemical models. Chemical modeling of aqueous systems II. In (eds. D. C. Melchior and R. L. Bassett) Am. Chem. Soc. Symp. Ser. 416,461–475

White A. F., Bullen T.D., Davison A.V., Vivit D.V., Schulz M. S., David D.W., 1999. The role of disseminated calcite in the chemical weathering of granitoid rocks. Geochim. Cosmochim. Acta 63, 1939–1953

White A. F., Brantley S.L, 2003. The effect of time on the weathering of silicate minerals: why do weathering rates differ in the laboratory and field? Chem. Geol. 202, 479– 506

West J.A., Galy A., Bickle M, 2005. Tectonic and climatic controls on silicate weathering Earth Plan. Sci. Lett. 235, 211-228

Wels C., Leslie S., Beckie R., 1997. The influence of surface sorption on dispersion in parallel plate fractures. J. Cont. Hydrol. 28, 95-l 14

Zhu C.,2005. In situ feldspar dissolution rates in an aquifer. Geochim. Cosmochim. Acta 69, 1435–1453.

3. Field experiment of CO_2 injection

A field experiment consisting on injection of CO_2 saturated water in subsurface aquifer was performed. The aim was to evaluate the effect of CO_2 perturbation on an equilibrated water-rock system where time, water-rock ratio and reservoir properties can be estimated. Emphasis was put on the behavior of dissolved trace elements and on mineral reactivity.

3.1. Introduction

The aim of this field experiment was to evaluate the impact of CO_2 perturbation on water-rock equilibrium with special focus on remobilization of dissolved metals species. Previous field experiment have shown that CO_2 injection under supercritical conditions in deep saline aquifer produced important increasing in concentration of metals species (Fe, Mn) in the reservoir water (Kharaka 2006, 2009). Suggested sources of dissolved Fe and Mn were oxy-hydroxides phases. Several other field experiments worked on simulation of CO_2 sink in subsurface aquifer (Zheng et al 2012). For example, shallow CO_2 injection at the MSU-ZERT field test showed rapid and systematic increases in the aqueous concentrations of major and trace elements (Kharaka et al., 2010). Authors conclude that chemical reactions occurring during CO_2 perturbation are a combination of dissolution effect, ions exchange, desorption, pH and redox control and highlighted the need for a comprehensive characterization of the rock-metal associations in the subsurface and the redox conditions to better constrain model results.

Several previous works, based on numerical model simulation highlighted that sinks from deep CO_2 reservoir storage could potentially have significant effect on the fate and transport of heavy metals in sub-surface water (Siirila et al. 2012, Vong 2011). In particular, Wang and Jaffe (2004) showed by numerical approach that the CO_2 injection could provoke significant increase in metals aqueous concentration due to dissolution of solid metal sulfur species such as galena (PbS).

Laboratory experiment performed by Little et al (2010) showed that exposure of natural minerals sampled from aquifer sediments, over a period of several months to CO_2 in batch reactor induced release of major cations species (Ca^{2+} and Mg^{2+}) and metals species by mineral dissolution. The release of major species was involved with major metals releases (Fe and Mn), and trace metals releases (essentially Co, Ba, U), provoked by lowering pH in response to CO_2 dissolution.

Further, hydrothermal sources were studied as natural analog of long term CO_2-water-rock dynamics. In particular Keating et al. (2010) highlighted the potential role of speciation by carbonate as a potential phenomenon for the fate and transport of trace metal element into CO_2 geothermal field. As mentioned by Apps et al (2010) and Zheng et al (2012), response to CO_2 perturbation is strongly dependent on mineral composition of reservoir and groundwater composition. The chemical processes potentially responsible for the mobilization of trace elements are the dissolution of carbonates (Kharaka et al., 2006), sulfides minerals dissolution (Wang and Jaffe, 2004; Zheng et al., 2009; Apps et al., 2010) and iron oxyhydroxide minerals dissolution (e.g., Kharaka et al., 2006, 2009), as well as surface reactions such as adsorption/desorption and ion exchange (Kharaka et al., 2006, 2009; Zheng

49

et al., 2009; Apps et al., 2010). Further, the pH buffer of groundwater induced by mineral dissolution appears as key parameter for potential consequence of metals release induced by CO_2 perturbation in groundwater.

As a part of this purpose, we performed a water CO_2-saturated injection into fractured sandstone bedrock mainly constituted by quartz, carbonate minerals and significant amount of iron oxides and relatively high concentrations of trace metals in rocks (U, As, Zn, Ba, Mo). We followed a push-pull test protocol, with special focus on the effect of CO_2 perturbation on pH, Redox and behavior of dissolved trace metals elements. A borehole was drilled especially for this operation in July 2011, borehole logging, previous packer and hydraulic test were performed in August and October 2011, and final CO_2 injection experiment was performed in December 2011.

3.2. Material and methods:

3.2.1. Experimental site: Geology, lithology

We performed our experiment in Lodève area (Languedoc Roussillon province, southern France). This area is composed by sedimentary bedrock with natural high concentration in metals, (Fe, Mn, U, As, Mo, Ba Cu and Zn). This region was exploited by for uranium by mining operation from 1970 to late 1990's. A large rehabilitation plan is now occurring in this zone. A lot of information was available concerning the local geology, hydrology and hydrogeology thanks to older mine operation. Previous investigations were conducted in this area to find suitable site to conduct this experiment.

The Lodève area is situated on the south-west limit of the Massif Central mountain, around 60 km on the north of Montpellier (French Mediterranean coast). This zone is characterized by a large permian sedimentary basin formation. The permian Lodève basin is composed by sandstone-shale succession of 100-400 m thickness. Permian bedrock is based on cambrian formation, composed by dolomite to shaly dolomite (See geological map on Fig. 3.2.1 and Fig.3.2.5, and geological section Fig.3.2.2). Permian shales and sandstones are characterized by a dark red-brown color (see Fig. 3.2.3) with red pelites and sandstones. Zones of metals mineralization are found mainly in the Autunian series, and are usually associated with faults in secondary mobilization zones.

These natural conditions appear as particularly interesting for studying the fate of numerous metal elements into the environment. A lot of studies concerning the geology, hydrogeology and geothermy are available in the literature (Vuillemenot and Toulhoat 1992, 1994; Beaucaire and Toulhoat 1987; Mathis et al. 1990). For those reasons, and the advantage of site access facilities, this area was chosen for our experiment (see Fig. 3.2.4).

The permian shale and sandstone are characterized as non-aquifer formations, low intrinsic permeability. Fluid circulations are mainly driven by secondary porosity (i.e. fractures) concentrated in fractured zones.
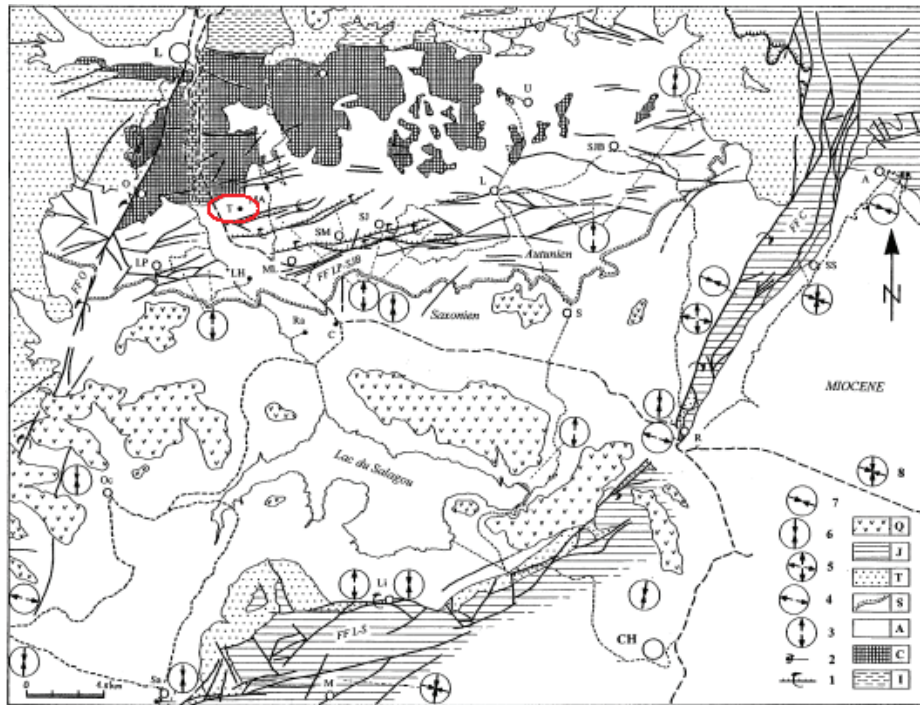
51

Fig. 3.2.1: Geological map of the Lodève Basin: cartographic and tectonic sketch. Experimental site location is highlighted by red mark. (*mod. Sheet Lodève 1/50.000*)

I: Infracambrian; C: Cambrian; A: Autunian; S: Saxonian; T: Triassic; J: Jurassic; Q: Quaternary.

1: Fault (direction, dip, direction of movement); 2: Axis of fold, direction of dumping; 3: Extension N160-20; 4: Extension N70-110; 5: Extensions N160-20 and N 70-110; 6: Compression N160-20; 7: Compression N90-120; 8: Compressions N160-20 and N90-120; FF-LP SJB: Le Puech-St Jean de La Blaquière fault beam; FFO: Olmet fault beam; FFC: Cévennes fault beam; FFL-S: Liausson-Salasc fault beam; L: Lodève; CH: Clermont l'Hérault; LP: Le Puech; ML: Mas Lavayre; SJ: St-Julien; SM: St-Martin; L: Loéras; U: Usclas; SJB: St-Jean de la Blaquière; S: Salelles; O: Olmet; Oc: Octon; Li: Liausson; Sa: Salasc; M: Mourèze; R: Rabieux; SS: St Saturnin; A: Arboras; MA: Mas d'Alary; T: Tréviels; LH: Les Hémies; Ra: Rabejac; C: Cartels.
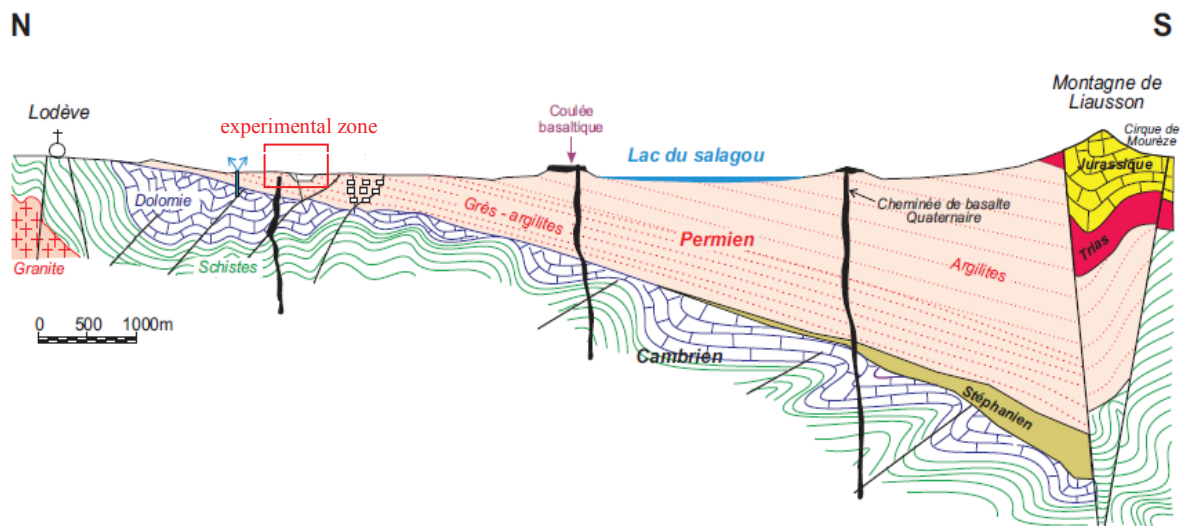

Fig. 3.2.2: Geological section of Lodève Basin. Geological formation exploited for uranium are in permian "Grès-argilite" formation (i.e. sandstone-shale). Permian formation is superposed on cambrien dolomite formation. Blue arrows indicate geothermal springs. Mine activities were performed by open pit exploitation and

underground galleries. The experimental site location is highlighted in red. (Sources: *Carte géologique BRGM de Lodève/Lodève geologic map*).

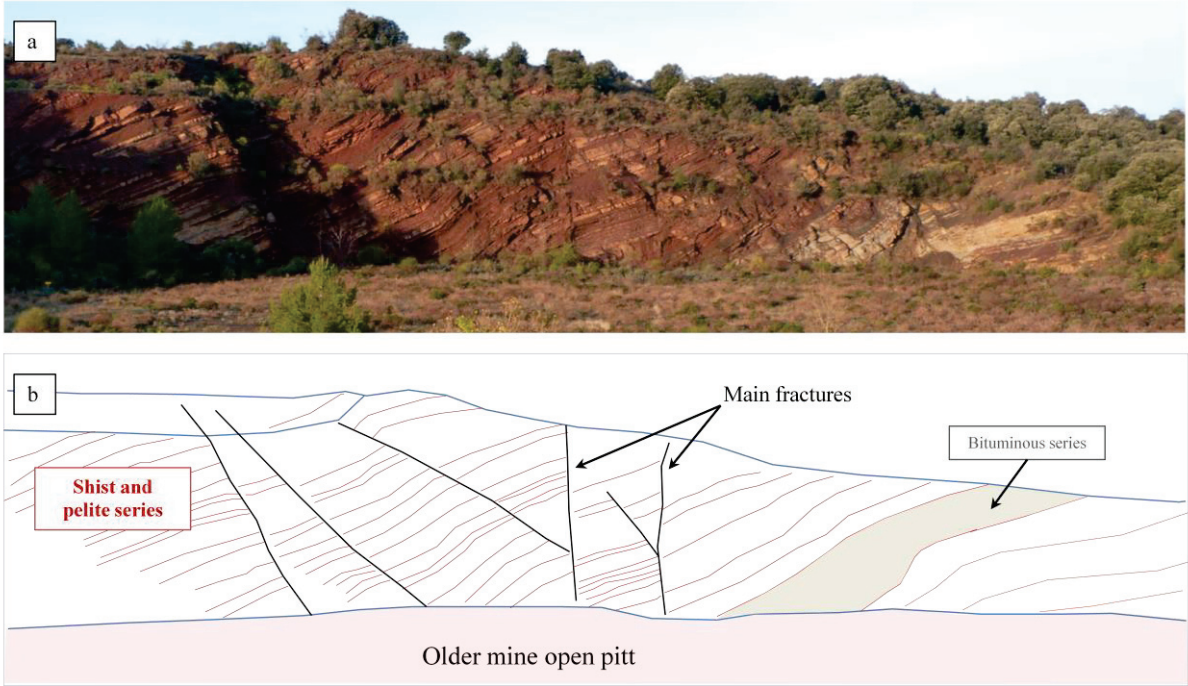Fig. 3.2.3: Picture of typical permian shale and sandstone formation (Autunian stage) (a), characterized by dark red color strata and dark red color due to the high concentration in iron oxides. Schematic representation in Fig.(b) highlights main fractures. Bituminous rich metal formations, on the left part of picture (a), are characterized by grey coloration.

Fig. 3.2.4: General photography of the experimental site

3.2.2. Borehole logging

A 116 m depth borehole was drilled specifically for this experiment in July 2011. Information concerning groundwater circulation and lithology were collected during drilling operations.

Drilling was performed by hammer drill technique. Rocks cuttings were directly sampled at the wellhead every meters. A qualitative description of cuttings was made to design a simplified geological log (see Fig 3.2.5). The borehole was equipped by cemented PVC pipe from 0 to 20 m depth in order to limit contamination of underground aquifer by surface and subsurface water.

Well camera logging allowed to identify fractured zone, and ore deposits, essentially composed by iron oxides (Ferrihydrite $FeOH_3$) and carbonates minerals (siderite, dolomite and calcite).
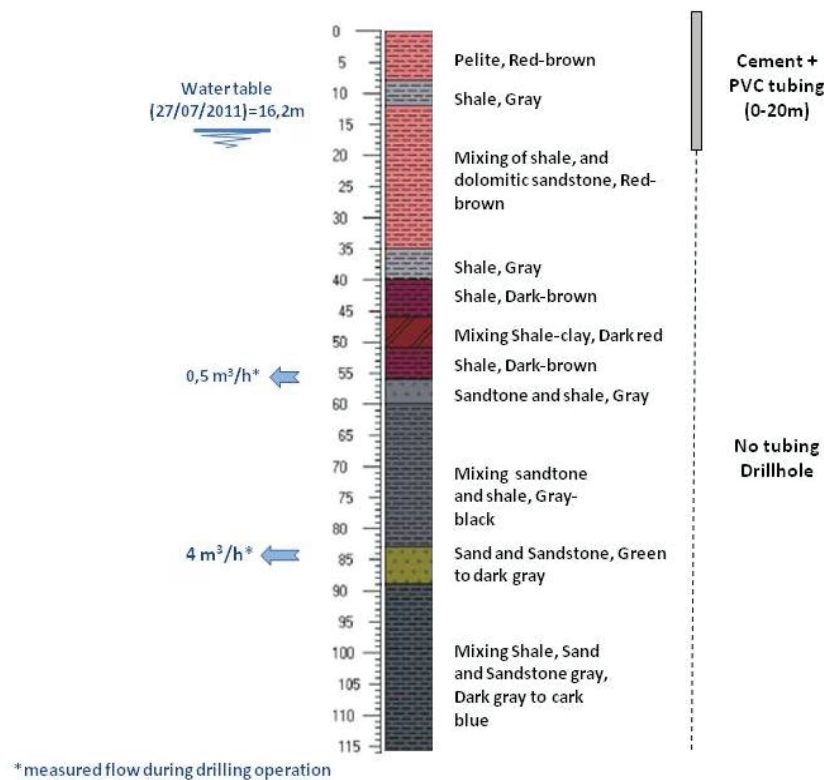
Fig. 3.2.5: Borehole geological log, describing from cuttings analyses and technical section. Water circulations observed during drilling operation are also mentioned.

During the drilling operations, two main water venues were identified at 56 m depth with measured flow of 0.5 m^3/h and 89 m depth with a measured flow of 4 m^3/h. Water table was measured 24 h after drilling operation at 16,2 m depth. Cuttings description analyses showed alternation between shale and sandstone rocks. Water circulations were mainly situated in fractured sandstone zones.

3.2.3. Hydraulic test and aquifer characteristics

A set of hydraulic tests and well geophysical logging were made to evaluate hydraulic properties of the sub-surface aquifer of the experimental site.

Flowmeter logging:

Flowmeter logging was performed to identify potential vertical movement of fluid and groundwater stratification.. Flowmeter logging was performed under pumping conditions, at constant pumping rate of 3.5 m^3/h. Results identified two transmissive fractured zones (see Fig. 3.2.8):

- a first zone between 42 m to 85 m with an average measured flow of 1.5 to 2 m^3/h
- a second zone from 85 m to 110 m, with an average measured flow of 3 to 3.5 m^3/h

Conductivity logging:

Conductivity logging data showed 3 different conductivity zones:

- a first zone with conductivity ranging from 1000 μS/cm to 2000 μS/cm from 16 m to 45 m depth,
- a second zone with homogeneous conductivity around 2300 μS/cm from 45 m to 88 m depth,
- a third zone characterized by a regular decrease from 2300 μS/cm to 2000 μS/cm from 88 m to 116m.

Temperature logging

Temperature logging identified 2 main zones:

- a first zone with a weak increase from 14°C to 15.5°C, corresponding to a temperature gradient of +0.02°C/m, from 15m to 89 m depth,
- a second zone with higher temperature increase from 15.5°C to 17°C, corresponding to a temperature gradient of +0.06°C/m from 90 m to 116 m depth.

Camera logging

Camera logging was made essentially to identify fractured zones and main lithology. Observations showed shale and sandstone, with pronounced red color. In correlation with previous results, two fractured zones with vertical faults opened by several millimeter space at 56,5m depth and between 86m and 91m depth were identified (see Fig 3.2.7). These results were correlated with water inflow observed at 56 m and 90 m depth observed during drilling operations, measured flows by flowmeter logging (Fig.3.2.7).
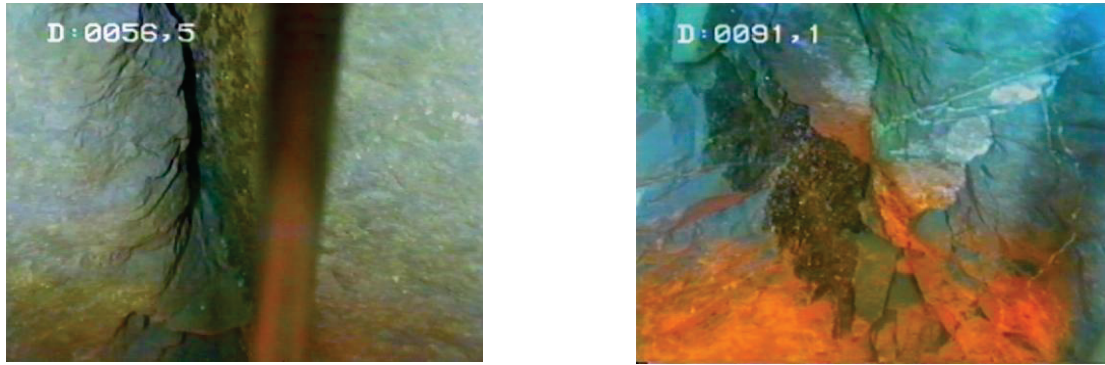
Fig. 3.2.7: photography of fractured zones identified by well camera logging, at 56,5m depth; and 91,1m depth.
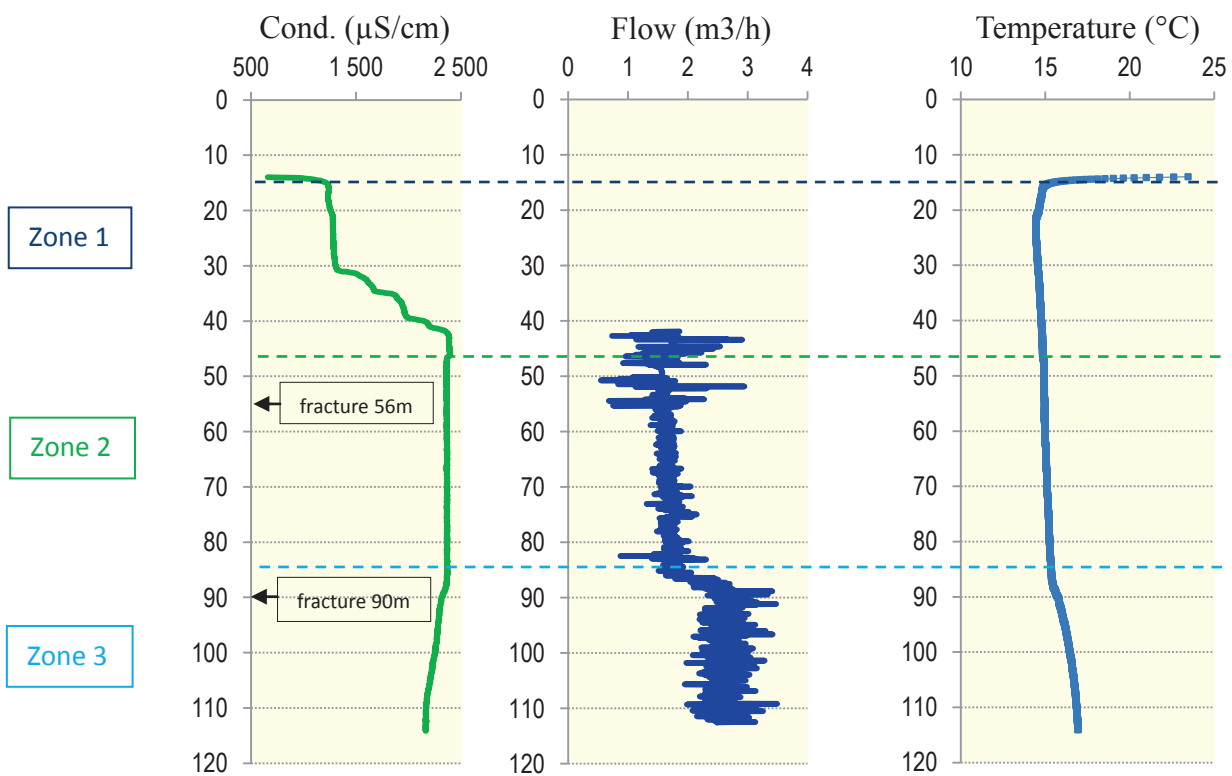
Fig. 3.2.8: Conductivity (µS/cm), temperature (°C) and flowmeter (m³/h) logging results, plotted as function of depth (m). Identified Zone 1, Zone 2 and Zone 3 and 56 m and 89-91m fractured zones are also reported.

Well logging results showed 3 main groundwaters units (Fig. 3.2.8):

- Zone 1, at 15-45 m depth characterized by low temperature and conductivity,
- Zone 2, at 45-90 m depth characterized by higher homogenous conductivity, low vertical flow, moderate temperature gradient, and fractured zone at 56m,
- Zone 3, at 90-115m depth with decrease in conductivity, a positive temperature and flow gradient, both correlated with fractured zone at 90 m depth.

Packers tests

Double packers system was tested to isolate fractured zones. (Fig. 3.2.11 and 3.2.12). Two packers tests (i.e. Packer test 1 and Packer test 2) were performed to isolate 89m depth and 56m depth fractured zones respectively (Fig. 3.2.9). During Packer test 1, hydraulic charge measured in the well increased by 8 meters (from -16,4m depth to -8,4m depth) comparing to initial conditions. During Packer test 2, hydraulic charge measured in the well increased by 11,4m (from -16,4m depth to -5m depth). These results suggested that hydraulic charge in Zone 1 and Zone 2 (Fracture 2) were superior to Zone 3 (Fracture 3). The groundwater inflow in Zone 1 was caused by a fractured zone situated at 30m depth. These results suggested two vertical groundwater movements between Zone 1, Zone 2 and Zone 3, caused by a differential hydraulic gradient (Fig. 3.2.9).

.
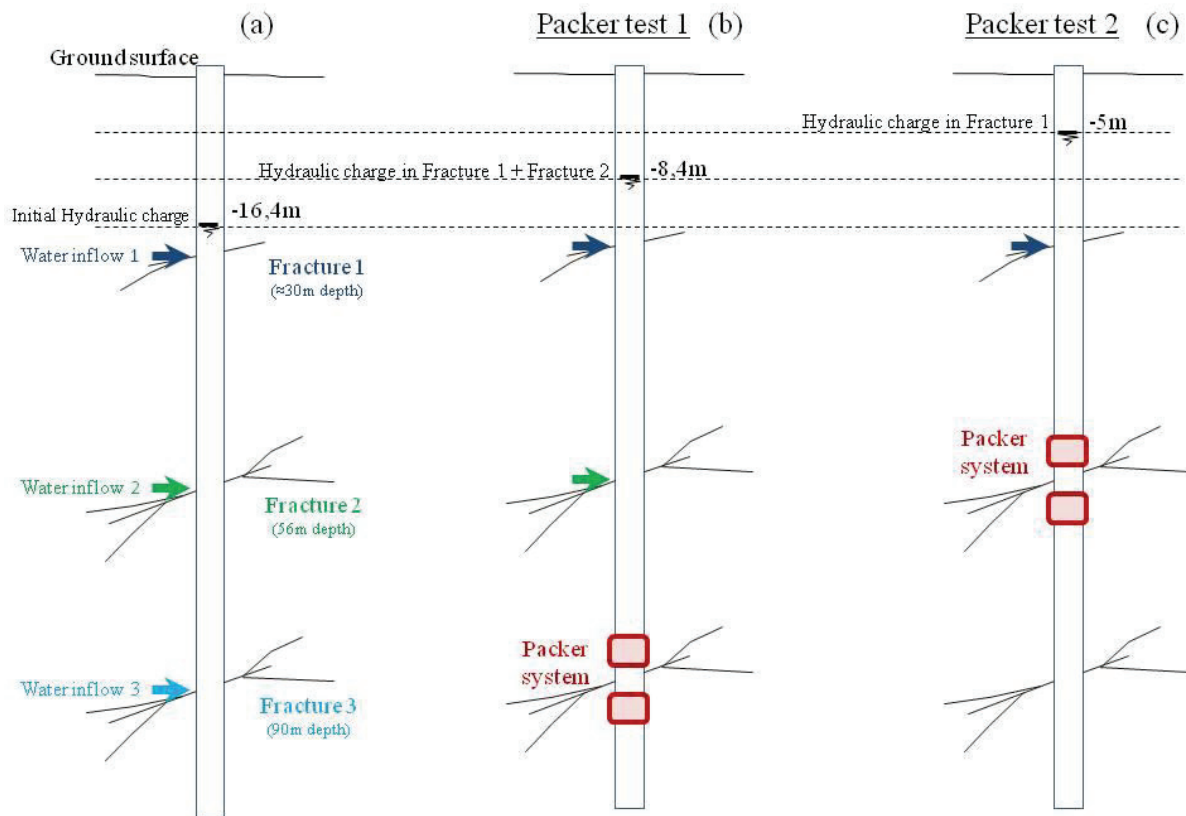
Fig.3.2.9: Schematic diagram representing different water tables, measured at 16.4 m depth before packers test (a), at 8.4 m depth during packers test in Fracture 3 (b), and at 5 m depth during packers test in Fracture 2 (c).

Measured debit during in Fracture 2 and Fracture 3 was 0.5 m^3/h and 3 m^3/h respectively. These relatively low debits suggested a low pore-water velocity within the surrounded fractured zones. Observations made on hydraulic charges showed a groundwater flow discharge from Fracture 1 to Fracture 2 and 3, and from Fracture 2 to Fracture 3

57

at initial condition, as illustrated in Fig. 3.2.10..
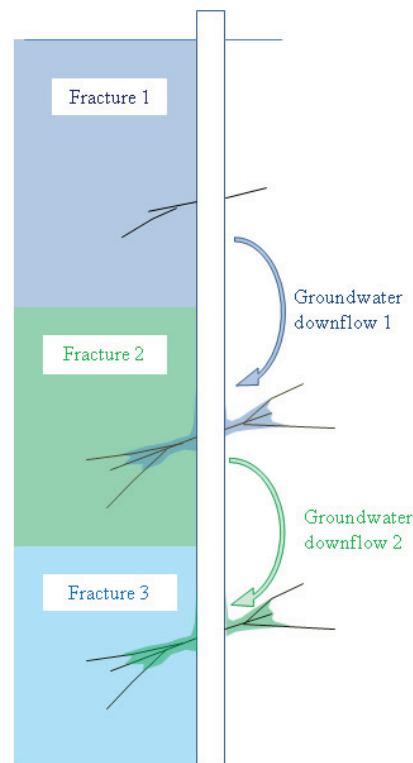
Fig.3.2.10: Schematic representation of groundwater down gradient occurring into the experimental borehole. Due to the differential in-situ hydraulic pressure between Fracture1, Fracture2 and Fracture3, an internal groundwater flow is occurring from upper fracture to lower fracture zones.

During packer test, both groundwater from Fracture 1 and Fracture 2 were sampled. Groundwater from Fracture 2 were sampled by pumping within packer system, and groundwater from Fracture 1 was collected by manual sampler at 30 m depth. Both groundwaters showed similar pH=7.3, alkalinity $(6 \cdot 10^{-3}$ mol/L) and $Fe^{(II)}$ concentration ($\approx 1.3 \ 10^{-5}$ mol/L), but a different signature in SO_4 and Cl^-. This last point will be discussed in part 3.3.2.

3.2.4. Push-pull test

Push-pull test protocol is a useful method to obtain a wide range of aquifer physical, chemical and microbiological properties (Istok et al. 1997, 2001; Haggerty et al. 1998). The push-pull test is an adapted method to single-well experiment.

A push-pull test consists of a pulse type injection of a prepared test solution into a single monitoring well, followed by the extraction test solution/groundwater mixture. The test solution contains a non reactive tracer and one or more reactants. During the extraction phase, tracers, reactants and possible reaction products are monitored continuously to obtain breakthrough curves. Evolution in concentration of non reactant tracer breakthrough curve is used to quantify fluid dynamic processes,

58

such as dispersion, advection, diffusion and mixing, and the amount of recovery of the injected solution at the end of the push-pull test. A comparative approach of both reactant and non-reactant breakthrough curves can be used to estimate the reaction rate affecting concentration of reactive tracer (MacGuire 2002, Lee 2010, Hageman H.J. 2003, Knecht 2011, Istok 2001). Single well push-pull test is commonly used in both applied and research project, and lot of data have been already published. Further, previous CO_2 injection experiment was performed following the same protocol (Matter 2007). The protocol of our experiment was specifically adapted to our field conditions.

3.2.4.1. Injection zone and in-situ monitoring

A double packer system, was used to isolate Fracture 2 (56 m depth) and Fracture 3 (89m depth). Packer system, pumping system and sampling-line were constituted by stainless steel and inert plastic material, in order to avoid pollution by metal or plastic corrosion. This system was entirely dimensioned and produced specifically for this project. A first experiment without CO_2 was performed using uranine ($C_{20}H_{10}Na_2O_5$) as a fluorescent inert tracer to evaluate the amount of recovery of the injected solution at the end of the push-pull test, and to select the most adapted zone for CO_2 injection experiment. A volume of $3m^3$ of water containing 0.5mg/L of uranine was injected and re-pumped few hours later. Results were more conclusive for Fracture 2 and water-CO_2 injection test was therefore dimensioned for this injection zone.
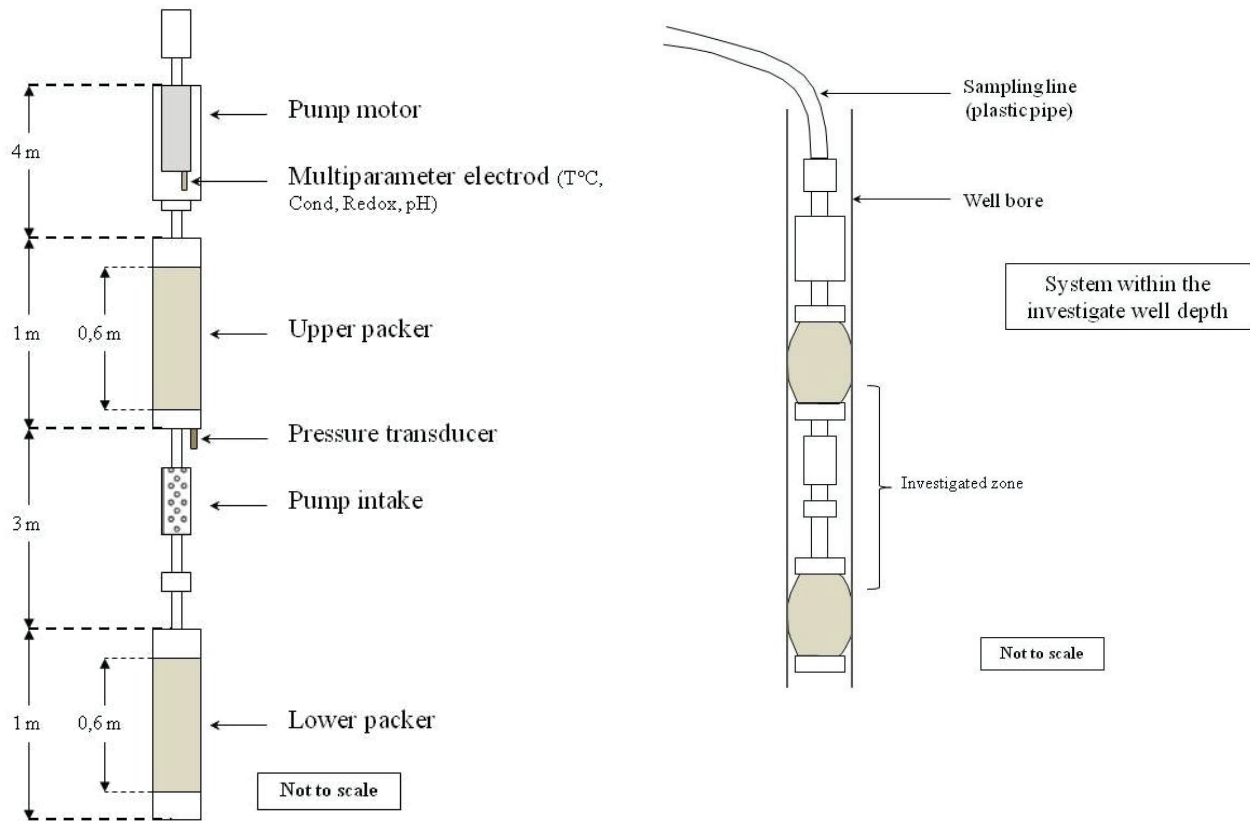
Fig. 3.2.11: Schematic representation of the coupled pumping-packer system used for sampling groundwater into the well.

A multiparameter electrode was installed into the packer system (Fig.3.2.11), in order to monitor pH, temperature, redox, dissolved oxygen, and conductivity at *in situ* conditions. Multiparameter electrode was calibrated at the groundwater temperature. A second multiparameters electrode was installed directly at the well-head, to evaluate the potential difference of physicochemical parameter between *in situ* conditions and surface conditions. Data measured at both in-situ and sub-surface conditions showed no significant differences. Data measured at the wellhead were used for final analyses.

A pressure sensor was installed to measure the pressure level into the injection/extraction line, and into the injection zone. The packer elastomer were filled up with water, at 18 bar pressure. The packer pressure was continuously controlled over the whole experiment, in order to control the potential extraction/intrusion of extern water into the injected zone. Over the whole push-pull test, packer pressure remain constant, meaning that no water extrusion/intrusion happened within the isolated zone.

Fig. 3.2.12: Photography of packer system installation

3.2.4.2. Injection extraction protocol

A volume of $3m^3$ of water was previously pumped from the 56m depth isolated zone. This water volume was temporally stored into plastique water tank at the surface. The water-tank was equipped with porous plastic pipes placed at the bottom, used to bubble a constant flux of CO_2 during approximately 12 hours (see Fig 3.2.13). The pH, temperature and redox was continu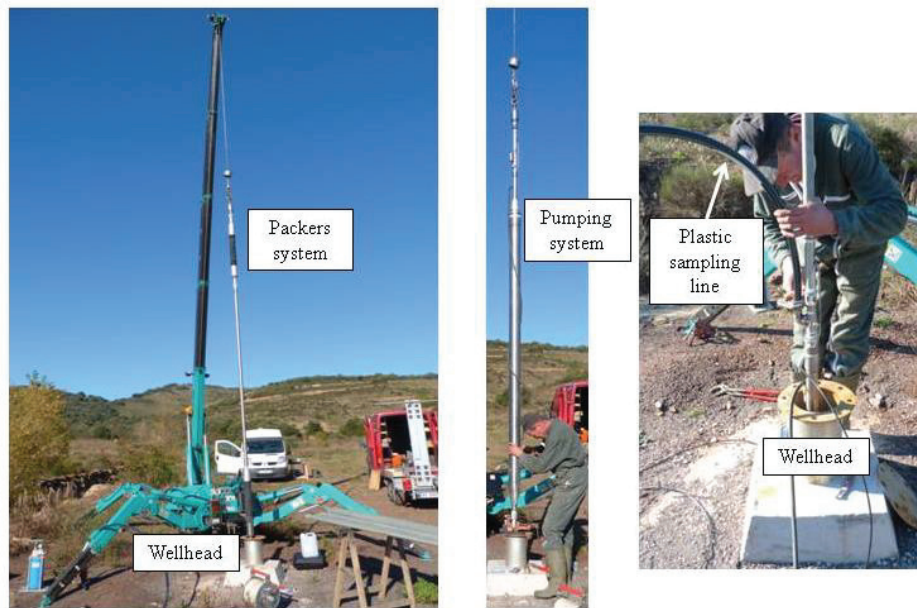ously monitored, during CO_2 dissolution. The CO_2 saturation was reached when pH stabilized around 5.6 while initial pH was 7.3, and pCO_2 was calculated at 1.2 atm. Sampling was made to analyze the ambient groundwater composition previously to injection. Samples were collected at the end of the $3m^3$ pumping phase, before and after CO_2 saturation.

Fig. 3.2.13: water tank used for CO_2 diffusion (left picture), interior of the water tank during the CO_2 diffusion (right picture).

The injection was performed at constant debit of $0.38m^3/h$ during 8 h. CO_2 was bubbling constantly into the water tank during the whole injection phase, to maintain the constancy of CO_2 saturation.

To reduce the risk of degassing, a peristaltic pump was used for injection. The advantage of using such a pump is that the fluid is simply pushed through a flexible tube, reducing fluid turbulence, and fluids are only in contact with the interior flexible tube, reducing the risk of contamination.

A laps time of 80 h was waited between the injection and the extraction phase (See Fig3.2.14). This range of "incubation" time was chosen because previous investigation showed very low velocity for groundwater circulation occurring naturally into the aquifer, (approximate at 0.5 m/day). Therefore the influence of transport on the groundwater reactivity was considered as acceptable for a water residence time of 80h in the aquifer. The natural gorundwater flow occuring within the aquifer was estimated at 0,5 m/day. Another reason was that water table was strongly influenced by rainfall episodes, according to water table monitored continuously within months preceding the injection experiment. As the current weather forecast provided dry period for a week during our experiment, 80 hours of incubation time was well adapted to avoid rain period during the entire experiment.
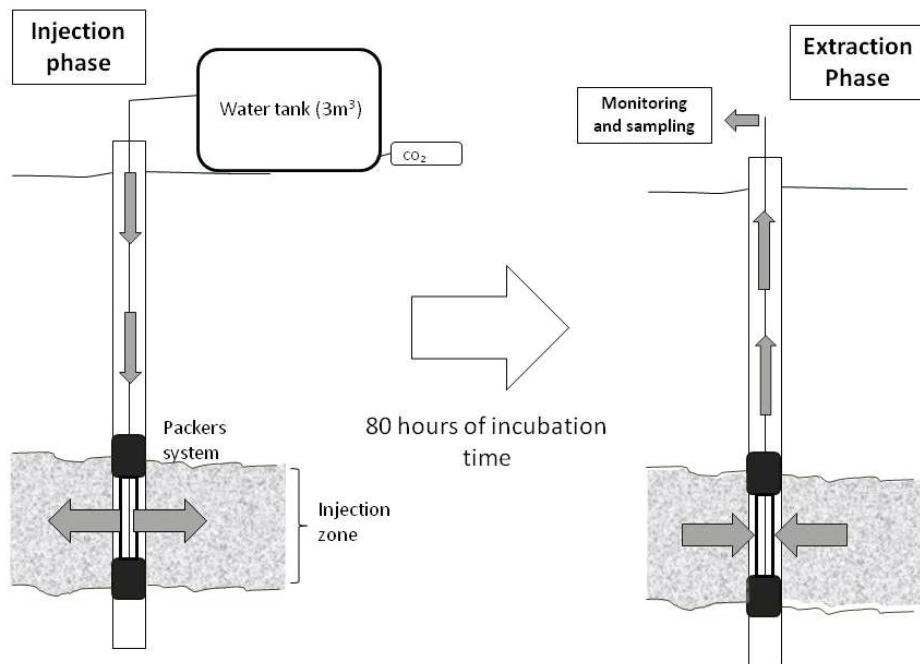
Fig. 3.2.14: schematic representation of the single well push-pull test.

It is important to mention that usual push-pull test protocol imposes to inject an inert tracer with the injected solution to evaluate in-situ rate calculation. However, classical inert tracers are organic molecules such as uranine ($C_{20}H_{10}Na_2O_5$). Despite this molecule has good properties of inert tracer and low sorption capacity, a risk of complexation with dissolved metals could alter chemical analyses for trace metals elements. Another classical inert tracer consists on using salt (NaCl). However addition of NaCl would modify significantly the ionic strenght of the solution, and influencing the water-rock interaction process. The best suitable inert tracer would have been isotopic tracer such as ^{2}H or chemical tracer such as Br^-. But for time, material, and budget issues, we could'nt use such tracers for this experiment. Therefore, we preferred use natural chemicals elements such as Li or Cl as natural tracers.

The pumping phase was performed at a constant debit of 0.38 m^3/h, during 72h. The aim of this pumping phase was to re-pump an equivalent volume ranging between 5 to 8 times the injected volume until recovering the initial condition.

3.2.5. Sampling protocol

Groundwater sampling has to be done properly as unrepresentative samples can lead to misinterpretations of ground-water-quality data. A sampling protocol unsuitable can significantly alter the chemical concentration of the sampled fluid, especially for trace elements analyses. Samples obtained from a poorly constructed well, or using improper sampling equipment, or improperly preserved, can bias the result (Nielson 1991, Yeskis and Zavala 2002).

Concentration measured by chemical analyses are usually elemental concentration, i.e. the total quantity of elements per unit of volume. The main difficulty to manage is that chemical species are not conservative. By variation of temperature, pressure, redox conditions (etc.), species concentrations can be significantly modified between the sampling and the measurement.

Iron can precipitate rapidly under the form of oxides minerals and trap other traces metals (As, Zn, U etc.) (Le Gern et al 2003), by adsorption or precipitation. Therefore, the sampling protocol has to be adapted to avoid oxidation of Iron or other metals, which could distort chemical analyses for traces metals species (Benoit 1994, Taylor and Shiller 1995, Windom et al 1995). Concentration of chemical elements can be also significantly influenced by the presence of colloidal particles (from 1nm to 1μm size), due to adsorption on surface particles. Therefore a filtering system was used on the field to minimize the presence of colloid phase.

Samples used for major cations/anions analyses (Ca^{2+}, Mg^{2+}, K^+, Na^+, NO_3^-, SO_4^{2-}, Cl^-, F^-) were filtered on the field using 0,45μm filter, and stored into a refrigerated box.

Samples for traces metals analyses were collected at the wellhead. A 4 liters bottle previously filled by inert gas N_2 (Fig.3.2.15) was used to collect water.

Fig. 3.2.15: (a) 4 liters bottle filled up by inert gas N_2, (b) sampling was performed directly at the wellhead

After water sampling, the 4 liters bottle was open into a glove box system isolated from the atmosphere, previously filled up with N_2 (Fig.3.2.16). Into the glove box, samples were filtered using 0,2 μm filter. Different series of 14ml samples were taken into polypropylene bottles.

Each samples were acidified by adding few microliters of HNO_3 (norma pur 70%), in order to get a sampled solution of pH 2 to 4. A total of 40 samples series were collected continuously during the experiment.
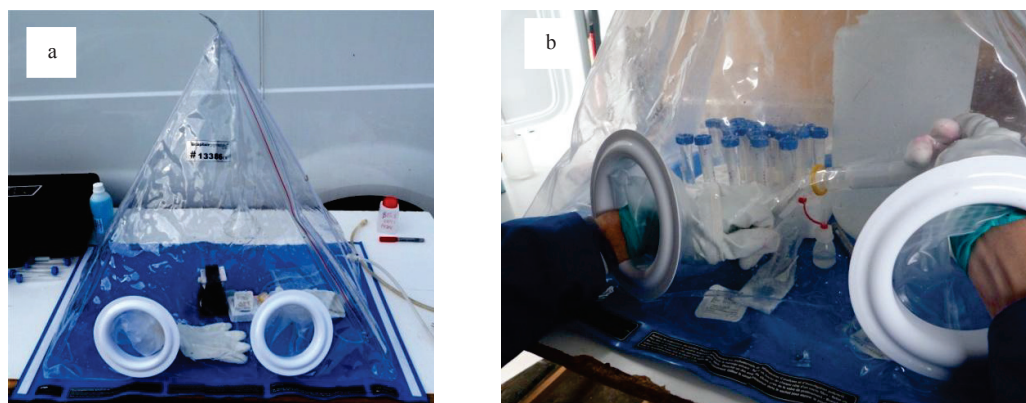
Fig.3.2.16: (a) glove box system (b) filtering with 0,2 μm filter under glove box

Another samples series were filtered using ultrafiltration cell, performed under pressure of N_2 with ultrafiltration cell equipped with 10 kDa filter (Fig.3.2.17). A time of nearby 40min was needed to get a filtered volume of 14ml. Therefore, only a 10 ultra-filtered samples were collected.
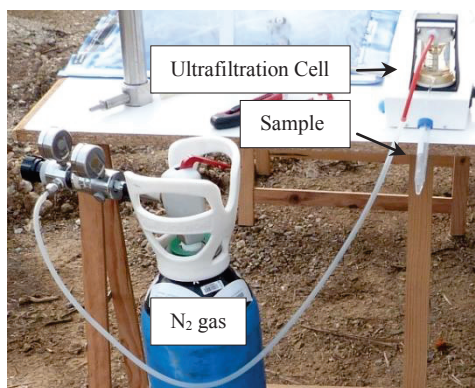
Fig. 3.2.17: Ultrafiltration system

Samples filtered under ultra filtration cell were used for traces metals analyses highly influenced by colloidal phase, such as aluminum.

All of the chemicals elements analyses with their specific sampling protocol are presented in table 3.2.1.

3.2.6. Field Measurement

3.2.6.1.   pH, Redox, alkalinity measurements

The pH measurement is crucial and difficult to realize in natural condition (Ritz and Collins 2008). As a part of CO_2-water-interaction studies, the pH measurement has to be done as precise as possible. Two different pH electrodes were used: **Hanna® HI 9828** and **WTW® pH 340i**

A three point calibration was done using pH 4, 7 and 10 buffer solutions at the beginning of each monitoring set. Electrodes was calibrated by methods using Nernst equation at the groundwater temperature of each pH electrode. All of the electric potential were measured at each calibration point at the groundwater temperature to compare with automatic temperature correction. During the experiment, the extern temperature and groundwater temperature were quite similar (nearlly 16°C), therefore the effect of temperature variation on the pH measurement was minimized. The pH measurement error is estimated at 0,1 pH unit for both pH electrodes.

The multiparameter electrode HI 9828 was used for a continuous monitoring during the pumping phase, and the electrode pH 340i was used for alkalinity titration. Continuous pH measurement was performed under continuous flux using a specific cell, installed directly at the well head (Fig.3.2.18). By this system, physico-chemical parameters pH and Redox were recorded into a system isolated from the atmosphere. The automatic routine recorded a dataset of one measure every 10 minutes during the 72 hours of pumping phase.

Redox measurement was performed with Ag/AgCl electrode (ref: HI 1296D). Redox was measured in ORP (i.e.Oxydo Reduction Potential), in mV. Redox measurement ORP differ from Eh measurement, (measured by Standard Hydrogen Electrode). As Redox measurement for equilibrium calculation is more appropriate in Eh units, empirical correction factor determined from redox buffer standard solution measurement with both SHE and Ag/AgCl electrodes (at fixed temperature) were to dtermien Eh. Correction of ORP to Eh values were made by adding 200 mV to the ORP value.

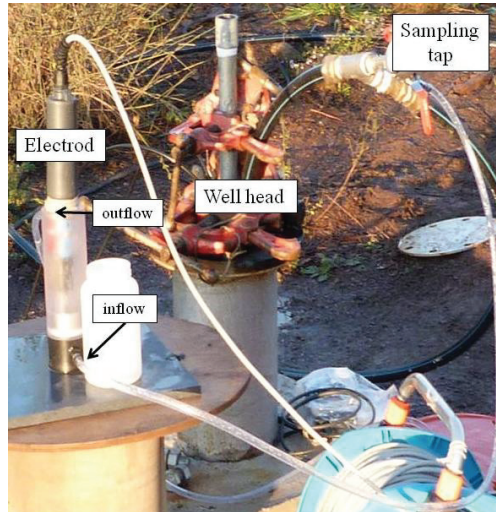Alkalinity was measured on the field by titration with H_2SO_4 and the equivalent point was estimated by the Gran method.

Fig. 3.2.18: continuous pH measurement at the wellhead during pumping phase.

Other physico-chemical parameters (T°C, dissolved Oxygen, conductivity, salinity) were monitored continuously with multi-electrode HI 9828, calibrated using specific solution (Ref.:Quick Calibration **HI 9828-25).**

67

3.2.6.2. Fe^{II} measurements

Dissolved iron can play a significant role in the transfer of other metals elements and on the redox control of the solution (Criaud and Fouillac 1986). Dissolved iron exists under two oxidation states, $Fe^{(II)}$ and $Fe^{(III)}$. The oxidation of $Fe^{(II)}$ by the oxygen of the atmosphere can be significantly fast (Stumm and Lee 1961, Davids and Seed 1983) and $Fe^{(II)}/Fe^{(III)}$ have to be measured as soon as possible after sampling.

The $Fe^{(II)}$ concentration was measured using photometer AQUALYTIC® Multidirect AL450. This test is made by sampling solution into 10ml cell and reacting with specific reagent (ref: IRON(II)LR).
The $Fe^{(II)}$ measurement test is based on a single tablet reagent containing 3-(2-Pyridyl)-5,6-bis (4-phenylsulphonic acid)-1,2,-triazine (PPST) formulated with a decomplexing/reducing agent in an acidic buffer. The test is carried out simply by adding a tablet to the sample of the tested water. The decomplexing/reducing agent breaks down weakly complexed forms of Iron. This ferrous iron, together with any originally present in the sample, reacts with PPST to form a pink coloration.

The intensity of the colour produced is proportional to the Iron concentration and is measured by comparison against Lovibond permanent colour glass standards (ref. Lovibond Iron method 6). It is important to take in mind that the measurement of $Fe^{(II)}$ corresponds to the total iron species with oxidation state II. Therefore, $Fe^{(II)}$ values includes free Fe^{2+} plus potential complexed form such as $FeSO_4{}^0{}_{(aq)}$ or $FeHCO_3{}^+{}_{(aq)}$.

Protocol was tested for both filtered and non-filtered solution, and no differences were showed. Detection limit were 0,1-1,8 mg/L. Measurement values were close to the detection limit before the injection test. After injection test, samples was diluted by 5 to be under the maximum detection limit. Each measurement was made in two different samples for the same sampling series, and good repeatability was observed.
Unfortunately, total $Fe^{(t)}$ could not be measured on the field. Therefore $Fe^{(t)}$ was measured in laboratory. Further $Fe^{(III)}$ could not be measured by this photometer on the field, and $Fe^{(III)}$ was deduced from the difference between $Fe^{(II)}$ and $Fe^{(t)}$.

3.2.7. Laboratory measurement

In Table 3.2.1 presents the analytical technique and sampling protocol for each measured elements. Analyses were performed at the laboratory of Analytical Resources (RESA) at INERIS. Major element concentration was analyzed by ionic chromatography. Cations analyses and anions analyses were done separately in two different set, using Metrohm® chromatograph IC 850 for anion and IC 872 for cation. Sample had to be diluted by 5 to 10 in order to get solution concentrations suited for detection limit (0,5 to 10 mg/L). Dilution factor is included in the accuracy values mentioned in Table3.2.1. The total dissolved organic carbon (DOC) was analyzed by chemical oxidation technique, using Shimadzu® TOC-V$_{CSH}$ machine.

Manganese, iron, lithium, and silicium analyses were performed by Inductively Coupled Plasma Atomic Emission Spectroscopy (ICP-AES), model Jobin Yvon® HORIBA Ultimate 2. Samples for iron analyses was diluted by 10. Another set of analyses was performed specifically for calcium and lithium, in order to compare measured values with ionic chromatography analyses.

Other metals elements (As, Cd, Cr, B, Ba, Cu, Rb, Sr, Zn, Mo, Pb, Al) were analyzed by Inductively coupled plasma mass spectrometry (ICP-MS), model Perkin Elmer® ELAN 6100 DRC, equipped with an ammoniac collision reaction cell.

For major ionic concentrations analyses, accuracy was estimated between 0,5 and 3%.

Analyses	Sampling protocole	Analytical Technique	Accuracy
TOC	0,45 μm filtration	Chemical Oxidation	1%
Ca^{2+}	0,45 μm filtration	Ionic Chromatography	2%
Mg^{2+}	0,45 μm filtration	Ionic Chromatography	2%
Na^+	0,45 μm filtration	Ionic Chromatography	2%
K^+	0,45 μm filtration	Ionic Chromatography	2%
SO_4^{2-}	0,45 μm filtration	Ionic Chromatography	0,5%
Cl^-	0,45 μm filtration	Ionic Chromatography	1%
NO_3^-	0,45 μm filtration	Ionic Chromatography	3%
F^-	0,45 μm filtration	Ionic Chromatography	3%
Fe	0,2 μm filtration with N_2 + Acidification HNO_3	ICP AES	<5%
Mn	0,2 μm filtration with N_2 + Acidification HNO_3	ICP AES	<5%
Si	0,2 μm filtration with N_2 + Acidification HNO_3	ICP AES	<5%
U	0,2 μm filtration with N_2 + Acidification HNO_3	ICP AES	<5%
Li	0,2 μm filtration with N_2 + Acidification HNO_3	ICP AES	<5%
Cd	0,2 μm filtration with N_2 + Acidification HNO_3	ICP MS	<5%
Cr	0,2 μm filtration with N_2 + Acidification HNO_3	ICP MS	<5%
B	0,2 μm filtration with N_2 + Acidification HNO_3	ICP MS	<5%
Ba	0,2 μm filtration with N_2 + Acidification HNO_3	ICP MS	<5%
Cu	0,2 μm filtration with N_2 + Acidification HNO_3	ICP MS	<5%
Rb	0,2 μm filtration with N_2 + Acidification HNO_3	ICP MS	<5%
Sr	0,2 μm filtration with N_2 + Acidification HNO_3	ICP MS	<5%
As	0,01 μm filtration with N_2 + Acidification HNO_3	ICP MS	<5%
Zn	0,01 μm filtration with N_2 + Acidification HNO_3	ICP MS	<5%
Mo	0,01 μm filtration with N_2 + Acidification HNO_3	ICP MS	<5%
Pb	0,01 μm filtration with N_2 + Acidification HNO_3	ICP MS	<5%
Al	0,01 μm filtration with N_2 + Acidification HNO_3	ICP MS	<5%

Table 3.2.1: List of sampling protocol and analytical method for elemental analysis of each chemical element

3.2.8. Calculation Method

Analyses of the effect of CO_2 perturbation on groundwater composition was made by studying the evolution of measured concentrations and physicochemical parameters (temperature, pH, redox) before and after water-CO_2 injection.

In order to identify potential reaction paths induced by CO_2 perturbation, simulation was performed using updated version of geochemical computer code PhreeqC (Parkhust and Appelo 1999) with updated database wateq.4f (Ball and Nordstrom 1991).

3.2.9. Redox Measurement and calculation

The perturbation of pCO_2 and pH itself has no direct influence on the redox condition. However, behavior of minor and trace metals are strongly influenced by redox condition. Numerous chemical reactions occurring into natural groundwater are resulting from coupled pH-redox reactions, because protons and electrons are interdependent in most of chemical reactions.

The Eh value was calculated by the Nernst equation:

$$Eh(volts) = Eh^{\circ} + \frac{2.3RT}{nF} log \frac{[oxidant]}{[reductant]} \qquad (3.3.8)$$

Where Eh° is a standard or reference value at which all substances involved are at unit activity and n is the number of transferred electrons.

3.2.10.   Graphs of Concentration Plot

Signal deconvolution Breakthrough curves were constructed by plotting elements concentrations as a function of the Injected/Pumped volume ratio. This method allows to normalised the evolution of measured concentration as a function of the pumped volume.

3.3.Results

3.3.1. pH-Alkalinity and major elements cocentrations

For most of the breakthrough curves, the maximum concentration was observed during the first hours of pumping, with a rapid decrease to baseline concentration after few hours of pumping. The general trend of breakthrough curves suggest a low extension of the plume injected around the injection borehole. The return to baseline concentrations was observed after a pumped stage corresponding to nearly twice the injected volume. We compared concentration at peak arrival time with baseline contrations to evaluate the enrichment induced by CO_2 water injection on the groundwater chemistry (see table A.1).

During the pumping phase, lower pH values were observed in the early stage of pumping. It is important to note that lower pH values of extracted fluids were equal to pH of injected solution (i.e. pH 5.7). At the begining of the pumping phase, an increasing in alkalinity by a factor of 2 was observed (from $5 \ 10^{-3}$ to $1.11 \ 10^{-2}$ mol/L). Peak of alkalinity is measured within the lower pH values. At the end of pumping phase, alkalinity was similar to baseline concentration.

The CO_2 partial pressure calculated using pH and alkalinity showed $pCO_2=1,2$ atm for lower pH and $pCO_2=1,5 \ 10^{-2}$ atm at the end of the pumping phase (see Fig.3.3.2).

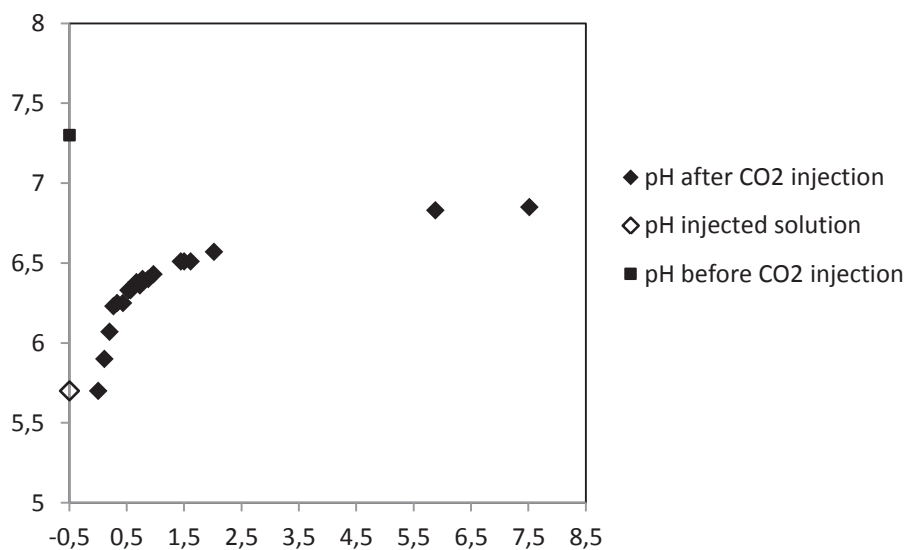Fig. 3.3.1: pH plotted as a function of volume pumped.

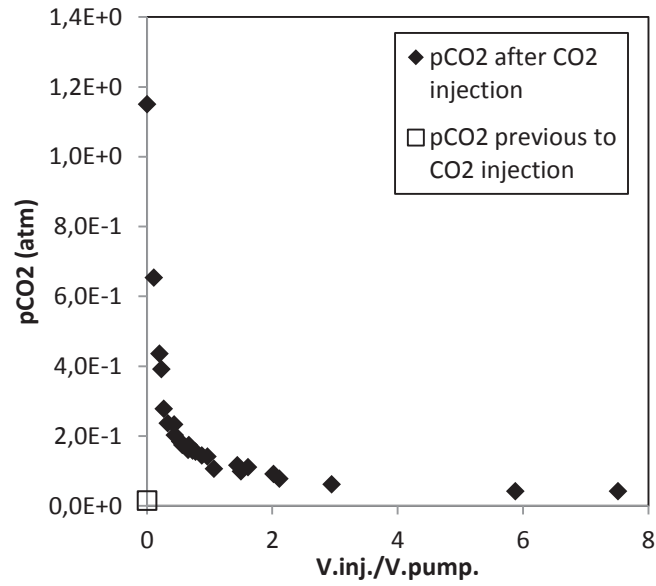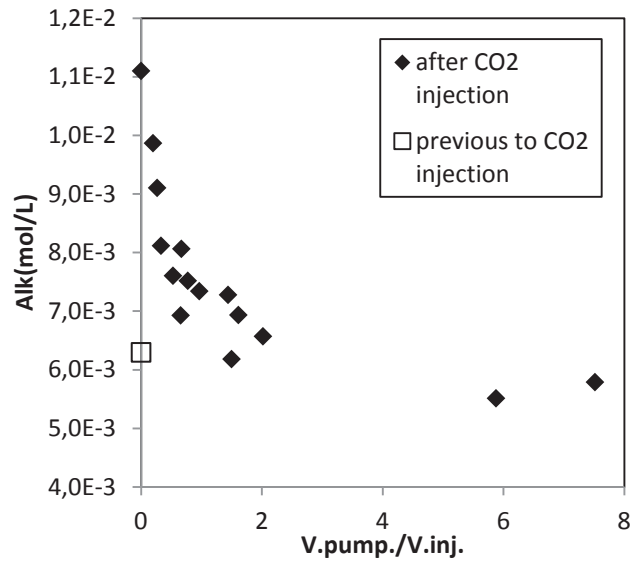Fig.3.3.2: pCO2 plotted as a function of pumped volume

Fig.3.3.3: Akalinity plotted as function of pumped volume

An increase of about 30% was observed for Ca^{2+} (from 1 to 1.4 10^{-3} mol/L) and Mg^{2+} (from 5 to 6.7 10^{-3} mol/L). Similarly to alkalinity Ca2+ ad Mg2+ conentration have the highest value in the early stage of pumping phase Fig. 3.3.4.
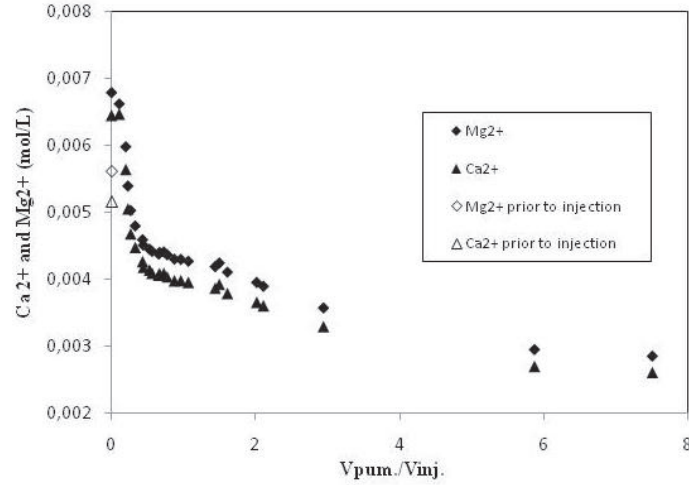
Fig. 3.3.4: Ca^{2+} and Mg^{2+} plotted as function of Vpumped/Vinjected.

Alkalinity measurement was performed directly on the field by acid titration with HNO_3 on samples continuously collected during pumping phase. Analyses of our experiment showed that alkalinity was enriched by a factor 2 between baseline concentration and after perturbation of CO_2 into the aquifer (from $6.2 \ 10^{-3}$ mol/L to $1.11 \cdot 10^{-2}$ mol/L). As showed in Fig.3.3.1 and Fig 3.3.3, electrochemical measurement of pH during the pumping phase showed an inverse correlation with alkalinity. Further the pH values of pumped fluid were similar to pH of injected solution (i.e. pH=5.7). We suggest that during the time interval of 80h between injection and the pumping phase, CO_2 perturbation produced mineral involving production of alkalinity. However, alkalinity production did not induce pH modification, we suggest that production of dissolved basic carbonate species by mineral dissolution was not sufficient to buffer pH perturbation.

Considering the charge balance:

$$2(Ca^{2+})+2(Mg^{2+})+(K^+)+(Na^+) = (Cl^-)+2(SO_4^{2-})+(HCO_3^-)+(F^-)+3(NO_3^-) \qquad (3.3.1)$$

In our case, dominant cations are Ca^{2+}, Mg^{2+}, and Na^+, and dominant anions are HCO_3^- and SO_4^{2-}, therefore neutral balance can be simplified as:

$$2(Ca^{2+})+2(Mg^{2+})+(Na^+) = 2(SO_4^{2-})+(HCO_3^-) \qquad (3.3.2)$$

Further, only Ca^{2+} and Mg^{2+} concentration are affected by CO_2 perturbation. Therefore the production of positive charges by cations (Ca^{2+} and Mg^{2+}) release was compensated by both anions SO_4^{2-} and HCO_3^-. In our pH and concentration range, sulfate was considered as none active species. Thus, we suggest the buffering capacity of the system by production of hydrogenocarbonate is inhibited by the high sulfate concentration.

74

After the CO_2 injection and during the whole pumping phase, Na^+ and K^+ concentrations are not affected by CO_2 perturbation and remained quite constant. In mol per litre concentration, alkalinity and the sum of Ca^{2+} and Mg^{2+} was correlated by:

$$\Delta Alkalinity_{(mol/L)} = \Delta Ca^{2+}_{(mol/L)} + \Delta Mg^{2+}_{(mol/L)} \qquad (3.3.3)$$

This suggests that the alkalinity production is induced by mineral dissolution, such as carbonate minerals dissolution (reaction *(3.3.4)*), a positive correlation was verified between alkalinity and the sum $Ca^{2+} + Mg^{2+}$, see Fig.3.3.5.
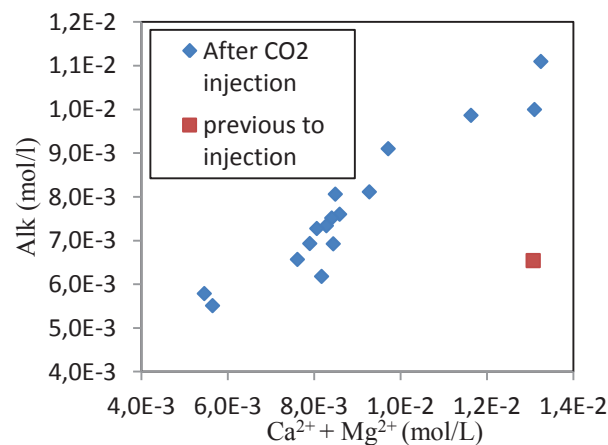
Fig.3.3.5: Plot of alkalinity versus sum of Ca^{2+} and Mg^{2+}, a linear correlation is verified after the CO_2 injection, this correlation is not verified for groundwater composition previous to injection (red point)

Further, a perfect linear correlation is verified between Ca^{2+} and Mg^{2+} concentration (see Fig3.6.6). This correlation was verified in both groundwaters compositions after CO_2 injection. This suggests that Ca^{2+} and Mg^{2+} concentration was imposed by dolomite dissolution stoichiometric reaction. Saturation index calculation indicate $SI_{(Dolomite\ ordered)} = +0,80$ for groundwater compositions before CO_2 injection, and $SI_{(Dolomite\ ordered)} = -1,85$ after CO_2 injection. Groundwater compositions indicated a under-saturation state in dolomite, with slow increase in SI values following the extraction phase (see Fig. 3.3.7).
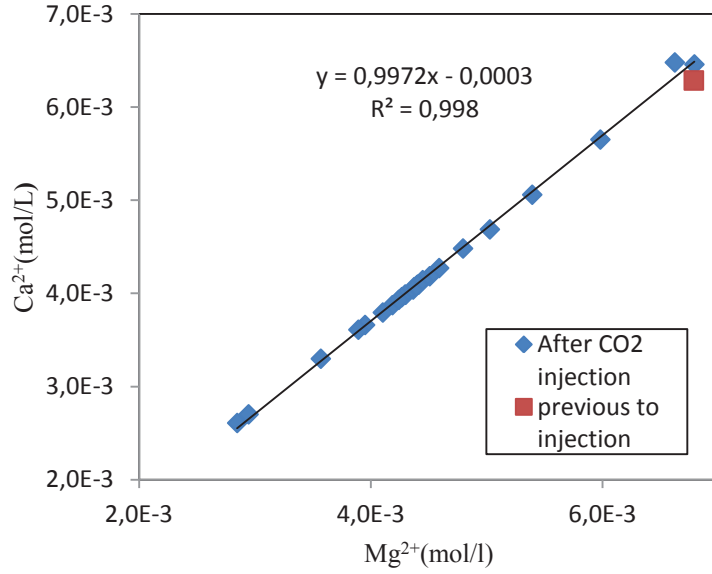
Fig.3.3.6: Plot of [Ca^{2+}] concentration as a function of [Mg^{2+}] in mol/L,
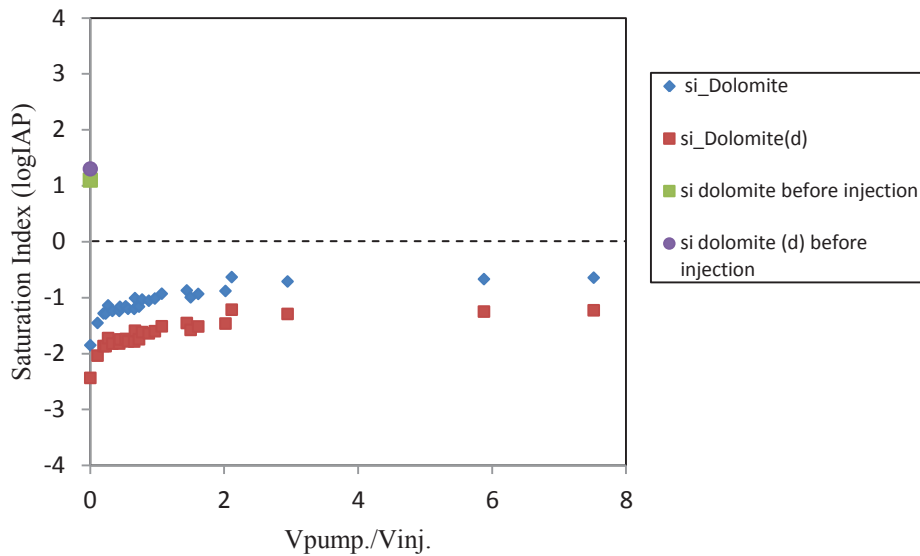
Fig.3.3.7: Saturation Index calculation (log IAP) plotted versus the pumped volume (Vpump./Vinj.)

This suggests that dissolution of mineral (calcite and dolomite) occurred and induced a production of HCO_3^- species. Therefore we suggest that the potential production of dissolved carbonates is the dissolution of carbonate minerals, following reactions *(3.3.4)* and *(3.3.5)*, and combined reaction *(3.3.6)*:

$$CaCO_3 \leftrightarrow Ca^{2+} + CO_3^{2-} \qquad (3.3.4)$$
$$Ca,Mg(CO_3)_2 \leftrightarrow Ca^{2+} + Mg^{2+} + 2CO_3^{2-} \quad (3.3.5)$$
$$CO_3^{2-} + H^+ \leftrightarrow HCO_3^- \qquad (3.3.6)$$
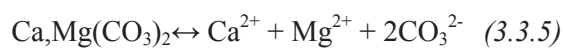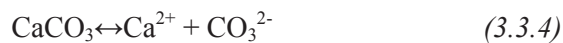
Similar to Ca^{2+} and Mg^{2+}, Sr increase by approximately 30% compared to injected solution, and B increase by a factor 2, from 4.6 10^{-5}mol/L to 8.4 10^{-5} mol/L. These two elements can be associated to carbonate minerals dissolution.

Our findings confirms observations in similar field experiments i.e. Kharaka et al. (2006, 2009), Kharaka and Cole (2011), Matter et al. (2007), and Zheng et al. (2012). Zheng and co-workers (2012) suggested that buffering capacity of reservoir in response to perturbation was too low due to limited calcite and dolomite reactive surface area and/or abundance, or low dissolution kinetics in the observed time scale of the experiment. Both possibilities can explain our results.

Further, in our experimental condition, the predominance of inactive pH-species SO_4^{2-} on the charge balance comparing to active base i.e. HCO_3^- would affect the neutralization capacity in response to pH perturbation by CO_2.

3.3.2. Cl^-, SO_4^{2-}, Na^+, K^+ and F^- concentrations

No significant variations were observed for Na^+, K^+, F^-. The Cl^- and SO_4^{2-} concentrations were not enriched compared to injected solution, and showed a significant decrease over the entire pumping phase.

On first, sulfate concentration were similar between injected solution and first pumped water volumes, about $1 \cdot 10^{-2}$mol/L (see fig. 3.3.8). A significant decrease in sulfate is observed over the entire pumping phase. Final concentration at the end of the pumped phase is 50% lower compared to injected solution and baseline water, from $1 \cdot 10^{-2}$ mol/L to $4,7 \cdot 10^{-3}$ mol/L. Further, an inverse correlation is observed between chloride and sulfate (fig. 3.3.8). The concentrations in chloride in the injected solution and in first pumped volumes are comparable, nearly $7 \cdot 10^{-4}$ mol/L. Therefore, chloride concenttration is considered as not influenced by CO_2-water-rock interaction. Chloride however is usually considered as a natural inert tracer. An increase in chloride concentration was observed over the entire pumping phase: at the final stage of pumping phase, chloride concentration is nearly two times higher comparing to injected solution (Fig. 3.3.8).
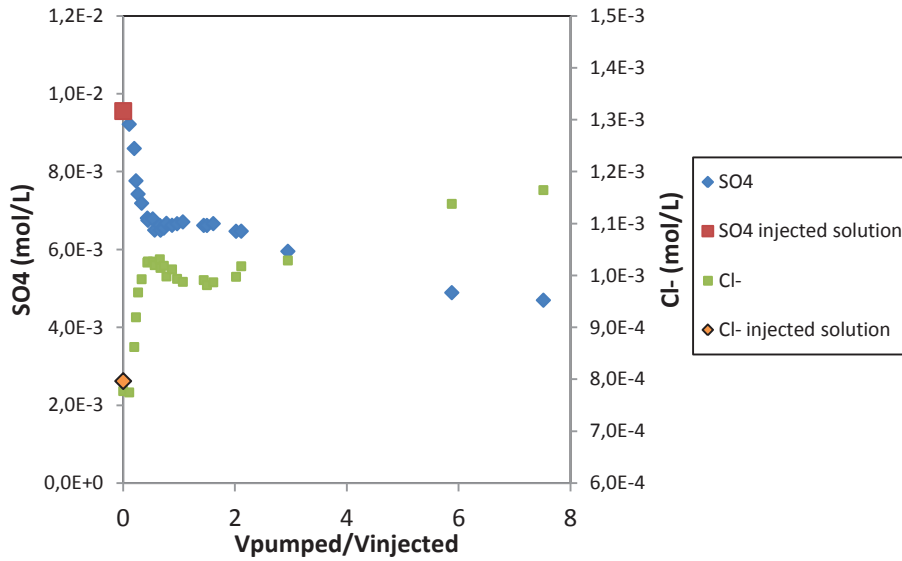
Fig. 3.3.8: Cl- and $SO_4^=$ concentrations plotted as a function of the pumped volume (Vpump./Vinj.)

A similar trend to sulfate was observed for lithium, however observed variation in Li^+ concentrations were included in the analytical error imposed by chemical analyses. Lithium concentrations measured by ICP-AES varied from $5.3 \cdot 10^{-5}$ mol/L to $4.8 \cdot 10^{-5}$ mol/L, with an accuracy of $\approx 1 \cdot 10^{-5}$ mol/L. Therefore the evolution of Li^+ behavior could not be used.

A linear correlation was observed between $SO_4^=$ and Cl^-, (Fig. 3.3.9).
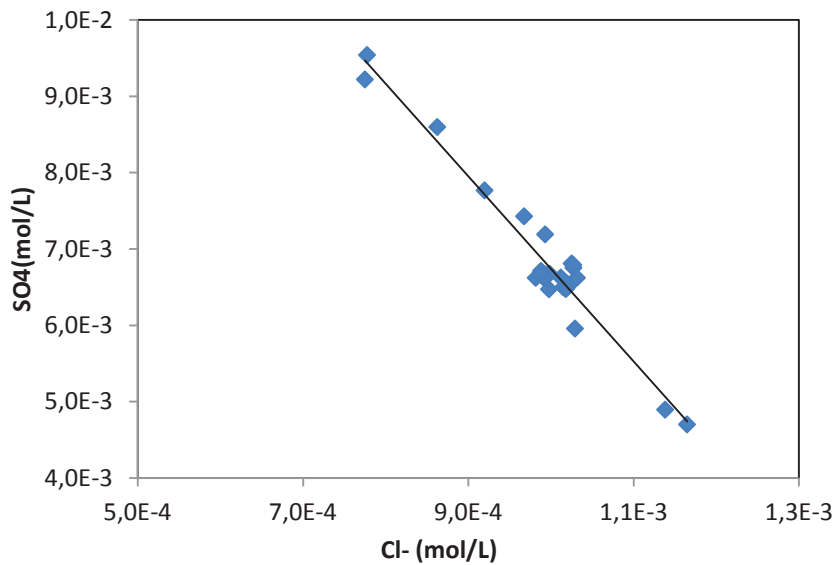
Fig. 3.3.9: $SO_4^=$ concentrations plotted as a function of Cl-

According to these results, Cl^- and SO_4^{2-} concentrations can be considered as non influenced by CO_2-water-rock interaction, or by water-rock exchange. Nevertheless Cl^- and SO_4^{2-} concentrations showed significant variation over the entire pumping phase (see Fig 3.3.9).

78

Since both elements are considered to be not reactive we propose that, chloride and sulfate concentrations were influenced by the possible mixing between different reservoirs with different SO_4^{2-} and Cl^- signatures. As previously developed in part 3.2, hydrogeophysical logging and packer test identified 3 different hydrogeological units within the entire borehole, designated as Fracture 1 ($\approx$-30m depth), Fracture 2 (-56m depth) and Fracture 3 (-89m depth). Hydraulic gradient measurement revealed a groundwater discharge from Fracture 1 to Fracture 2. Push pull test was performed in Fracture 2 isolated by packer system, where a volume of 3 m^3 was previously pumped to prepare CO_2 saturated injected solution. Therefore injected solution, previously pumped in Fracture 2 would present a chemical signature influenced by both groundwater signature in Fracture 1 and Fracture 2 waters. Finally, we noted that Fracture 1 groundwater (sampled during packer test) showed similar concentration in chloride and sulfate to injected solution. However, sulfate concentration can be influenced by both acido-basic and redox reactions, for example by reduction/oxydation of HS^-. However, redox measurement and calculation showed oxidative conditions before and after CO_2 perturbation, suggesting a total oxidation of HS^- in SO_4^{2-} in the aquifer. Furthermore, sulfate concentration was very high compared to other major ionic species. Thus the SO_4 variation due to potential oxydation or water-rock exchange could be negligible.

Therefore, the evolutions of sulfate and chloride during the pumping phase may correspond to (Fig 3.3.10):

- Water samples collected during first stage of pumping are characterized by Fracture 1 chemical signature (rich in SO_4^{2-}, poor in Cl^-),
- Water samples collected during final stage of pumping are characterized by Fracture 2 chemical signature (poor in SO_4^{2-}, rich in Cl^-).

Evolution of SO_4^{2-} and Cl^- will be used to estimate the influence of transport processes (see part 3.7).

Fig.3.3.10: conceptual hydrogeological model proposed to evaluate the evolution of Cl- and SO42- over the entire pumping phase.
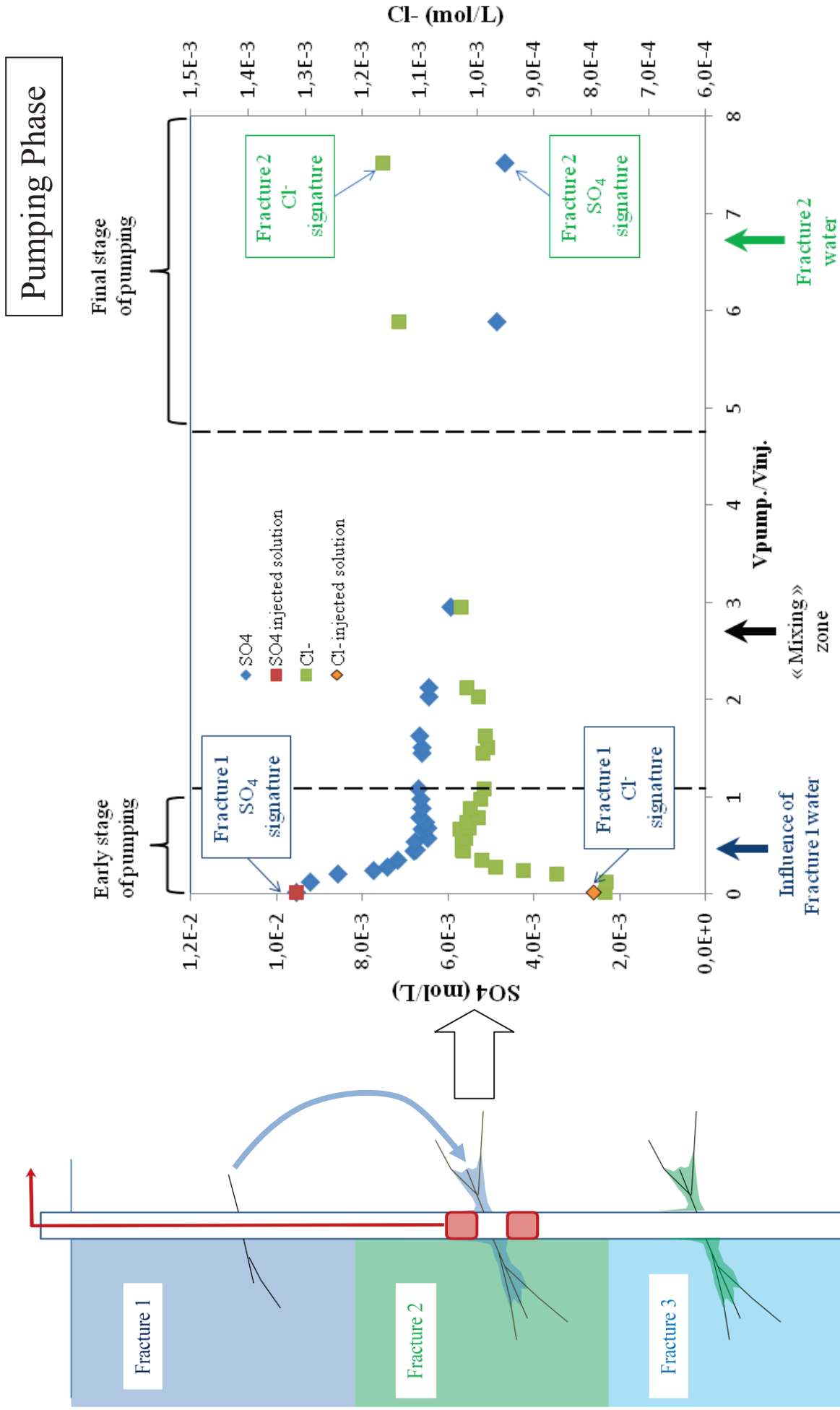
3.3.3. Minor and trace metals behavior

Despite the observed low variations in major element concentration,, the level of dissolved metals showed important enrichment compared to baseline concentrations.

3.3.3.1. Metal speciation

A characteristic feature of most dissolved metals is their tendency to form hydrolyzed species and to form complexed species by combining with inorganic anions such as HCO_3^- or SO_4^{2-}. The formation of aqueous complexes influence their mobility by increasing their solubility. One of the potential factors of mobilization of trace metal elements related to the CO_2-water rock interaction processes is the importance of bicarbonate complexes in the transport of divalent metals (Keating et al 2010, Zheng et al 2012). Speciation of dissolved bivalent metals M^{II} can operate into the aqueous phase by forming metals-bicarbonate or metal-sulfate complexes. Metals complexes are thermodynamically more stable than free M^{2+}. In the pH range of our experiment ($5.7 \leq pH \leq 7.3$), the dominant form of dissolved carbonated is anion hydrogenocarbonate HCO_3^-. In our case, main bivalent dissolved metals are Zn^{2+}, Mn^{2+} and Fe^{2+}. These elements can form weak complexes with SO_4^{2-} and HCO_3^-. Due to the high concentration in sulfate, and hydrogenocarbonates anions, speciation with SO_4 and HCO_3^- cannot be neglected. Reactions of speciation are listed in table 3.3.1.:

Reactions	log K*
$Fe^{2+} + HCO_3^- \leftrightarrow FeHCO_3^+$	2
$Mn^{2+} + HCO_3^- \leftrightarrow MnHCO_3^+$	1,95
$Zn^{2+} + HCO_3^- \leftrightarrow ZnHCO_3^+$	2,1
$Fe^{2+} + SO_4^{2-} \leftrightarrow FeSO4_0$	2,39
$Mn^{2+} + SO_4^{2-} \leftrightarrow MnSO4_0$	2,25
$Zn^{2+} + SO_4^{2-} \leftrightarrow ZnSO4_0$	2,34

*Thermodynamic data from database NIST46.3

Table 3.3.1: chemical reaction of speciation of bivalent metals

Direct measurement of metal complexes are difficult. Geochemical modeling was used to estimate proportion of complexes concentration compared to free bivalent metals concentrations. Calculation was run for the different water sample composition, collected at different lapstime of the pumping phase. and results are showed in Fig 3.3.11.

Results showed higher complexed proportion for water presenting higher CO_2 perturbation. For example about 50% of the total dissolved Zn is complexed (30% $ZnHCO_3^+$ + 20% $ZnSO_4^0$). At the end

of the pumping phase, with water composition close to baseline water composition, 43% of total Zn is complexed (25% $ZnHCO_3^+$ + 18% $ZnSO_4^0$). For dissolved iron, 43% of total dissolved iron is complexed (25% $FeHCO_3^+$ + 15% $FeSO_4^0$). Result for manganese and iron are comparable.

These results showed that complexed forms of divalent metals are not negligible, and therefore could have a potential influence on chemical equilibrium with metals species. The relase of bivalent metal release was potentially strongly influenced by speciation with HCO_3^- and SO_4^{2-} anions. Further, the effect of complexation could significantly affect the occurrence in Fe^{II}, and thus Fe^{II}/Fe^{III} and proportion as well.
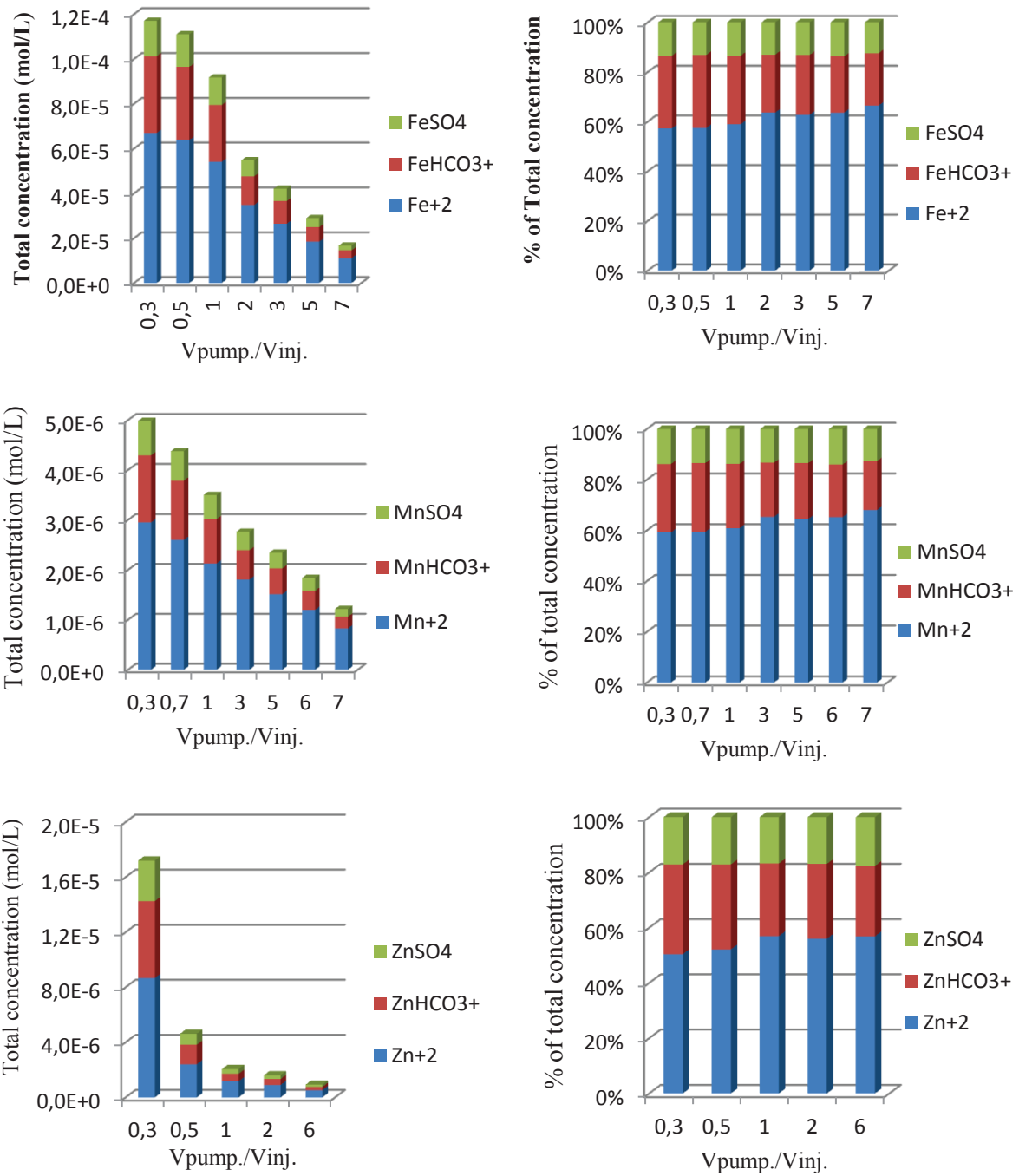
Fig.3.3.11: Result of calcualted speciation metal concentration plotted versus the pumped volume for Fe, Mn and Zn. Results are showed in concentration (mol/L): figures (b)(d)(f) and percentage: figures (a)(c)(e)

3.3.3.2.   Iron behavior and redox perturbation

Iron showed significant enrichment. The $Fe^{(II)}$ concentration, measured on the field, showed enrichment by a factor 5 (1 to 5 10^{-5} mol/L) and $Fe_{(t)}$ showed an enrichment by a factor 10 ($1 \cdot 10^{-5}$ to $1,3 \cdot 10^{-4}$ mol/L), see Fig3.3.12.
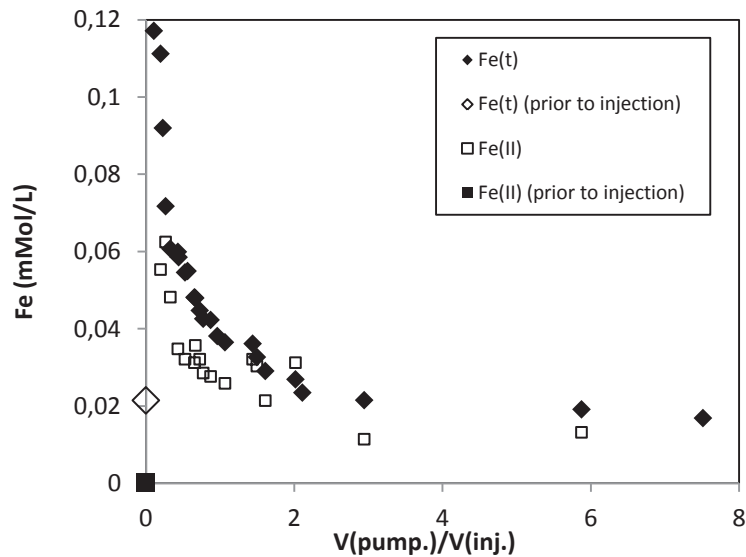
Fig. 3.3.12: Fe(t) and Fe(II) plotted as function of Vpumped/Vinjected.

Saturation index were calculated for baseline water and at the peak of pCO_2 perturbation (i.e. first samples collected during the pumping phase). to evaluate main effects of CO_2 perturbation on water-rock equilibrium, and potential main sources of dissolved iron.

Fe^{II}, Redox measurement and calculation

Only few chemical elements are important in the natural redox system (Fe, S, Mn, and C). Equilibrium between all the redox systems generally does not occur, except for some geothermal water (Stumm and Morgan 1996, Beaucaire and Toulhoat 1987, Criaud and Fouillac 1986). At the mineral-water interface, redox buffering capacity is due to the presence of electron donors or receptors on the solid surface, such as $Fe(OH)_{3(s)}$, $Fe_2O_{3(s)}$, $FeCO_{3(s)}$, $MnO_{2(s)}$ or $FeS_{2(s)}$. Therefore, a mixed potential or a potential following the predominant system might govern the redox state of groundwater. Redox was mesured by a standard electrode. Since redox sensitive species such as iron are present in significant concentrations, the electrochemical redox measurement corresponds to an equilibrium which involves

solid components such as ferric hydroxide or oxyhydroxide. Thus, the corresponding Eh values can be calculated by the Nernst equation for the ferrous/ferric species (Criaud and Fouillac 1986).

In our experiment, the injected solution was prepared with $3m^3$ of water previously pumped into the aquifer. This water was temporally stored during 12 hours into a plastic water tank, and saturated in CO_2 by a bubbling system, before re-injection (see Fig. 3.2.13). During this laps-time, an equilibrium with the oxygen of the atmosphere may have occurred. A low redox increase was measured at the electrode and few iron oxides deposits were observed at the bottom of the water tank, showing that oxidation of the injected solution occurred. Therefore a potential perturbation of redox into the aquifer in addition to CO_2 perturbation had to be considered.

Redox potential was estimated using Fe^{II}/Fe^{III} couples, in the $Fe-CO_2-H_2O$ system (Stumm and Morgan 1996).

Following reactions were considered:

$$Fe^{2+} + 2H_2O \leftrightarrow FeOOH_{(s)} + 3\ H^+ + e^- \qquad (3.3.9)$$

$$Fe^{2+} + 3H_2O \leftrightarrow Fe(OH)_{3(s)} + 3H^+ + e^- \qquad (3.3.10)$$

$$FeCO_{3(s)} + 3H_2O \leftrightarrow Fe(OH)_{3(s)} + 2H^+ + HCO_3^- + e^- \qquad (3.3.11)$$
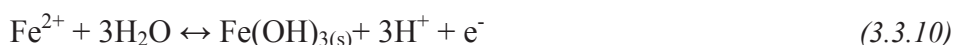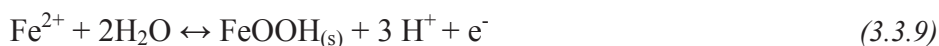
Considering the reactions with oxihydroxide iron *(3.3.9)* and hydroxide *(3.3.10)*, the Eh equation can be expressed by:

$$Eh = Eh_0 - 0{,}18pH - 0{,}0592\log a(Fe^{2+}) \qquad (3.3.12)$$

Where the term Eh_0 is defined as standard value for the specific redox couple. Using measured pH and $Fe^{(II)}$, the Eh of the solution was calculated and compared to the electrochemical measurement $Fe^{(II)}$ measured on the field corresponds to free Fe^{2+} plus complexed $Fe^{(II)}$. In our case, groundwater composition presented high concentrations in HCO_3^- (10^{-2}mol/L), and SO_4^{2-} (10^{-2}mol/L), therefore iron species $FeHCO_3^+$ and $FeSO_4^0$ cannot be neglected in the free Fe^{2+} calculation. Thermodynamic equilibrium calculation was used to estimate the concentration of free Fe^{2+}.

Eh_0 values were chosen for FeOOH well crystallized phase, i.e. $E_0 = 1.06V$ for Ferryhydrite $Fe(OH)_3$ (Serrebrennikov, 1977), $E_0 = 0{,}81V$ for goethite α-FeOOH (Ball and Nordstrom 1991), $E_0 = 0.88V$ lepidocrocite γ-FeOOH (Langmuir, 1969).

Considering the equilibrium siderite-ferryhidrite (reaction *(3.3.11)*), redox potential was estimated by the pe-pH relation:

$$pe = 16 - 2pH + \log(HCO_3^-) \qquad (3.3.12)$$

$$\text{with: } pe = Eh \times \frac{F}{2{,}303RT}$$

85

Calculated Eh was plotted versus measured Eh:
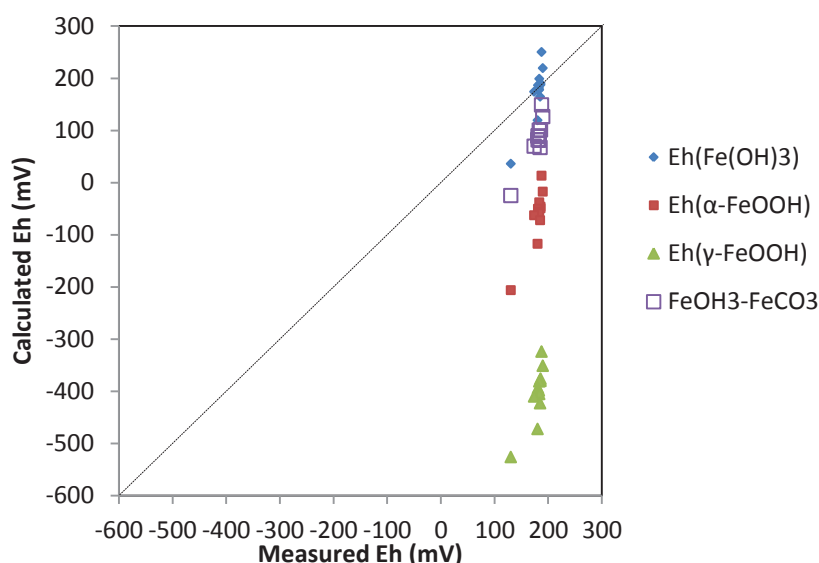
Fig. 3.3.13: Comparison between measured Eh and calculated Eh using $Fe^{2+}/Fe(OH)_3$, $Fe^{2+}/FeOOH$ redox and $FeCO_3/Fe(OH)_3$ redox couple.

The difference between measured Eh and calculated Eh is comprised between 2 mV to 40 mV for ferryhidrite Fe^{2+}-$Fe(OH)_3$, and ferryhidrite-siderite equilibrium (see Fig.3.3.13), while Eh values calculated from equilibrium with goethite (α-FeOOH) and lepidocrocite (γ-FeOOH) produced inconsistent values, with differences between measured and calculated Eh ranging from 150 mV to 300 mV.

These results suggested that the conditions in our experiment, redox potential is nearly controlled by Fe^{2+}-$Fe(OH)_3$ and siderite-$Fe(OH)_3$ equilibrium. Eh values range between +20 and +250 mV, suggesting that the groundwater in this system can be considered as oxic/sub-oxic waters (including these of baseline conditions previous to pCO_2 perturbation), with relatively low variation of Eh. This confirms our hypothesis of the weaky redox perturbation during the CO_2 injection. Due to the oxidative conditions, organic matter was considered as oxidated, and having negligible effect on redox control.

Previous works from Beaucaire and Toulhoat (1987) on the groundwater in the area of Lodève, and Criaud and Fouillac (1986) on CO_2 rich thermal water from Massif Central mountain have shown that groundwater potential redox can be estimated by the equilibrium with hydrous ferrous oxide FeOOH, ferric oxide $Fe(OH)_3$ and ferrous carbonate $FeCO_3$.

Chemical reactions involving iron oxide/hydroxide (reaction *3.3.2* to *3.3.4*) are both acido-basic and redox dependent. A useful tools to study reaction sensitive to combined effect of redox and pH is the predominance Eh-pH diagram or pe-pH diagram.

A pe-pH diagram was constructed for a system containing Fe, CO_2, H_2O, and solid phase ferrihydrite $Fe(OH)_3$, $FeCO_3$ (siderite), $Fe(OH)_2$ and Fe^0. Reactions used to construct the pe-pH diagram are listed in table 3.3.2.

reaction	pe function	
$Fe^{3+} + e- = Fe^{2+}$	$pe=13+ \log((Fe^{3+})/(Fe^{2+}))$	(1)
$Fe^{2+} + 2e- = Fe(s)$	$pe=-6,9 + 1/2 \log(Fe^{2+})$	(2)
$Fe(OH)_3(s) + 3H^+ + e- = Fe^{2+} + 3H_2O$	$pe=16 - \log(Fe^{2+}) - 3pH$	(3)
$Fe(OH)_3(s) + 2H^+ + HCO_3^- + e- = FeCO_3(s) + 3H_2O$	$pe= 16 - 2pH + \log(HCO_3^-)$	(4)
$FeCO_3(s) + H^+ + 2e- = Fe(s) + HCO_3^-$	$pe= -7 - 1/2 \, pH - 1/2 \log(HCO_3^-)$	(4)
$Fe(OH)_2(s) + 2H+ + 2e- = Fe(s) + 2H_2O$	$pe= -1,1 - pH$	(5)
$Fe(OH)_3(s) + H^+ + e- = Fe(OH)_2(s) + H_2O$	$pe= 4,3 - pH$	(6)
	pH function	
$FeCO_3(s) + 2H_2O = Fe(OH)_2(s) + H^+ + HCO_3^-$	$pH= 11,9 + \log(HCO_3^-)$	(7)
$FeCO_3(s) + H^+ = Fe^{2+} + HCO_3^-$	$pH= 0,2 - \log(Fe^{2+}) - \log(HCO_3^-)$	(8)

Table 3.3.2: equation used for the construction of pe-pH diagram for the Fe-CO$_2$-H$_2$O system
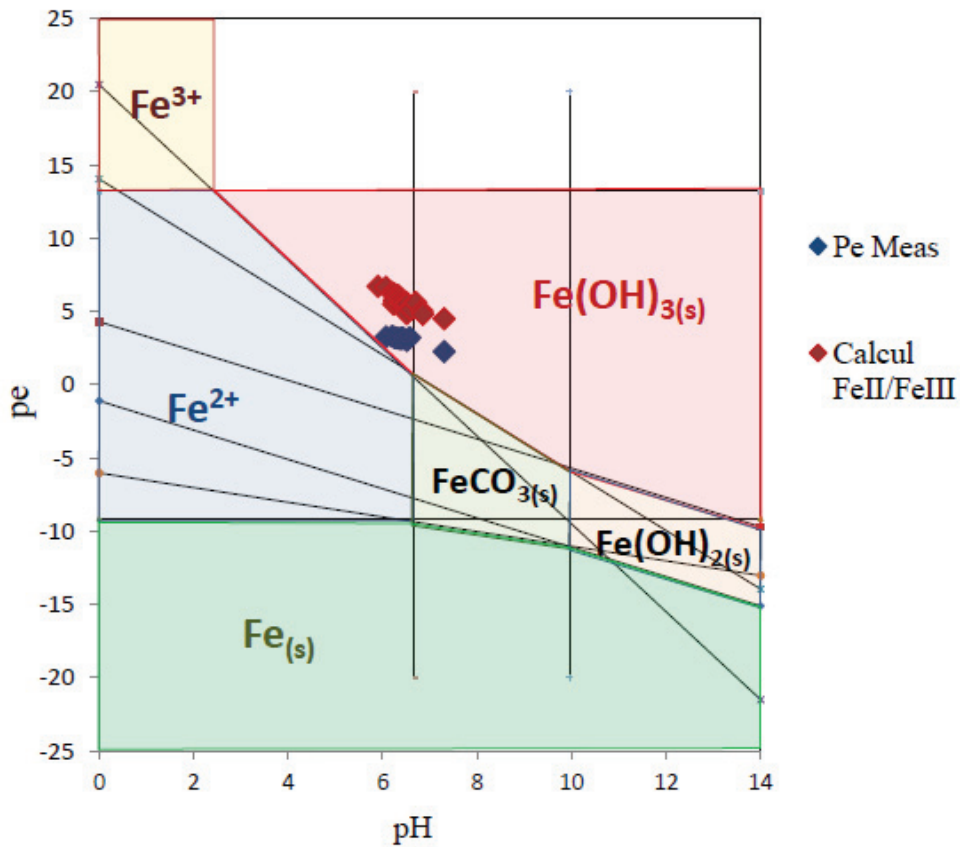
Fig. 3.3.14: pe-pH diagramm for the system Fe, CO$_2$, H$_2$O. Stability field of solid phases and aqueous species Solid phases are Fe(OH)$_3$ amorphous, FeCO$_3$ (sidérite), Fe(OH)$_2$ and Fe. Carbone total C$_T$=10^{-2} mol/L, dissolved species of Fe$^{(II)}$ and Fe$^{(III)}$=10^{-5} mol/L. Data corresponding to measured pe (in blue) and calculated pe (in red) are reported

Fig. 3.3.14 shows that water pe and pH corresponding to our experiment. We see that predominant iron species in our experiment are Fe(OH)$_{3(s)}$, and Fe^{2+} (see Fig.3.3.15). However, considering the

analytical and equilibrium calculation uncertainty, we can consider that water are close to triple point Fe^{2+}-$FeCO_3$-$Fe(OH)_3$.

Given the dominant reaction of pH-redox domain (see pe-pH functions *(3)*, *(4)* and *(8)* in table 3.3.2), for a given pe value, a small change in pH produce a significant variation on Fe^{2+}, while small changing in Fe^{2+} or Redox would have a low effect on pH. As showed in Fig. 3.3.14, redox variations during our experiment were slights comparing to pH variation, suggesting that iron behavior in our system is more dependent on the pH perturbation.

Baseline solution are saturated with respect to siderite and over saturated with respect to ferrihydrite. After CO_2 injection both phase are undersaturated:

	siderite	ferrihydrite
	$FeCO_3$	$Fe(OH)_3$
Previously to injection	**0,25**	**1,88**
After CO_2 injection	**-1,06**	**-2,37**

Table3.3.3: Saturation index for siderite and ferrihydrite phase in groundwater before and after CO_2 injection

We propose that the CO2 perturbation is responsible for the dissolution of ferrihydrite $Fe(OH)_3$ and siderite $FeCO_3$. Both reactions however participate to the iron release:

$$Fe(OH)_3 + 3H^+ \leftrightarrow Fe^{3+} + 3H_2O$$
$$FeCO_3 + H^+ \leftrightarrow Fe^{2+} + HCO_3^-$$
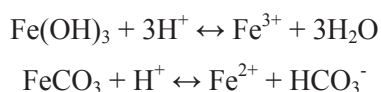
Further, saturation was calculated for all chemical compositions measured continuously over the pumping phase, and plotted versus the pumped volume (see Fig.3.3.13). We can see a good correlation between $SI_{Fe(OH)3}$ and dissolved iron in solution, with a gradual increase of SI forward the saturation state over the entire pumped phase. This confirms that potential source of iron release following the pCO_2 perturbation was induced by dissolution of iron hydroxide ferrihydrite $Fe(OH)_3$ via reaction *(5)* in table 3.3.2.

SI for siderite showed a weak decrease after CO_2 injection, but no clear correlation between siderite SI and dissolved iron concentration was observed over the entire pumping phase.
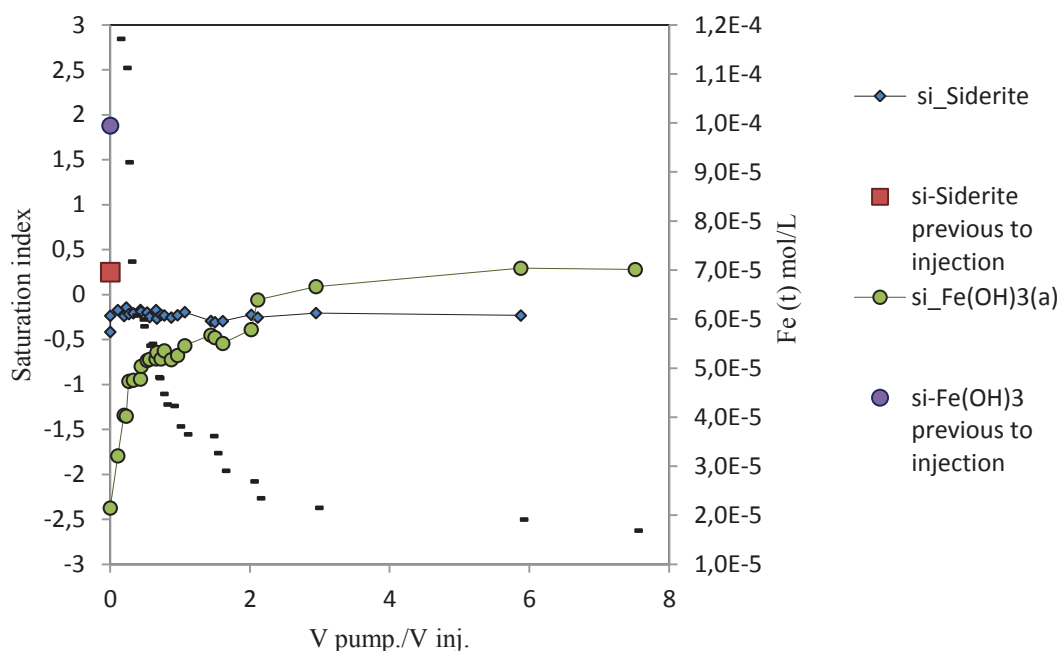
Fig.3.3.15: Plot of SI Fe(OH)$_3$ and FeCO$_3$, and total dissolved iron Fe(t) plotted versus pumped volume (Vpump./Vinj.)

Saturation index calculation using pH, redox and water composition suggested that source of iron release induced by pCO$_2$ perturbation was controlled firstly by ferrihydrite reactivity, with potential participation of siderite.

Ferrihydrite is a trivalent iron amorphous mineral specie, with high solubility. According to chemical analyses, dissolved iron is present in both Fe^{II} and Fe^{III} species, in nearly equal proportions. Therefore, we propose than main source of bivalent iron might be the dissolution of siderite, and main source of trivalent iron might be the dissolution of ferrihydrite. However, it is important to keep in mind that the boundary domains between solid phases and dissolved species are based on specified activity values, and that the validity of stability domain as thermodynamically defined equilibrium conditions is dependent on the reliability of the free-energy data. In particular, iron hydroxide Fe(OH)$_3$ is a substance of variable crystallinity which has different ΔG_0 values, depending on its crystalline form. Therefore, considering Fe(OH)$_3$ as a main source of dissoled Fe^{III} is a plausible scenario, but the occurrence of other iron oxides dissolution forms cannot be ignored.

Further, these calculations suggest that reactivity is firstly controlled by acidification due to pCO$_2$ perturbation. According to thermodynamic equilibrium calculation, and range of redox variation, reactivity appears as dominated by pH perturbation.

However, bivalent iron concentration appears significantly high despite measured oxidative condition. This large proportion of bivalent iron can be explained by complexation of Fe^{2+} with dissolved SO$_4^{2-}$ and HCO$_3^-$, which kept the concentration of divalent iron relatively high for oxidative condition.

90

3.3.3.3. Manganese behavior

An important increase of Mn was observed, with an enrichment by a factor of 5 (Fig.3.3.16).
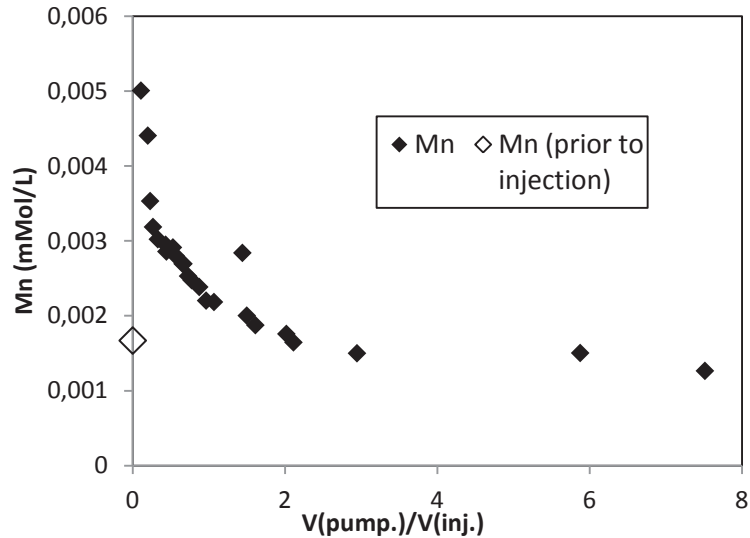
Fig. 3.3.16: Mn plotted as function of Vpumped/Vinjected

Potential sources for dissolved manganese could be dissolution of manganese oxides or hydroxide such as pyrolusite (MnO_2), pyrochroïte ($Mn(OH)_2$) or manganite $MnOOH$. Thermodynamic calculation results show that all of these phases were undersaturated before and after pCO_2 perturbation. Therefore, the dissolution of manganese oxide-hydroxide phase could not be clearly identified in the range of pCO_2 variation of this experiment

On the other hand, a good correlation was observed between SI index of manganese carbonate rhodocrosite ($MnCO_3$) and CO_2 injection (see Fig 3.3.17).Baseline water appeared weakly undersatured before CO_2 injection, and clearly under saturated after CO_2 injection. Dissolution of Rhodocrosite $MnCO_3$ could be the potential main source of dissolved following chemical reaction:

$$MnCO_3 = Mn^{2+} + CO_3^{2-} \qquad\qquad \log K=-10,58$$
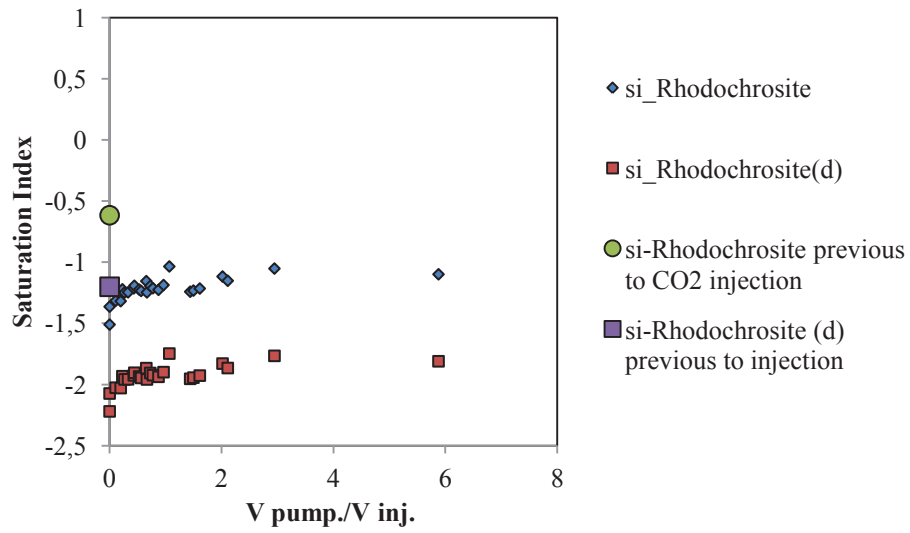
Fig. 3.3.17: saturation index of rhodocrosite ordered and rhodocrosite disordered (d) plotted as a function of pumped fluid

3.3.3.4. Arsenic behavior

Arsenic showed an increase by a factor 2 (Fig3.3.18).
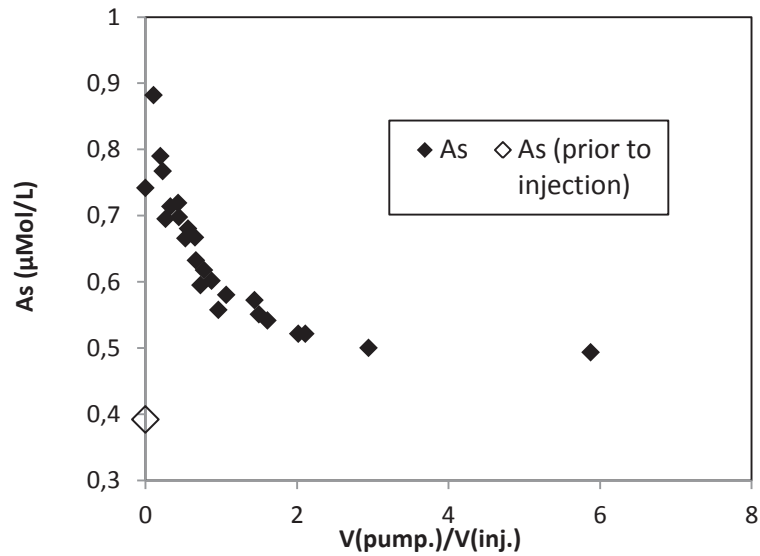
Fig. 3.3.18: Mn plotted as function of Vpumped/Vinjected

Thermodynamic equilibrium calculation did not identify particular mineral phase as a source arsenic. A potential source for As could be the dissolution of sulfur mineral (As_xS_x). However, due to the high amount in SO_4 of our experiment, and oxidative condition, dissolution of sulfur minerals could not be clearly identified by thermodynamic approach. Equilibrium calculation using thermodynamic database are difficult for application to trace elements such as arsenic. Another potential important source of As could be dissolution of metals oxide-hydroxide. Arsenic can be present as cosorbed elements on the iron oxyhydroxides surface(Stumm and Morgan 1996, Waychunas 2002). Redox condition measurement suggest that predominant dissolved arsenic species is under the form of arsenate H_2AsO^{4-} (i.e. As$^{(V)}$). Appelo et al. (2002) showed that release of sorbed arsenic in groundwater from iron hydroxides surface are influenced by the presence of dissolved carbonate in solution. The sorption of carbonate on ferryhydrite reduces the sorption capacity of As by displacing effect of carbonate on sorbed arsenate As$^{(III)}$ and arsenite As$^{(V)}$.

3.3.3.5. Zinc behavior

The higher enrichment was observed for Zn, with an enrichment by a factor of 25 (Fig 3.3.19).
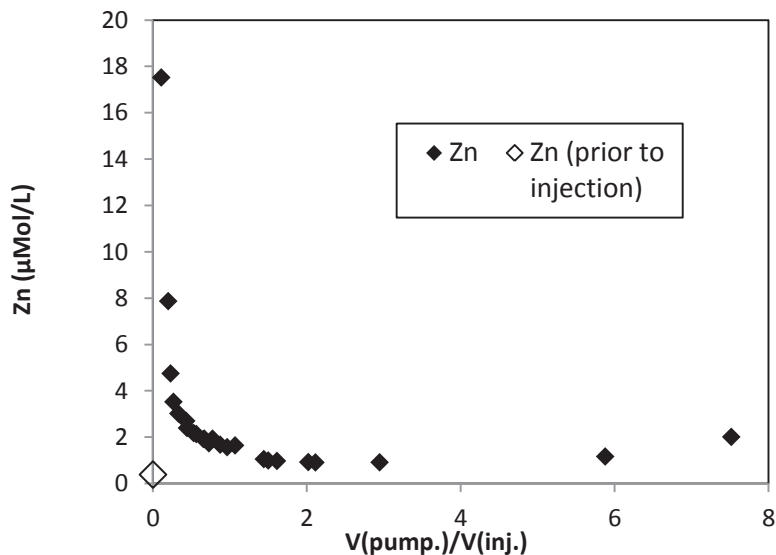
Fig. 3.3.19: Mn plotted as function of Vpumped/Vinjected

Thermodynamic equilibrium calculation did not identify particular mineral phase as a source for Zn. A potential source for Zn could be the dissolution of sulfur mineral (ZnS, ZnS_2, etc.). However, due to the high amount in SO_4 concentration of our experiment, and oxidative condition, dissolution of sulfur minerals could not be clearly identified. Another source for Zn could be the dissolution of carbonate. Similarly to As, another potential important source of Zn could be dissolution of metals oxide-hydroxide. Indeed, Zn and As can be present as cosorbed elements on the iron oxihydroxides surface (Stumm and Morgan 1996, Waychunas 2002). Zinc enrichment is significantly higher than other dissolved metals. These different trends can be explained by a differential speciation phenomenon. In particular dissolved Zn and As concentrations were comparable previously to injection in both water and rock, with a ratio Zn/As comprised between 1 and 1.7. However, following the CO_2 injection test, Zn was enriched by a factor of 25, and As was only enriched by a factor of 2 (Fig.3.5.5 and table A.2). Gräffe et al. (2004 and 2005) studied the co-sorption and desorption of Zn and As on goethite surface. They studied the desorption of $Zn^{(II)}$ and $As^{(V)}$ at pH=5.5 from goethite surface, and showed that relatively more $Zn^{(II)}$ was released than $As^{(V)}$. One possible reason may be the elongated apical Zn-O bonds, when the O atoms are shared with Fe^{3+} and/or As^{5+} centers. The elongated Zn-O is weaker and more prone to attack by H_3O^+. Ding et al. (2000) proposed that Zn-Fe complexes on the iron hydroxide surface are weaker than As-Fe surface complexes, due to greater energy differences between the lowest unoccupied molecular orbital (LUMO) of the adsorbate and the highest occupied

molecular orbital (HOMO) of the sorbent and the consequently lower potential molecular energies of the Zn-Fe vs. As-Fe sorption complex. This explanation could be correlated with our experimental results.

3.3.3.6. Molybdenum behavior

Contrary to other elements, molybdenum concentration showed an inverse correlation to other dissolved metals, with a decrease by a factor 2 following the CO_2 injection, and a slowly increase over the pumping phase before returning to initial concentration, as showed in Fig. 3.3.20. The behavior of Mo as a function of pH, redox and different solution chemistry was extensively developed as part of mine and industrial waste water management. According to our calculation, dissolved Mo was under the anionic form MoO_4^{2-}. Morrison and Spandler (1992) studied the precipitation and sorption of Mo on iron oxides for use in chemical barriers in groundwater remediation. Their works showed that sorption percentage of MoO_4^{2-} on ferric oxide surface is maximum for acid to neutral pH range (from 2 to 7) and significantly decrease from neutral to basic pH (from 7 to 12). Therefore, acidic perturbation caused by CO_2 injection would have increased the sorption of MoO_4^- on ferric oxide surface. Another possibility to explain the opposite behavior of Mo is the precipitation of $FeMoO_4$ involved with release of Fe^{2+}. Thermodynamic calculation showed a slight increase of saturation index of $FeMoO_4$ before and after injection, but this variation was included in the analytical error, therefore this hypothesis could'nt be formally confirmed.
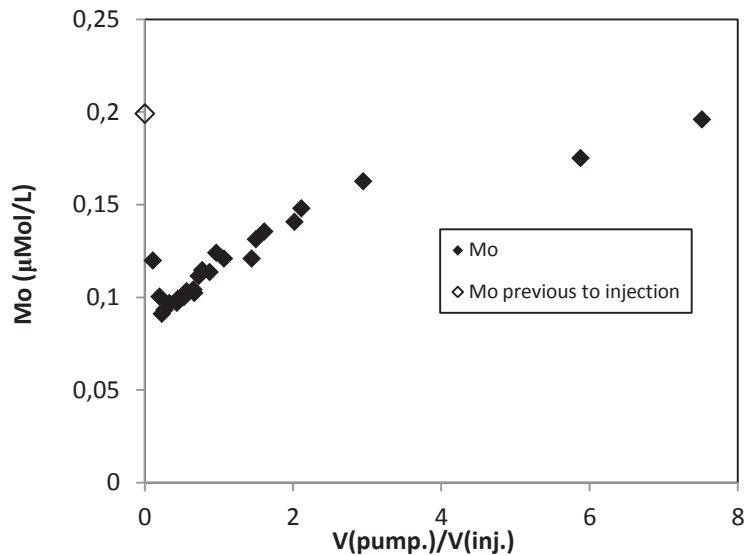
Fig. 3.3.20: Mo plotted as function of Vpumped/Vinjected

3.3.4. Effect of fluid dynamic on chemical concentration

Elements concentrations presenting major modifications induced by pCO_2 perturbation were Fe, Mn, Zn, As.

Concentrations of reactive elements can be plotted as function of time since injection stopped (Fig. 3.3.21) In this case, two phases can be identified: a first phase of 80 h following the water-CO_2 injection called "incubation time", and a pumping phase of 72 h (i.e. from 80 h to 142 h) (see Fig 3.3.21).

During the first phase, chemical composition of the injected solution is modeified by CO_2-water-rock interaction and mixing with the baseline aquifer water. As previously mentioned, the natural groundwater flow was considered as negligible in our experimental site. Between the time since the injection stopped, and the start of the pumping phase, the aquifer portion impacted by injection can be considered as a system with constant volume, pressure and temperature, with no transfer or exchange of matter. We assume that influence of natural groundwater flow occurring into the aquifer was negligible. This system can be considered as thermodynamically isolate, where we assume that the increase in dissolved concentrations was mainly driven by chemical reaction induced by pCO_2 perturbation, and mixing with aquifer water.

On the second phase, the measured concentration corresponds to fluid samples collected during pumping phase. During this phase, a forced transport process was induced by pumping, and measured concentrations were influenced by two factor that are CO_2-water-rock interaction, and fluid dynamic (mixing, advection, dispersion, diffusion). The influence of mixing within the baseline aquifer water on the measured concentrations increase as the pumping volume increases.

The effect of fluid dynamic on measured concentration during the pumping phase cannot be neglected and have to be estimated to quantify the actual concentration added by CO_2 water-rock interaction and evaluating *in-situ* rate of metals release.
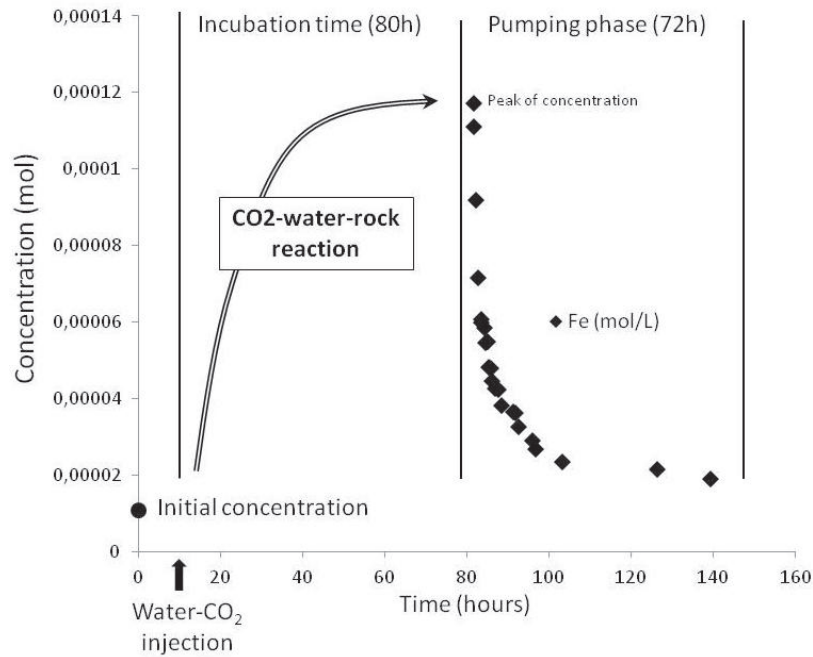
Fig.3.3.21: Breakthrough curve resulted from push-pull test. Chemical concentration of reactive species (Fe) is plotted as function of time since CO_2-water injection ended. The incubation time of 80h, and the pumping phase are mentioned. The chemical concentration previous to injection is indicate in order to appreciate the enrichment in concentration induced by CO_2-water injection.

Therefore, two different stages were considered in the analysis of mineral reactivity:

- A first phase, corresponding to the phase between the previous to injection condition and first pumped sample 80h after CO_2 injection, where measured concentrations are considered are mainly driven by CO_2-water-rock interaction process

- A second phase, corresponding to measured data over the pumping phase, where transport and mixing effect have to be evaluated

3.4. Estimation of *in-situ* reaction rate of metal release calculation

Push-pull test results were determined by breakthrough curves analyse (Istok et al 1997, Haggerty et al 1998). Similar techniques were tested in a wide range of environmental issues, such as chloride solvent degradation (Lee et al 2010), nitrate degradation (Boisson 2010), or to evaluate storage capicity of reservoir. Haggerty, Istok and coworkers (1997, 1998, 2001) developed a method based on assumption that the injected test solution is well mixed within the portion of the aquifer assayed by the test, and that the retardation factor induced by hydraulic parameters (advection, diffusion, dispersion, mixing) is the same for the tracer and the reactant. Differential trend between the reactant and the tracer breakthrough curves can be used to estimate the in situ reaction rate of the reactant. The relative concentration of the reactant $c_d(t)$ (i.e. the measured concentration divided by the injected concentration) can be expressed as (Jury and Roth 1990):

98

$$c_d(t) = c_{tr}(t)\exp(-kt) \qquad (3.4.1)$$

Where c_{tr} is the relative concentration of the tracer, and k corresponds an in situ reaction rate. Therefore equation *(3.4.1)* can be rewritten as:

$$ln\left(\frac{c_d(t)}{c_{tr}(t)}\right) = -kt \quad (3.4.2)$$

For this simple case, we can obtain an estimation of k by measuring $c_{tr}(t)$, $c_d(t)$ and applying a linear fitting by least-square technique on a semi-log plot of $ln((c_d(t)/c_{tr}(t))$ versus time t (Levenspiel 1989). Equt 3.4.2 can be adapted to push-pull test using conservative tracer and the reactant that undergoes a first order or pseudo first order of reaction. In our case, dissolution of oxide minerals induced by CO_2 perturbation and involved pH acidification appeared as not ruled by a first order of reaction. A method based on mass balance transfer can be used to estimate in-situ reaction rate (Matter et al 2007). This technique was used to evaluate the dependence of reaction rate with pH and pCO_2. In particular, this method has been adapted to analyse our experimental results concerning metal releases in order to estimate in-situ reaction rate induced by CO_2 perturbation.

3.4.1. Mass transfer balance

In our experiment, artificial inert tracer was not added into the injected solution (see part 3.4). Indeed, trace metal concentration can be easily influenced by complexation or variation of ionic strength. Thus, adding important quantity of ionic (NaCl) or fluorescent (uranine) tracer would have probably influenced chemical reactions. We adopted sulfate as conservative tracer, since its concentration was not influenced by redox and water-rock interaction, and injected solution had a different signature comparing to baseline water in the aquifer.

Measured solute concentrations enabled breakthrough curves for each solute to be plotted as a function of pumped volume. The background (i.e. previously to injection) solute concentrations were subtracted from the measured values to account for pre-injection concentrations in the ambient aquifer water. The injected solution is mixed with the ambient aquifer water. Samples collected at the wellhead during the pumping phase represent a mixture of injected water and ambient aquifer water.

A dilution ratio can be calculated by:

$$\frac{(C_{measured} - C_{background})}{C_{injected}} = \text{Dilution ratio} \qquad (3.4.4)$$

A mass transfer calculation can be made using the inert tracer (i.e. SO_4^{2-}) breakthrough curve, and the recovery percentage for the injected solution can be quantified by:

$$\frac{\text{Extracted Mass}}{\text{Injected Mass}} \times 100 = \text{Recovery of injected solution (\%)} \qquad (3.4.5)$$

The inert tracer concentration breakthrough curve is considered as influenced exclusively by hydraulic factors such as solutes losses due to advection, dispersion or diffusion. Breakthrough curves of reactive solutes are used to quantify bulk rock dissolution. The total mass of all recovered solutes was derived by integration of the breakthrough curves. The total mass of solutes obtained by water-rock reactions was derived from mass balance calculations using the dilution factors calculated from inert tracer solution concentrations.

Therefore, mass balance and recovery proportion was calculated for each reactive tracer, i.e. Fe, Mn, Zn and As and non reactive tracer SO_4^{2-}. All of the results are summarized in Table 3.4.1:

	Fe	Mn	Zn	As	SO_4
Injected Mass (mol)	0.0255	0.00405	0.00204	0.00118	28.2
Extracted Mass (mol)	0.2193	0.01118	0.01081	0.01207	18.20
Mass added by reaction (mol)	0.2981	0.01096	0.01349	0.01676	0
Recovery (%)	-	-	-	-	64.5

Table 3.4.1: Mass Balance and Recovery Proportions for Iron, Manganese, Zinc, Arsenic and Sulfate. The extracted mass is corrected by background concentration in the ambient aquifer water. Sulfate was used as conservative tracer in the single well push-pull test, the mass added by CO_2-water-rock reaction was corrected for about 65% recovery.

The rate of element release, is reflected in the rate of change of the corrected solute concentration. The recovery proportion based on the conservative sulfate tracer was 65% (Table 3.4.1) and (Fig. 3.4.1).
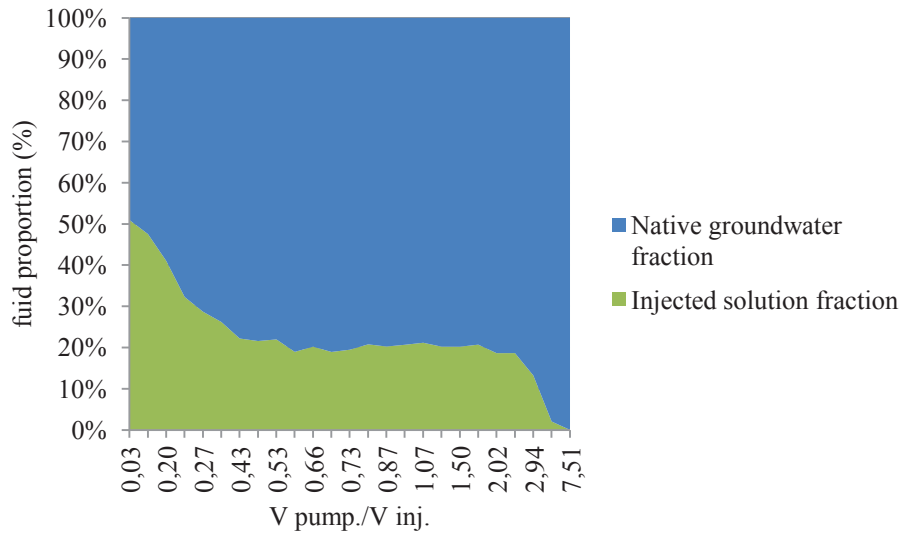
Fig. 3.4.1: proportion estimated of native groundwater fraction as a function of pumped fluid

The measured cation concentrations in the retrieved water samples reflect mixing between the ambient aquifer water and the injected solution plus the addition of elements by water-rock reactions. Therefore, assuming a binary mixing between the injected and ambient waters (Fig.3.4.2), we can calculate the term C_{mix} by the following equation:

$$C_{mix} = X \times C_{inject} + (1 - X) \times C_{ambient} \qquad (3.4.6)$$

where X is the fraction of the injected solution estimated from sulfate concentrations, and $C_{ambient}$ is the background aquifer groundwater composition previous to injection. Fraction of the injected solution (or dilution factor) was calculated with sulfate.

The difference between the measured solute concentrations (C_{meas}) and the mixing value (C_{mix}) is attributed to the dissolution of the bulk rock and defined as C_{react} in Table 3.4.2. Computations, which account for the dilution and hence for the 65% recovery fraction, show that the following total masses are added by reactions: $2.98 \cdot 10^{-1}$ mol of iron, $1.10 \cdot 10^{-2}$ mol of manganese, $1.68 \cdot 10^{-2}$ mol of arsenic and $1.35 \cdot 10^{-2}$ mol of zinc.

101
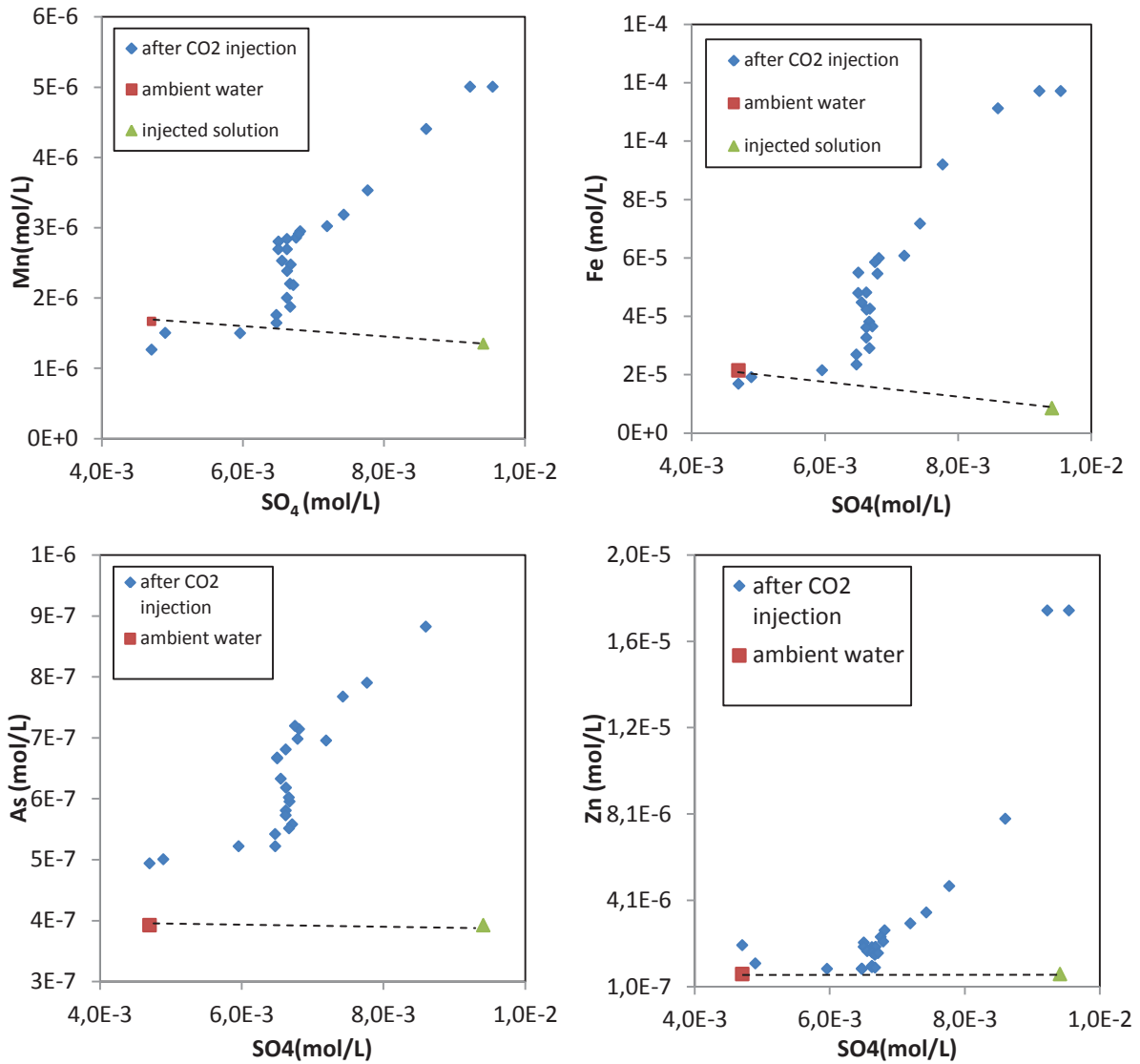
Fig.3.4.2: Reactive chemical elements (Fe, Mn, As, Zn) versus inert tracer (sulfate), illustrating the mixing line between the native groundwater and the injected solution as well as the data from water samples extracted after the CO_2 injection. All extracted water samples are above the mixing line, indicating increased concentration due to dissolution reactions.

3.4.2. *In-situ* rate of release estimation

Average bulk rock dissolution rates were estimated by elements release rates using the following rate equation (Matter et al 2007):

$$R = \frac{C_{react}(t) \cdot V_{pumped}}{t_r \cdot A} \qquad (3.4.7)$$

Where R is the in-situ dissolution rate, of the rock in contact with the interacting fluid ($mol/m^2/h$). The term t_r defines the time since the injection stopped, A designs the surface rock in contact with the reactive fluid into the aquifer. C_{react} is the concentration of the element resulting from the CO_2-water-rock interaction. C_{react} corresponds to the measured concentration corrected by ambient concentration of the aquifer previously to injection, and corrected by a dilution factor induced by physical transport processes (diffusion, dispersion and advection).

aquifer For each water samples, the term C_{react} can be calculated from the measured concentration $C_{meas.}$ using equation *(3.4.4)* and the correction factor, calculated by sulfate mass transfer. The dilution factor was estimated by mass balance of SO_4^{2-}, considered as non reactive tracer in our case.

It is important to note that rock surface area designed by A is a parameter deduced from the porosity of the rock. In our case, we used the total surface area of mineral in contact with fluid (estimated with the porosity).

The aquifer volume influenced by the pushpull process is estimated assuming (1) a radially symetrical flow field around the injection well (cylindrical model) and (2) an effective connected porosity of 2%, Since one parcel of injected solution travelled a greater radial distance from the injection point than the previous one, each extracted water sample is representative for a specific region of influence (i.e., aquifer volume) with a specific radial distance (r) from the well. The aquifer volume and radial distance for each cylinder was computed assuming the radially symetrical model. The geometric surface *(A)* of each specific cylindrical aquifer volume was calculated using the estimated aquifer porosity and the radial distance. Since each water sample is representative of one cylinder (Fig. 3.4.3), the rock surface area in contact with reactive fluid is defined for each cylinder.

Assuming that the aquifer affected by injection-extraction experiment is an homogeneous confined aquifer with 2% of connected porosity and 3 m thickness (corresponding the inter-packer distance), the radius of each cylinder representing the total volume of water+rock can be estimated for each pumped volume. Therefore, the radius affected by $3m^3$ of injected volume is about 15 m, while the total radius corresponding to the 22,5 m^3 pumped volume at the end of the extracted phase is about 116 m.

103
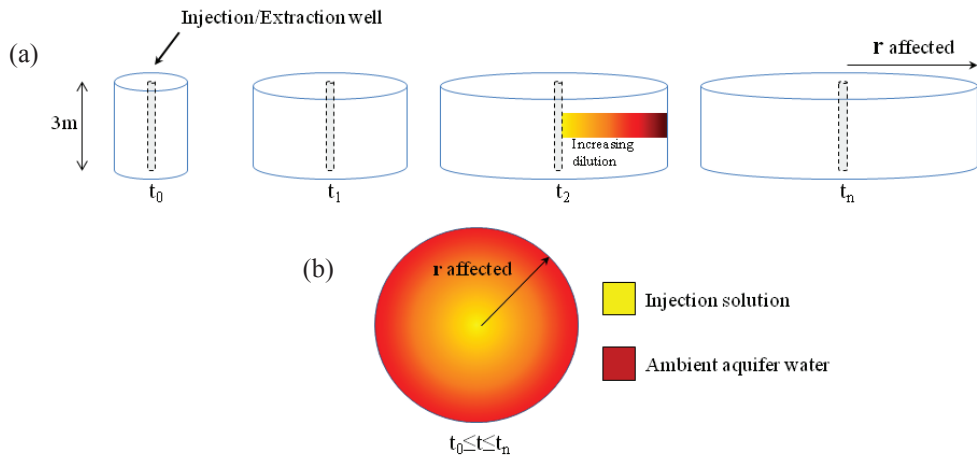
Fig. 3.4.3: Single-well push-pull test schematic indicating (a) the proportion of aquifer close to the injection/extraction well with increasing dilution away from the well and (b) the plan view of the radially symetrical aquifer model (adapted from Istok [2002] and Matter [2007]).

For each water samples, the corresponding differential volume $\Delta V(t)$ can be calculated by:

$$\Delta V(t) = V_{pump.(t)} - V_{pump.(t-1)} \qquad (3.4.8)$$

The total surface rock A in contact with interacting fluids was estimated assuming a reservoir rock composed by homogeneous spherical grain of 2mm radius and the total volume of aquifer portion affected corresponding to each pumped volume, composed by 2 mm spherical grains, and 2% connected porosity.

Therefore, in situ reaction rate can be calculated by equation *(3.4.7)* for each water samples collected at time t_r, considering to ΔV volume of extracted fluid as:

$$R = \frac{C_{react}(t) \cdot \Delta V(t)}{t_r \cdot A} \qquad (3.4.9)$$

Estimations for Fe, Mn, As and Zn release are showed in table 3.4.3.Therefore, for each water samples, a bulk rock dissolution rate *R* can be calculated using equation *(3.4.9)*, considering C_{react}, the reaction time t_r, which corresponds to the elapsed time since the injection stopped, *A* the total surface rock in contact with interacting water, and the pumped volume $V_{pump.}$.

104

Pumped Volume	Reaction Time (h)	Injected solution fraction	Native groundwater fraction	Fe$_{meas.}$	Fe$_{mix}$	Fe$_{react.}$	Mn$_{meas.}$	Mn$_{mix.}$	Mn$_{react.}$	Zn$_{meas.}$	Zn$_{mix.}$	Zn$_{react.}$	As$_{meas.}$	As$_{mix.}$	As$_{react.}$
m^3	hours			mol/L	mol/L	mol/L	mol/L	mol/L	mol/L	mol/L	mol/L	mol/L	mol/L	mol/L	mol/L
0.1	80.2	0.509	0.491	1.17E-04	9.26E-06	1.08E-04	5.01E-06	1.51E-06	3.50E-06	1.75E-05	7.96E-07	1.67E-05	8.82E-07	4.42E-07	4.40E-07
0.323	80.8	0.475	0.525	1.17E-04	9.31E-06	1.08E-04	5.01E-06	1.52E-06	3.49E-06	1.75E-05	8.04E-07	1.67E-05	7.90E-07	4.46E-07	3.45E-07
0.593	81.6	0.410	0.590	1.11E-04	9.40E-06	1.02E-04	4.41E-06	1.54E-06	2.87E-06	7.88E-06	8.20E-07	7.06E-06	7.67E-07	4.52E-07	3.15E-07
0.685	81.8	0.322	0.678	9.20E-05	9.53E-06	8.25E-05	3.53E-06	1.57E-06	1.97E-06	4.76E-06	8.40E-07	3.92E-06	7.42E-07	4.61E-07	2.81E-07
0.798	82.1	0.287	0.713	7.18E-05	9.58E-06	6.22E-05	3.19E-06	1.58E-06	1.61E-06	3.53E-06	8.49E-07	2.68E-06	7.42E-07	4.65E-07	2.77E-07
0.989	82.6	0.262	0.738	6.08E-05	9.62E-06	5.11E-05	3.02E-06	1.59E-06	1.44E-06	3.03E-06	8.54E-07	2.17E-06	6.95E-07	4.67E-07	2.28E-07
1.296	83.4	0.222	0.778	6.00E-05	9.68E-06	5.03E-05	2.95E-06	1.60E-06	1.35E-06	2.71E-06	8.64E-07	1.84E-06	7.14E-07	4.71E-07	2.43E-07
1.326	83.5	0.216	0.784	5.86E-05	9.69E-06	4.89E-05	2.86E-06	1.60E-06	1.26E-06	2.40E-06	8.65E-07	1.54E-06	7.19E-07	4.72E-07	2.47E-07
1.584	84.2	0.220	0.780	5.46E-05	9.68E-06	4.49E-05	2.91E-06	1.60E-06	1.31E-06	2.19E-06	8.64E-07	1.32E-06	6.98E-07	4.72E-07	2.26E-07
1.688	84.4	0.189	0.811	5.50E-05	9.72E-06	4.52E-05	2.80E-06	1.61E-06	1.19E-06	2.14E-06	8.71E-07	1.27E-06	6.66E-07	4.75E-07	1.91E-07
1.965	85.2	0.202	0.798	4.82E-05	9.71E-06	3.85E-05	2.69E-06	1.61E-06	1.09E-06	1.93E-06	8.68E-07	1.06E-06	6.81E-07	4.73E-07	2.07E-07
2	85.3	0.189	0.811	4.80E-05	9.72E-06	3.83E-05	2.69E-06	1.61E-06	1.09E-06	1.94E-06	8.71E-07	1.07E-06	6.67E-07	4.75E-07	1.93E-07
2.18	85.7	0.195	0.805	4.48E-05	9.72E-06	3.51E-05	2.53E-06	1.61E-06	9.23E-07	1.74E-06	8.70E-07	8.73E-07	6.33E-07	4.74E-07	1.59E-07
2.32	86.1	0.208	0.792	4.26E-05	9.70E-06	3.29E-05	2.48E-06	1.60E-06	8.75E-07	1.94E-06	8.67E-07	1.08E-06	5.95E-07	4.73E-07	1.23E-07
2.62	86.9	0.202	0.798	4.23E-05	9.70E-06	3.26E-05	2.38E-06	1.60E-06	7.80E-07	1.68E-06	8.68E-07	8.14E-07	6.18E-07	4.73E-07	1.45E-07
2.89	87.6	0.207	0.793	3.81E-05	9.70E-06	2.84E-05	2.20E-06	1.60E-06	5.99E-07	1.58E-06	8.67E-07	7.08E-07	6.02E-07	4.73E-07	1.29E-07
3.2	88.4	0.212	0.788	3.65E-05	9.69E-06	2.68E-05	2.18E-06	1.60E-06	5.83E-07	1.65E-06	8.66E-07	7.86E-07	5.58E-07	4.72E-07	8.55E-08
4.32	91.4	0.202	0.798	3.62E-05	9.71E-06	2.65E-05	2.84E-06	1.61E-06	1.23E-06	1.06E-06	8.68E-07	1.92E-07	5.81E-07	4.73E-07	1.07E-07
4.493	91.8	0.202	0.798	3.27E-05	9.71E-06	2.30E-05	2.00E-06	1.61E-06	3.97E-07	1.00E-06	8.68E-07	1.32E-07	5.73E-07	4.73E-07	9.92E-08
4.832	92.7	0.207	0.793	2.91E-05	9.70E-06	1.94E-05	1.88E-06	1.60E-06	2.72E-07	9.80E-07	8.67E-07	1.13E-07	5.51E-07	4.73E-07	7.84E-08
6.053	95.9	0.186	0.814	2.69E-05	9.73E-06	1.72E-05	1.76E-06	1.61E-06	1.49E-07	9.33E-07	8.72E-07	6.08E-08	5.42E-07	4.75E-07	6.69E-08
6.332	96.7	0.186	0.814	2.35E-05	9.73E-06	1.38E-05	1.65E-06	1.61E-06	3.57E-08	-	-	-	5.22E-07	4.75E-07	4.69E-08
8.834	103.2	0.132	0.868	2.15E-05	9.81E-06	1.17E-05	-	-	-	-	-	-	5.22E-07	4.80E-07	4.14E-08
17.628	126.4	0.020	0.980	1.92E-05	9.97E-06	9.19E-06	-	-	-	-	-	-	5.01E-07	4.92E-07	8.74E-09
22.542	139.3	0.000	1.000	1.69E-05	1.00E-05	6.90E-06	-	-	-	-	-	-	-	-	-

Table 3.4.2: Mass balance calculation for Fe, Mn, Zn and As

Pumped Volume	Reaction Time (h)	pH	pCO$_2$	Surface Area	LogR(Fe)	log R(Mn)	logR(Zn)	logR(As)
m^3	hours		atm	m^2	mol/m^2/h	mol/m^2/h	mol/m^2/h	mol/m^2/h
0.1	80.3	5.6	1.15E+00	157.00	-6.067	-7.556	-6.877	-8.457
0.323	80.9	5.7	6.54E-01	507.11	-6.232	-7.722	-7.041	-8.727
0.593	81.6	5.9	5.00E-01	931.01	-6.441	-7.992	-7.600	-8.950
0.685	81.8	6.07	4.36E-01	1075.45	-7.064	-8.687	-8.388	-9.532
0.989	82.6	6.23	2.79E-01	1552.73	-7.118	-8.670	-8.490	-9.469
1.296	83.4	6.25	2.37E-01	2034.72	-7.041	-8.612	-8.477	-9.357
1.688	84.4	6.33	1.85E-01	2650.16	-7.101	-8.679	-8.653	-9.475
2.18	85.7	6.36	1.75E-01	3422.60	-7.231	-8.810	-8.834	-9.575
2.32	86.1	6.38	1.59E-01	3642.40	-7.833	-9.409	-9.319	-10.262
2.62	86.9	6.4	1.56E-01	4113.40	-7.563	-9.184	-9.165	-9.916
2.89	87.6	6.4	1.45E-01	4537.30	-7.714	-9.390	-9.318	-10.057
3.2	88.4	6.43	1.42E-01	5024.00	-7.727	-9.391	-9.261	-10.224
4.32	91.4	6.47	1.07E-01	6782.40	-7.320	-8.651	-9.461	-9.713
4.493	91.8	6.51	1.11E-01	7054.01	-8.212	-9.974	-10.200	-10.577
6.332	96.7	6.57	9.19E-02	9941.24	-7.579	-10.165	-10.453	-10.047

Table 3.4.3: Rate of reaction estimated for each reactive chemical elements (Fe, Mn, As, Zn) calculated at each pumped volume. Values of total surface of rock in contact with fluids A (m^2) are reported, and values of pH, pCO$_2$ and reaction time (hours)

3.4.3. Influence of pH and pCO_2 on rate of release

Fig. 3.4.4 show the estimate rate R as a function of log (H^+) and pCO_2. The pCO_2 values were calculated from pH and alkalinity measurements.
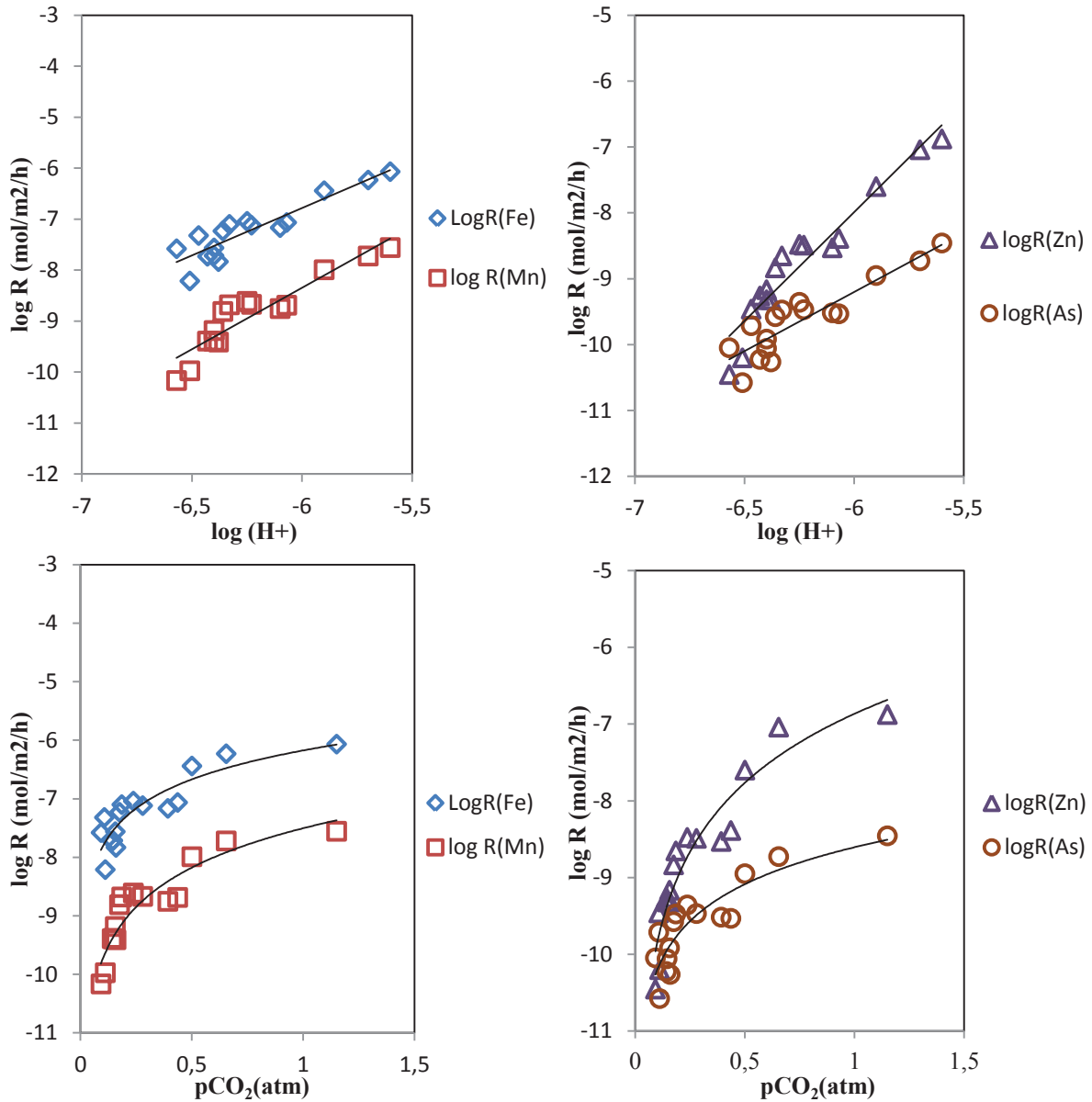
Fig3.4.4: in-situ reaction rate for Fe, Mn, As, Zn, plotted as a function of log(H+) and pCO2.

We found that in-situ reaction rate are ranging from $8.56 \cdot 10^{-7}$ to $4 \cdot 10^{-9}$ mol/m^2/h for Fe, $4.63 \cdot 10^{-9}$ to $1.73 \cdot 10^{-12}$ mol/m^2/h for Mn, $3.49 \cdot 10^{-9}$ to $2.2 \cdot 10^{-11}$ mol/m^2/h for As, $1.33 \cdot 10^{-7}$ to $3.52 \cdot 10^{-11}$ mol/m^2/h for Zn. Rates decreases are correlated to an increase in pH from 5.7 to 6.85. Variations of in-situ reaction rate as a function of pH and pCO_2 variation are different for each individual reactive chemical element.

107

In order to quantify the influence of pH on reaction rate, the following relation was used:

$$R = k[H^+]^n \qquad (3.4.10)$$

Where R is the rate of release ($mol/m^2/h$), k is the coefficient of reaction rate ($mol/m^2/h$), $[H^+]$ the proton concentration, and *n* is the reaction order. To quantify the influence of pH variation on the in-situ dissolution rate, coefficient k and *n* can be calculated by linear regression using the last square criterion. Results are showed in Table 3.4.4.

	k	n	R^2
R(Fe)	4.9	1.94	0.82
R(Mn)	5.86	2.36	0.78
R(Zn)	12.2	3.35	0.89
R(As)	2.04	1.87	0.79

Table 3.4.4: Empirical rate law for reaction of Fe, Mn, As, Zn as function of pH, coefficient determination R^2

3.4.4. Discussion

The release of dissolved metals induced by CO_2 injection into groundwater was estimated in this experiment. As expected, dissolved CO_2 provides protons that accelerate mineral dissolution. Dissolution of the bulk rock material was clearly indicated in this *in situ* experiment by a shift upward from the mixing lines with dilution of the injected solution by aquifer water (see Fig.3.4.2). An enrichment of dissolved iron, manganese, zinc and arsenic was observed. A corrected concentration was calculated using mass balance calculation of sulfate as inert tracer to estimate the part of dissolved elements actually mobilized by CO_2-water-rock interaction processes. Using the calculated mass transfer terms of Fe, Mn, As, Zn, the incubation time, and the calculated surface areas, bulk rock dissolution rates of aquifer material were estimated.

The dependence of in-situ reaction rate on pH and pCO_2, was used to determine empirical rate laws to correlate the rate of release of elements and bulk rock dissolution reaction as function of pH for each individual reactive chemical elements, i.e. Fe, Mn, As and Zn.

For range of pH increase from 5.7 to 6.7, the in situ dissolution rate increases by 2 order of magnitude for Fe, Mn, and As, and 4 orders of magnitude for Zn.

Zinc is known a very mobile element in the environment, due to high reactivity with pH, and speciation with sulfate and carbonate. The source of zinc could be the desorption from the oxi-hydroxide minerals or carbonate minerals, plus the combined effect of speciation with carbonate and sulfate (Gräfe and Sparks 2005, Gräfe et al 2004).

Desorption from ferrihydrite can be also proposed for As, however but in lower proportion, this element is not influenced by secondary reaction of speciation with HCO_3^- and SO_4^{2-} anions, as developed previously. The release of As by desorption from iron hydroxide surface could be issued from the competitive sorption with carbonate (Appelo et al 2002, Arai et al 2004, Brechbül 2012).

It is important to highlight that in-situ reaction rate calculation is theoretically possible for elements for which no effect of precipitation or sorption reactions occur. In the particular case of iron, geochemical calculation showed potential precipitation of goethite (α-FeOOH) and hematite (Fe_2O_3). Although, goethite and hematite are more stable than ferrihydrite (Stumm and Morgan 1996). Their kinetic of precipitation are slower than dissolution kinetics of ferrihydrite. Schwertmann and coworkers works (1983, 2003, 2004) on the effect of pH and temperature on the conversion of ferrihydrite to goethite/hematite showed that half-life reaction of conversion in the pH range 5 to 7 and 15°C ranging from hundred days to several years. Therefore, these reactions were considered as negligible on the iron concentration and dissolution kinetic of Ferrihydrite $Fe(OH)_3$.

Saturation index calculation suggested dissolution of iron oxide as main source of dissolved metals.The influence of pH on rate release was calculated by empirical rate law which describe the rate of dissolution as a function of H^+ concentration. In our case, dissolution rate were determined per square meter of the bulk rock in contact with reacting fluid estimated by porosity. Since iron oxides is a major constituent of the bulk rock, this relation can be applied to iron release, but higher incertitude does exist for other reactive elements. Our calculation shows that the rate of realease of oxi-hydroxide metals as a function of H^+ obeys to a second order rate law for Fe, Mn and As, and fourth order for Zn suggesting that dissolution of Fe, Mn, As and Zn minerals requires protonation of 2 to 4 metals atoms on the "oxide-hydroxide mineral surfaces". Previous works on parameters influencing the rate of dissolution of minerals, metals carbonate and oxides dissolution rate is influenced by effect of carbonate and sulfate lignads affinity of the reaction (Stumm and Morgan 1996; Lasaga 1998; Pokrovsky et al 2002, 2004, 2005, Brantley et al. 2008, Bruno et al 1992, 2000; Pokrovsky and Schott 2002).. The combination of these different phenomena might explain the complex order of reaction of oxide this dissolution on surface metal oxide and carbonate. However such assumption should be verified by experimental protocol based on pure mineral phase by measuring rate of dissolution under different pH.

To conclude, in this part we proposed a method to quantify rate of release of reactive metals (Fe, Mn, Zn, As) for application to single push-pull test experiment. SO_4 and Cl^- concentrations in the injected solution had a different signature compared to the aquifer, thus were used as inert tracers only affected by fluid dynamic (i.e. dispersion, advection, diffusion, mixing). We estimated a fluid dynamic

correction factor by the difference between injected and extracted amount of Cl^- and SO_4. The amount of metal release resulting was estimated by the total measured concentration over the entire pumping phase, corrected by fluid dynamic factor. The influence of pH on release of metals was used to estimate a field rate of release, considering an homogeneous porosity. These results highlights the role of hydroxide iron dissolution in the release of metals induced by artificial CO_2 injection in aquifer. A kinetic reaction rate of ferrihydrite dissolution was estimated using empirical rate law and indicates that mechanism of ferrihydrite dissolution is ruled by a complex order of reaction, close to two. We propose that this complex order of reaction can be explained by the influence of complexation by sulfate and dissolved carbonate on the affinity of dissolution reaction and on complexation of active oxide surface site.

3.4.5. Estimation of reactive surface area of iron oxide

In the previous section, the rate of element release was estimated considering that dissolution affect an homogenous bulk rock

As previously developed, during the 80h of incubation time, no transfer/exchange of matter occurred into the aquifer. Therefore, variation in chemical concentration were considered as exclusively influenced by chemical reaction. During this phase, variation of reaction affinity can estimated between initial condition after the injection of CO_2.

3.4.5.1.   Influence of mineral reactive surface area

As extensively developed in part 1 and 2, in situ kinetic rates are extremely difficult to determine. In particular, the comparison between mineral weathering rates determined in the laboratory and in the field reveals large discrepancies. One of the main reasons for this discrepancy is due to the difficulty of estimating the reactive surface area of minerals (RSA). However, this estimation is necessary to model and predict the evolution of a CO_2-water-rock system. Alternative approach exists to estimate reactive surface area of minerals using chemical data (Marini et al 2000, Malmstrom et al 2000, Sciewlevski and Zuddas 2010, Rillard and Zuddas 2012). Since the amount of reaction per unit of time is dependent of RSA variable, and RSA is poorly constrained, we can take the approach of using fluid chemical compositions to calculate RSA's accounting for the observed fluid compositions.

3.4.5.2.   Kinetic rate of reaction calculation and estimation of reactive surface area

The dissolution of ferrihydrite $Fe(OH)_3$ was identified as the major source of Fe(III) release. In our experiment, pH varied from neutral (pH=7.3) in baseline water, to acidic condition after the CO_2 injection (pH=5.7). Considering the dissolution of ferrihydrite $Fe(OH)_3$ in acidic condition, we can write:

$$Fe(OH)_3 + 3H^+ \leftrightarrow Fe^{3+} + 3H_2O \qquad \log K=12{,}56^*$$

$$^*\log K \text{ value was taken from wateq.4f database}$$

Ferrihydrite dissolution induced release of trivalent iron Fe^{3+}. Further, kinetic constant of reaction rate does exist for ferrihydrite dissolution in acidic and neutral condition (Pallandri and Kharaka 2004). The field rate of dissolution can be calculated by:

$$R_i = \frac{\Delta n_i}{\Delta t} \qquad (3.4.11)$$

111

where n corresponds to the number of mole added by reaction of the ith reactive species, and t tends for the time of reaction, therefore R_i is explained in mol/time. We can estimate the total mol of Fe^{3+} added by $Fe(OH)_3$ dissolution $T(Fe^{III}_{.react})$ by:

$$T(Fe^{III}_{react}) = (Fe^{III}_{react} - Fe^{III}_{previous\ to\ injection}) \times V\ pump. \qquad (3.4.12)$$

Where the reactive time corresponds to the time since the injection stopped, Fe^{III}_{react} is the total number of moles of iron added by reaction, and V the pumped volume. The term R_i can be calculated between the time since injection stopped, where iron concentration is considered as equal to previous to injection concentration, and the peak of iron, observed after 0,323 m^3 of pumped fluid . This point corresponds to an elapsed time of 80,9 hours since the injection stopped. As previously mentioned, Fe^{3+} was estimated by difference between Fe^{II} concentration and Fe(t).
Ri can be defined as follows:

$$Ri = \frac{T(Fe^{III}react.)}{Reactive\ time} \qquad (3.4.13)$$

Kinetics dissolution rate can be determined using empirical rate law (Lasaga et al. 1994, Steefel and Lasaga 1994), including a pH dependency (Palandri and Kharaka 2004), defined as follows:

$$\bar{R_\iota} = k\ (1 - \Omega)^n \qquad (3.4.14)$$

Where Ω is the saturation index, n is the reaction order defined as a function of Ω, here chosen as equal to n=1, and k is defined as :

$$k = \begin{bmatrix} k_{25}^{nu} exp\left[\frac{-Ea}{r}\left(\frac{1}{T} - \frac{1}{298,15}\right)\right] \\ + k_{25}^{H+} exp\left[\frac{-Ea}{r}\left(\frac{1}{T} - \frac{1}{298,15}\right)\right] \times a_{H+} \end{bmatrix} \qquad (3.4.15)$$

Where r is the gas constant, T the temperature in Kelvin, k_{25}^{H+} and k_{25}^{nu} at kinetic rate constants determined at 25°C for neutral and acidic conditions respectively. The activity of H$^+$ was fixed at pH=5.7, which corresponds to the pH of the injected solution and to the pH of the first sample collected 80h after injection.
Following constants are defined for ferrihydrite $Fe(OH)_3$ dissolution kinetic (Palandri and Kharaka 2004):

	neutral mechanism		acid mechanism	
	k_{25} (mol/m^2/s)	Ea (kJ/mol)	k_{25} (mol/m^2/s)	Ea (kJ/mol)
Ferrihydrite Fe(OH)$_3$	2.52×10^{-12}	62.76	2.34×10^{-7}	43.54

Table 3.4.5: constant rate values (k) and activation energy values (Ea) used to calculate R_i

Since R and $\bar{R}$ are defined, reactive surface area can be defined by:

$$R_i = S\bar{R}_i \qquad (3.4.16)$$

Where R_i corresponds to field dissolution rate, calculated by equation (3.4.11), and $\bar{R}_i$ corresponds to the absolute dissolution rate. Calculated values for all of the parameters are listed in Table 3.4.6:

Parameters	units	calculated values
R_i	mol/s	$5.051 \cdot 10^{-8}$
$\bar{R}_i$	mol/m^2/s	$2.954 \ 10^{-12}$
Reactive time	hour	80,9
pH in situ		5.7
T(Fe^{III}react)	mol	0.0147
S_i	m^2	17100

Table 3.4.6: List of parameter values used to quantify kinetic dissolution rate and results for reactive surface area calculation

This result suggests that, at the peak of concentration of iron, the corresponding total RSA of ferrihydrite is equal to 17100 m^2, (Table 3.4.6).

Fe$^{(III)}$ oxide such as ferrihydrite are known to have large specific area. Shwertmann (1991), Hiemstra and Van Riemsdijk (2009) works based on BET method and multisite surface complexation model showed values range of 300 to 600 m^2/g for natural and synthetic ferrihydrite. Our results are consistent with these data, suggesting that such important specific area for Ferrihydrite are plausible.

It is important to note that high values of reactive surface area are not measurable by classical field technique used to evaluate porosity of soil and aquifer, based usually on hydraulic or electrical resistivity tests. It is important to keep in mind that by our calculation the total concentration of Fe^{3+} was considered as issued from ferrihydrite dissolution, thus the production of Fe^{3+} by oxidation of Fe^{2+} is considered as negligible. This hypothesis was made considering the important effect of Fe^{2+} speciation. According to speciation calculation (see part 3.3), 40% of total dissolved Fe is complexed

by SO_4^{2-} and HCO_3^-. Therefore the oxidation of Fe^{2+} on Fe^{3+} was considered as negligible comparing to total Fe^{3+} concentration.

3.5. Conclusion on field experiment

We performed a field experiment consisting on injection of water saturated in CO_2 following a single well push-pull test protocol in subsurface aquifer. The aquifer zone was situated in fractured sandstone, composed by quartz, dolomite, significant amount iron oxide-hydroxide and trace metals elements (Mn, Zn, As).

Chemical analyses of water samples collected after CO_2 injection showed, decrease in pH (from 7.3 to 5.7), increase in alkalinity by a factor two(from $6 \cdot 10^{-3}$ to $1 \cdot 10^{-2}$ mol/L), and increase in pCO_2 (from 1 10^{-2} to 1,2 atm). Concerning major chemical elements, a weak increase in cations (+30% for Ca^{2+} and Mg^{2+}) was observed. Higher enrichments were observed for dissolved metals, with increases by one order of magnitude for Fe and Zn, by factor five for Mn, and by a factor two for As.

Thermodynamic calculation was used to identify main reactions paths that may controlled fluid composition, and metal speciation. Our results suggested that alkalinity production, calcium and magnesium release involved the dissolution of dolomite. Release of iron involved the dissolution of iron hydroxide ($Fe(OH)_3$) and carbonate minerals ($FeCO_3$). E_h values were calculated from Fe^{II}/Fe^{III} measurements and compared to measured values. Our results suggested that redox conditions were controlled by reaction involving Fe^{II}-Ferrihydrite-Siderite. We proposed that source of Fe^{II} was dissolution of siderite and source of Fe^{III} was dissolution of ferrihydrite. Main enrichments were observed for divalent metals (Zn^{II}, Fe^{II} and Mn^{II}) potentially enhanced by speciation with hydrogenocarbonates and sulfates in the aqueous phase. Speciation calculation showed that proportion of 40% to 50% of total manganese, iron, and zinc was under the form of complex with sulfate and carbonate.

Rates of release for dissolved metals were estimated by using measured concentration of Fe, Mn, Zn and As as a function of time since injection stopped and pumped volume. The influence of mixing between injected solution and baseline aquifer water was estimated by calculating percentage of recovery of injected mass of SO_4, identified as inert tracer. We found a good correlation between rate of release and pH and pCO_2. Rates of release were calculated by empirical rate law as a function of H^+ concentration and revealed that involved reactions followed second order of reaction for Fe, Mn and As, and third order for Zn. Assuming that main sources of metal are dissolution of metal oxides, our results suggest that in our experimental conditions, dissolutions of metals oxide are not elementary reactions, but follow a complex order of reactions. Other mechanism such as complexation by carbonate and sulfate would affect dissolution of iron oxide.

We suggest that dissolution kinetics of iron oxides were enhanced by formation of aqueous complexe and formation of surface ligand on metals oxides surfaces. Complexation of Fe^{II} might also affected the redox conditions by maintaining high concentration of Fe^{II} in solution and influencing the Fe^{II}/Fe^{III} proportion.

However, main sources of arsenic and zinc could not be properly identified by thermodynamic approach. Mobilization of these elements were probably a combination of different phenomenas such as desorption from hydroxide surfaces, dissolution of sulfur species or carbonate species..

Further, on the case of Ferrihydrite $Fe(OH)_3$ dissolution, estimated field rate was compared to kinetic rate constant of ferrihydrite dissolution determined for pure minerals phase. By this approach the proportion of reactive surface area of ferrihydrite was estimated. Results suggested a reactive surface area of several thousand square meters. Such a value cannot be quantified by classical available field investigation method (i.e.porosity or permeability measurement). Therefore this confirms the importance of taking into account the reactive surface area of mineral for evaluating the storage capacity of reservoir and the risk of dissolved metals involved with perturbation of pCO_2.

4.   General conclusion

The effect of CO_2 perturbation on water-rock interactions processes in natural system was investigated in two different time and space scales. In both cases the approach was based on using fluid chemical composition as input data to evaluate the effect of CO_2 perturbation on chemical equilibrium and kinetics of reactions in natural context.

In the first part of this work, our approach consisted on using chemical data from natural hydrothermal CO_2-rich water, representing system with long-term (>1000 years) interaction processes, over a large space scale (~100km^2). In the second part we performed a field experiment of CO_2-water mix injection in a subsurface aquifer to study the impact pCO_2 perturbation on groundwater composition and mineral-rock interaction processes, with special focus on dissolved metals behaviors. In the second case, observation time scale were 3 to 6 days, and space scale was ≤1000m^2.

The evolution of chemical compositions showed that CO_2 perturbation provoked systematic changes in pH, and alkalinity, as well as increase in the aqueous concentrations of naturally occurring major cations species. This increase in major cations and alkalinity was induced by minerals dissolution involved with fluid acidification. These observations were consistent with previous CO_2 injection experiments made in a deep sedimentary aquifer (Kharaka et al 2006, 2009), in a deep basaltic aquifer (Matter et al 2007), and in a shallow sedimentary aquifer (Kharaka 2010, Zheng 2012).

Release of chemical elements induced by CO_2 perturbation was studied by kinetic approach in order to estimate reactive surface area (RSA) of minerals using fluid chemical data. We found that for natural system such as geothermal field, the RSA cannot be determined by absolute values due to the lack of knowledge on the reaction time and reservoir properties. However order variation of mineral RSA can be estimated. Results showed that RSA could varied from two to four order of variation over the entire CO_2 perturbation.

Results of field experiment showed that release of major cations (Ca^{2+} and Mg^{2+}) involved with CO_2 perturbation was induced by carbonate mineral dissolution such as dolomite. However, the observed increase in dissolved calcium and magnesium was not significant (nearly 30%). Despite the low increase in major cations, an increase of about one order of magnitude was observed for dissolved metals cations such as iron, manganese and zinc, and an increase by a factor two for arsenic. Higher enrichments were observed for bivalent metals Mn^{II}, Zn^{II}, Fe^{II}. Chemical equilibrium calculation showed that 30% to 50% of total bivalent metals were complexed with hydrogenocarbonate and sulfate anions species. We propose that effect of complexation would explain the higher enrichment

for bivalent metals, by their affinity to complex which increases their solubility and accelerates their dissolution kinetics. Saturation index calculation showed that dissolution of metals oxide and hydroxide occurred after CO_2 injection. Considering effect of fluid dynamic (transport and mixing), we estimated a fluid dynamic correction factor by the difference between injected and extracted amount of Cl and SO_4. The amount of reactive elements resulting from the chemical reactivity has been estimated by the total measured concentration corrected by fluid dynamic factor. We proposed an empirical model of rate of metals releases $R=k[H^+]^n$. Results for iron and manganese showed that reaction operated following a second order of reaction. These results suggest that reaction are not elementary reaction. We propose that this complex order of reaction is explained by the influence of complexation by sulfate and hydrogenocarbonate on reaction mechanism.

This work highlighted that a small quantity of CO_2 is sufficient to mobilize significant quantity of dissolved trace metals in mineralized reservoir rocks. Therefore this point should be carefully viewed to improve the safety of CO_2 geological storage site. Enrichment in dissolved iron and manganese induced by CO_2 perturbation observed over our experiment are comparable to previous published results by Kharaka et al (2006, 2009) where 1600 tones of CO_2 was injected at 1500m depth in deep saline aquifer under supercritical states. In our case only $3m^3$ of water saturated in CO_2 (equivalent to approximately 6 kg of "pure" CO_2) was injected in non supercritical state. Considering these results, the presence of metal oxide on the reservoir rock, and the combined effect of complexation of metallic cations with major anions such as SO_4^{2-} and HCO_3^- should be evaluate for further investigation. Specific experiment for studying the dissolution kinetics of metals oxides as a function of pCO_2, pH, and anions concentration (such as carbonate and sulfate) might be interesting for future work. The use of metals isotop such as $^{68}Zn/^{66}Zn$; $^{57}Fe/^{54}Fe$ could constitute an interesting additional tool to identify main sources of dissolved metals, and may also be useful in the evaluation of complexation effect (Aucour et al 2011, Juillot et al 2011, Marechal and Albarède 2002).

To improve geochemical predictive models for long term CO_2 geological storage, our experimental results and interpretation must be extended and compared to larger scale and different geological context. Further, the Reactive Surface Area of minerals appears as a key parameter to define source terms in geochemical model applied to carbon sequestration environments. Because of the lack of site-specific data for key model parameters such as suitable kinetic rate and mineral reactive surface areas, our results clearly point to the need for a comprehensive characterization of the rock-metal associations and CO_2-water-rock interaction process in the subsurface to better constrain model results. Consequently, our geochemical model should be regarded as an exercise that yields a plausible, but uncertain interpretation of the chemical processes taking place in response to CO_2 perturbation in groundwater systems.

Despite the specific technological application, this work attempts to better understanding the basic of water-rock exchange occurring into natural environment. Phenomenology and model described will find a lot of implications in geosciences and environmental sciences, such as the underground waste storage, radioactive waste storage, geothermic, or mine waste water management.

References:

Aagard P., Helgeson H.C., Thermodynamic and kinetic constraints on reaction rates among minerals and aqueous solutions: I. Theoritical consideration, American Journal of Sciences, 1982, 282, pp 237-285

Angelone M., Gasparini C., Guerra M., Lombardi S., Pizzino L., Quattrocchi F., Sacchi E., Zuppi G.M., Fluid geochemistry of the Sardinian Rift-Campidano Graben (Sardinia, Italy): fault segmentation, seismic quiescence of geochemically ''active'' faults, and new constraints for selection of CO_2 storage sites, Applied Geochemistry, 2005, 20, pp 317–340

Appelo C.A.J, Van Der Weiden M.J.J., Tournassat C., Charlet A. Surface Complexation of Ferrous Iron and Carbonate on Ferrihydrite and the Mobilization of Arsenic, 2002, Environmental Sciences and Technology, 36, 3096-3103

Arai Y., Sparks D.L., Davis J.A., Effects of Dissolved Carbonate on Arsenate Adsorption and Surface Speciation

Aucour A.M., Pichat S., Macnair M.R., Oger P., Fractionation of Stable Zinc Isotopes in the Zinc Hyperaccumulator *Arabidopsis halleri* and nonaccumulator *Arabidopsis petraea*, 2011, Environ. Sci. Technol., vol. 45, pp 9212–9217

Bachu S., Sequestration of CO_2 in geological media: criteria and approach for site selection in response to climate change. Energy Conver. Mgmt, 2000, 41, pp 953-970

Bachu S., Sequestration of CO_2 in geological media in response to climate change: road map for site selection using the transform of the geological space into the CO_2 phase space. Energy Conver. Mgmt, 2002, 43, pp 87-102

Bachu S., Adams J.J., Sequestratin of CO_2 in geological media in response to climate change: capacity of deep saline aquifers to sequester CO_2 in solution. Energy Conver. Mgmt, 2003, 44, pp 3151-3175

Beaucaire C., Criaud A., Michard G., Contrôle des concentrations de certains éléments trace (As, Sb, Ge, U, Ra, Ba) dans les eaux du cézallier (Massif Central, France) Chemical Geology, 1987, 63, pp.85-99

Bénézeth P ,Ménez B, Noiriel C. CO_2 geological storage: Integrating geochemical, hydrodynamical, mechanical and biological processes from the pore to the reservoir scale . Chemical Geology, 2009, 265 : 1-2.

Bénézeth P, Palmer AD, Anovitz LM, Horita J. Dawsonite synthesis and re-evaluation of its thermodynamic properties from solubility measurements: Implications for mineral trapping of CO_2 . Geochim. Cosmochim. Acta, 2007, **71** : 4438- 55 .

Benoit G. Clean technique measurement of Pb, Ag and Cd in freshwater: a redefinition of metal pollution, 1994, Environmental Sciences and Technology, 28, pp. 1987-1991

Benson SM, and Cook , P. Underground Geological Storage . In: Carbon Dioxide Capture and Storage: Special Report of the Intergovernmental Panel on Climate Change (IPCC) . Cambridge University Press , Interlachen, Switzerland , 2005, pp. 5-1 to 5-134 .

Benson SM and Cole DR. CO_2 sequestration in deep sedimentary formations . Elements 4 (5), In: DR Cole and EH Oelkers (eds.) Carbon Dioxide Sequestration. 2008, pp. 305-310 .

Berner, R.A., Holdren, G.R. Mechanism of feldspar weathering. II: observations of feldspars from soils. Geochimica et Cosmochimica Acta, 1979, 43, 1173–1186.

Berner, R.A., Schott, J. Mechanism of pyroxene and amphibole weathering II. Observations of soil grains. American Journal of Science, 1982, 282, 1214–1231.

Boisson A., Etude multi-échelles des réactions de dénitrification dans les aquifères hétérogènes: Approches expérimentales de l'influence des écoulements sur la réactivité biogéochimique, PhD Thesis, Université Rennes 1 version 1 - 17 May 2011, 303 p.

Brantley S.L., Kubicki J. D.. White A. F., Kinetics of Water-Rock Interaction. 2008, Springer 852p.

Brechbühl Y., Christl I., Elzinga E.J., Kretzschmar R., Competitive sorption of carbonate and arsenic to hematite: Combined ATR-FTIR and batch experiments, 2012 Journal of Colloid and Interface Science, 377, pp. 313–321

Cantucci B., Montegrossi G., Vaselli O., Tassi F., Quattrocchi F., Perkins E.H. Geochemical modeling of CO_2 storage in deep reservoirs: The Weyburn Project (Canada) case study. Chemical Geology, 2009, 265, pp 181-197

Cidu R., Bahaj S., Geochemistry of thermal waters from Morocco, Geothermics, 2000, 29, pp.407-430

Chenevoy M., Piboule M., Hydrothermalisme spéciation métalliques hydrique des systèmes hydrothermaux, EDP Sciences, 2007. 619 p.

Chou L. and Wollast R. Study of the weathering of albite at room temperature and pressure with a fluidized bed reactor. Geochimica Cosmochimica Acta, 1984, 48, pp. 2205-2218.

Criaud A., Fouillac C., Etude des eaux thermominérales carboguzeuses du Massif Central 1. Potentiel d'oxydoréduction et comportement du fer, Geochimica et Cosmochimica Acta, 1986, 50, pp. 525-533

Criaud A., Fouillac C., The distribution of arsenic (III) and arsenic (V) in geothermal waters: Examples from the Massif Central of France, the Island of Dominica in the Leeward Islands of the Caribbean, the Valles Caldera of New Mexico, U.S.A., and southwest Bulgaria, Chemical Geology, 1989, 76, pp 259-269

Czernichowski-Lauriol I., Pauwels H., Vigouroux P., Le Nindre Y.M. The French Carbogaseous Province: An Illustration of Natural Processes of CO2 Generation, Migration, Accumulation and Leakage. Greenhouse Gas Control Technologies - 6th International Conference, Volume I, 2003, pp 411-416

Davidson W., Seed G., The kinetics of the oxidation of ferrous iron in synthetic and natural waters, Geochimica et Cosmochimica Acta, 1983, 47, pp.67-69

Davwn W., Seed G. The kinetics of the oxidation of ferrous iron in synthetic and natural waters, Geochimica et Cosmochimica Acta, 1983, 47, pp. 67-79

De Donder T., Lecons de Thermodynamique et de Chimie Physique (Lessons of Thermodynamics and Physical Chemistry)*,* Paris: Gauthier-Villars, 1920, 117 pp

Friedmann SJ, Geological carbon dioxide sequestration., Elements, 2007, 3, pp.179- 84

Fessenden JE, Stauffer , PH and Viswanathan , HS Natural Analogs of Geologic CO_2 Sequestration: Some General Implications for Engineered Sequestration. In: BJ McPherson and ET Sundquist (eds.). Carbon Sequestration and Its Role in the Global Carbon Cycle. American Geophysical Union, Geophysical Monograph 183 , Washington, D.C., 2009, pp. 135- 46 .

Gaus I., Pascal A., Andre´ L., Lions J., Jacquemet N., Durst P., Czernichowski-Lauriol I. and Azaroual M. Geochemical and solute transport modelling for CO2 storage, what to expect from it? Int. J. Greenhouse Gas Control, 2008, 2, pp. 605–625.

Gautier, J.M., Oelkers, E.H., Schott, J., Are quartz dissolution rates proportional to B.E.T. surface areas? Geochimica et Cosmochimica Acta, 2001, 65, pp.1059–1070.

Gilfillan SMV , Sherwood-Lollar B, Holland G , Blagburn D , Stevens S , Schoell M , Cassidy M , Ding Z , Zhou Z , Lacrampe-Couloume , G, Ballentine ,CJ Solubility trapping in formation water as dominant CO2 sink in natural gas fields, Nature, 2009, 458, pp.614 – 618.

Gilfillan SMV , Ballentine , CJ , Holland , G , Blagburn , D ,,Sherwood-Lollar B ,Stevens S , Schoell M, Cassidy M. The noble gas geochemistry of natural CO_2 gas reservoirs from the Colorado Plateau and Rocky Mountain provinces, USA . Geochim. Cosmochim. Acta, 2001, vol.72, pp. 1174- 98

Gräfe M., Sparks D.L., Kinetics of zinc and arsenate co-sorption at the goethite-water interface, Geochimica et Cosmochimica Acta, 2005, vol.69, pp.4573-4595

Gräfe M., Nachtegaal M., Sparks D.L., Formation of metal-Arsenate precipitates at the Goethite-Water Interface, Environmental Sciences and Technology, 2004,vol. 38, pp. 6561-6570

Grandstaff, D.E., Changes in surface area and morphology and the mechanism of forsterite dissolution. Geochimica et Cosmochimica Acta, 1978, vol.42, 1899–1901.

Gunter WD , Perkins , EH and McCann , TJ,Aquifer disposal of CO_2-rich gases: reaction design for added capacity . Energy Conversion and Management, 2008, vol. 34, pp. 941-948

Hageman K.J., Field J.A., Istok J.D., Schroth, "Forced mass balance" technique for estimating for transformation rates of sorbing solutes in groundwater. Environmental Sciences and Technology, 2003, 37, pp. 3920-3925

Haggerty R., Schroth M.H; Istok J.D., Simplified method of "push-pull" test data analysis for determing in situ reaction rate coefficients. Ground Water 1998, 36, (2), 314-324.

Haszeldine SR. Carbon Capture and Storage: How Green Can Black Be? Science 2009, **325** : 1647-1652

Helgeson H.C., Garrels R.M., Mac Kenzie F.T., 1969. Evaluation of irreversible reactions in geochemical processes involving minerals and aqueous solutions II. Applications. Geochim. Cosmochim. Acta 33, 455-481

Helgeson H. C., Brown T. H., Nigrini A., Jones T. A., 1970. Calculation of mass transfer ingeochemical processes involving aqueous solutions., Geochimica et Cosmochimica Acta 34, pp.569-592

Helgeson H. C., Delany J. M., Nesbitt H. W., Bird D. K.. Summary and critique of the thermodynamic properties of rockforming minerals. American Journal of Sci. ,1978, 229p

Helgeson H. C., Murphy W. M., Aagaard P. Thermodynamic and kinetic constraints on reaction rates among minerals and aqueous solutions. II. Rate constants. effective surface area. and the hydrolysis of feldspar. et Cosmochimica Acta, ,1984, vol.48, pp.2405-2432

Hendriks C.A., Black K., Underground storage of carbon dioxide. Energy Conver. Mgmt 1993, 34, pp 949-57

Hermanrud C, Andresen T., Eiken O., Hansen H., Janbu A., Lippard J., Bolås H.N., Simmenes T.H., Teige G.M.G., Østmo S. Storage of CO_2 in saline aquifers–Lessons learned from 10 years of injection into the Utsira Formation in the Sleipner area, Energy Procedia, 2009, 1, pp 1997-2004

Hitchon B. Aquifer Disposal of Carbon Dioxide . Geoscience Publishing Ltd., Sherwood Park, Alberta, Canada, 1996, pp. 165.

Hochella, Jr., M. F. and Banfield J. F. (1995) Chemical weathering of silicates in nature: a microscopic perspective with theoretical considerations. In Reviews in Mineralogy, vol. 31 (eds. A. F. White and S. L. Brantley). Mineralogical Society of America, Washington, DC, pp. 354–406.

Holloway S., Savage D., The potential for aquifer disposal of carbon dioxide in the UK. Energy Conver. Mgmt, 1993, 34, pp 925-932

Holloway S An overview of the underground disposal of carbon dioxide. Energy Convers Mgmt, 1997, 38:S193–S198

Holloway S, Pearce JM , Hards VL , Ohsumi T ,Gale J., Natural emissions of CO_2 from the geosphere and their bearing on the geological storage of carbon dioxide . Energy, 2007, **32** : 1194- 201.

Intergovernmental panel on Climate Change (IPCC), 2007 Climate Change 2007: The Physical Science Basis. Contribution of Working Group I to the Fourth,Assessment Report of the Intergovernmental Panel,on Climate Change [S Solomon , D Qin , M Manning ,,Z Chen , M Marquis, KB Averyt , M Tignor and HL Miller (eds.)]. Cambridge University Press , Cambridge, United Kingdom and New York, NY, USA , 996 pp.

Istok J.D., Humphrey M.D.; Schroth M.H; Hyman M.R.; O'Reilly K.T., Single well, "push-pull" test for in situ determination of microbial metabolic activities. Ground Water 1997, 4, 618-631.

123

Istok J.D., Field J.A., Schroth M.H., In situ determination of subsurface microbial enzymes kinetics, 2001, Groundwater, 39, pp. 339-355

Istok, J. D., J. A. Field, M. H. Schroth, B. M. Davis, and V. Dwarakanath (2002), Single-well ''push-pull'' partitioning tracer test for NAPL detection in the subsurface, Environmental. Sciences and Technology, 36, 2708–2716.

Juillot F., Maréchal C., Morin G., Jouvin D., Cacaly S., Telouk P., Benedetti M.F., Ildefonse P., Sutton S., Guyot F., Brown Jr. G.E., Contrasting isotopic signatures between anthropogenic and geogenic Zn and evidence for post-depositional fractionation processes in smelter-impacted soils from Northern France, 2011, Geochimica et Cosmochimica Acta, 75, pp. 2295-2308

Jury W.A., Roth K., Transfer functions and solute movement through soil, 1990, Boston: Birkhauser Verlag

Karamalidis A.K., Torres S.G., Hakala J.A., Shao H., Cantrell K.J., Carroll S., Trace Metal Source Terms in Carbon Sequestration Environments, Environmental Sciences and Technology, 2012, dx.doi.org/10.1021/es304832m

Keating E.H, Fessenden J., Kanjorski N., Koning D.J., Pawar R., The impact of CO_2 on shallow groundwater chemistry: observations at a natural analog site and implications for carbon sequestration, Environmental Earth Sciences, 2010, 60, pp 521-536

Kharaka Y.K., Cole D.R., Hovorka S.D., Gunter W.D., Knauss K.G., Freifeld B.M., Gaz-wtaer-rock interactions in Frio Formation following CO_2 injection: Implications for the storage of greenhouse gases in sedimentary basins, Geology, 2006, 34, pp 577-580

Kharaka Y.K., Cole D.R., Geochemistry of Geologic Sequestration of Carbon Dioxide in *Frontiers in Geochemistry: Contribution of Geochemistry to the Study of the Earth*, First edition. Edited by Russell S. Harmon and Andrew Parker. © 2011 Blackwell Publishing Ltd. Published 2011 by Blackwell Publishing Ltd.

Kharaka Y.K, Thordsen J.J., Hovorka S.D., Nance H.S., Cole D.R., Phelps T.J., Knauss K.G., Potential environmental issues of CO_2 storage in deep saline aquifers: Geochemical results from the Frio-I Brine Pilot test, Texas, USA, Applied Geochemistry, 2009, 24, pp 1106-1112

Koschel D, Coxam , J-Y , Rodier , L , Majer , V. Enthalpy and solubility data of CO_2 in water and NaCl(aq) at conditions of interest for geological sequestration. *Fluid Phase Equil*. 2006, **247** : 107-20

Knecht K., Schroth M.H., Schulin R., Nowack B., Development and Evaluation of Micro Push_Pull Tests to Investigate Micro-Scale Processes in Porous Media, Environmental Sciences and Technology 2011, 45, 6460–6467

Lackner KS. Carbon Dioxide Capture from Ambient Air . In: W Blum , M Keilhacker , U Platt , W Roether (eds.) The Physics Perspective on Energy Supply and Climate Change – A Critical Assessment, v. 2009 . Springer Verlag : Bad Honnef .

Lagneau, V , Pipart , A and Catalette , H. Reactive transport modeling of CO2 sequestration in deep saline aquifers . Oil & Gas Science and Technology, 2005, 60, pp. 231 – 47 .

Lasaga A. C., Rate laws of chemical reactions. In *Kinetics of Geochemical Processes*, Vol. 8 (ed. A. C. Lasaga and R. J. Kirkpatrick), 1981, pp. 1–68. Mineralogical Society of America.

Lasaga A. C. and Blum A. E., Surface chemistry, etch pits and mineral-water reactions, Geochimica et Cosmochimica Acta, 1986, 50, pp 2363-2379

Lasaga A. C. 1998. Kinetic Theory in the Earth Sciences. Princeton Series in Geochemistry.: 811 pp. Princeton, Chichester: Princeton University Press. ISBN 0 691 03748 5.

Lee J.H., Dolan M., Field J., Istok J. Monitoring bioaugmentation with single-well push-pull tests in sediment systems contaminated with trichloroethene. Environmental Sciences and Technology, 2010, 44, pp.1085–1092

Le Guern C., Baranger P., Crozet C., Bodénan F., Conil P., Arsenic trapping by iron oxyhydroxides and carbonates at hydrothermal spring outlets, Applied Geochemistry, 2003, 18, pp.1313-1323

Levenspiel O., The chemical reactor omnibook, 1989, Corvallis, Oregon State University Bookstore Inc.

Lewicki J , Oldenburg , C , Dobeck , L and Spangler , L. Surface CO2 leakage during the first shallow subsurface CO_2 release experiment. *Geophys. Res.Lett., 2007,* 34, L24402

Li X.F., Liu Y., 2010, First-principles study of Ge isotope fractionation during adsorption onto Fe(III)-oxyhydroxide surfaces, Chemical Geology, 278, pp.15-22

Lichtner P. C. (1996) Continuum formulation of multicomponentmultiphase reactive transport. In Reviews in Mineralogy, vol. 43 (eds. P. C. Lichtner, C. I. Steefel and E. H. Oelkers). Mineralogical Society of America, Washington DC, pp. 1–81.

Lichtner P. C. (1998) Modeling reactive flow and transport in natural systems. In Proceedings of the Rome Seminar on Environmental Geochemistry (eds. L. Marini and G. Ottonello). Pacini, Pisa, pp. 5–72.

Maher K. The dependence of chemical weathering rates on fluid residence time Earth and Planetary Science Letters, 2010, 294, 2010, pp 101-110

Maher K. The role of fluid residence time and topographic scales in determining chemical fluxes from landscapes Earth and Planetary Science Letters, 2011, 312, pp 48-58

Malmström M.A., Banwart S., Biotite dissolution at 25°C: the pH dependence of dissolution rate and stoichiometry, 1997, Geochimica et Cosmochimica Acta, 61, pp. 2779-2799

Malmström M., Destuni G., Banwart S.A., Strömberg B.H.E, 2000. Resolving the Scale-Dependence of Mineral Weathering Rates . Env. Sci. Tech. 34,. 1375-1378

Maréchal C., Albarède F., 2002, Ion-exchange fractionation of copper and zinc isotopes, Geochimica et Cosmochimica Acta, Vol. 66, pp. 1499–1509

125

Marini L., Ottonello G., Canepa M., Cipolli F. Water-rock interaction in the Bisagno valley (Genoa, Italy): application of an inverse approach to model spring water chemistry. Geochim. et Cosmochim. Acta, 2000, 64 (15), 2617-2635.

Mathews A., Emmanuel S., Levi L., Gvirtzman H., Erel Y., 2008, Kinetic fractionation of Fe isotopes during transport through a porous quartz-sand column, Geochimica et Cosmochimica Acta, vol.72 pp.5908-5919

Matter JG., Takahashi T; D, G., 2007, Experimental evaluation of in situ CO_2-water-rock reactions during CO_2 injection in basaltic rocks: Implications for geological CO_2 sequestration. Geochemistry, Geophysics, Geosystem, 8, (2), 1-19.

Mc Guire J., Long D.T., Klug M.J., Haak S.K., Hyndman D.W., Evaluating behavior of Oxygen, Nitrate, and Sulfate during recharge and quantifying reduction rates in contaminated aquifer. Environmental Sciences and Technology, 2002, 36, pp. 2693-2700

Michard G., Beaucaire C., Les eaux thermales des granites de Galice (Espagne): des eaux carbogazeuses aux eaux alcalines (Thermal waters from granites of Galicia (Spain): from CO_2-rich to high-pH waters), Chemical Geology, 1993, 110, 1993, pp 345-360

Michard G. Chimie des eaux naturelles, Principes de géochimie des eaux, Publisud, 2002, 461p.

Moore J., Lichtner P.C., White A.F., Brantley S.L. Geochimica et Cosmochimica Acta 2012, In Press, Corrected Proof, Available online 24 March 2012

Nielson D.M., Practical Handbook of Ground-Water Monitoring,1991; Lewis Publishers, 717 pp

Oelkers EH and Cole , DR. Carbon dioxide sequestration: A solution to a global problem. Elements, 2008, 4 pp.305-310

Palandri J.L, Kharaka Y.K, A compilation of Rate Parameters of Water-Mineral Interaction Kinetics for Application to Geochemical Modeling**,** U.S. GEOLOGICAL SURVEY, OPEN FILE REPORT 2004-1068, 2004, 64p.

Palandri JL , Rosenbauer , RJ and Kharaka , YK Ferric iron in sediments as a novel CO2 mineral trap: CO2 - SO2 reaction with hematite . Applied Geochemistry, 2005, **20** : 2038-2048 .

Pauwels H, Gaus I., Michel le Nindre Y., Pearce J.,Czernichowski-Lauriol I. Chemistry of fluids from a natural analogue for a geological CO2 storage site (Montmiral, France): Lessons for CO2–water–rock interaction assessment and monitoring Applied Geochemistry, 200,7 22, pp 2817-2833

Parkhust D. L., Appelo C.A.J., User's Guide to Phreeqc (version 2) – A Computer Program for Speciation. Batch-Reaction. One-Dimensional Transport. and Inverse Geochemical Calculations, 1999, U.S. Department of the Interior/ U.S. Geological Survey. Denver.Colorado.

Pearce JM, Baker J , Beaubien S , Brune S , Czernichowski-Lauriol I, Faber , E , Hatziyannis G , Hildebrand A ,Krooss BM, Lombardi S, Nador A, Pauwels H Schroot , BM. Natural CO2 accumulations in Europe: understanding long - term geological processes in CO_2 sequestration . In: J Gale and Y Kaya (eds.) *Greenhouse Gas Control Tech* . 2003, **1** , pp. 417-422

126

Plummer L. N., Wigley T. M. L., and Parkhurst D. L., The kinetics of calcite dissolution in CO2-water system at 5° to 60°C and 0.0 to 1.0 atm CO2, 1978, American Journal of Sciences. 278, pp 179–216.

Pokrovsky O.S., Schott J., Kudryavtzev D.I., Dupré B. Basalt weathering in Central Siberia under permafrost conditions, 2005, Geochimica et Cosmochimica Acta, vol. 69, pp. 5659-5680

Pokrovsky O.S., Pokrovsky G.S., Schott J., Galy A. Experimental study of germanium adsorption on goethite and germanium coprecipitation with iron hydroxide: X-ray absorption fine structure and macroscopic characterization, 2006, Vol. 70, pp. 3325-3341

Pokrovsky O.S., Schott J, Surface Chemistry and Dissolution Kinetics of Divalent Metal Carbonates, 2002, Environ. Sci. Technol. vol. 36, pp. 426-432

Prigogine I., Introduction to Thermodynamics of irreversible processes, Interscience Publishers, 1968, 147 p

Oelkers E. H. (1996) Physical and chemical properties of rocks and fluids for chemical mass transport calculations. Rev. Mineral. Geochem. 34(1), 131–191.

Raistruck M , Mayer B , Shevalier M , Perez RJ, Hutcheon I , Perkins E, Gunter , B. Using,Chemical and Isotopic Data to Quantify Ionic Trapping of Injected Carbon Dioxide in Oil Field Brines .
Environ. Sci. Technol. 2006, **40** : 6744-6749

Rillard J., Zuddas P. A field kinetic approach to study difference of mineral reactivity in response to natural CO_2 perturbation, *manuscript in preparation*

Rosenbauer RJ , Koksalan , T and Palandri , JL. Experimental investigation of CO_2 - brine - rock interactions at elevated temperature and pressure: Implications for CO2 sequestration in deep-saline aquifers . Fuel Processing Technology, 2005, **86** : 1581-1597

Salmon S.U., Malmstrom M.E., Quantification of mineral dissolution rates and applicability of rate laws: Laboratory studies of mill tailings, 2006, Applied Geochemistry, 21, pp.269-288

Sanjuan A, Michard G Influence of the temperature of CO2-rich springs on their aluminium and rare-earth element contents, Chemical Geology, 1988, 68, pp 57–67

Sasaki K., Fujii T., Niibori Y., Ito T., Hashida T.   Numerical simulation of supercritical CO2 injection into subsurface rock masses. Energy Conver. Mgmt 2008, 49, pp 54-61

Sciuto P. F. and Ottonello G. Water-rock interaction on Zabargad Island (Red Sea) - a case study: I. application of the concept of local equilibrium. Geochim. et Cosmochim. Acta, 1995, 59, pp. 2187-2206

Scislewski A, Zuddas P., 2010. Estimation of reactive mineral surface area during water–rock interaction using fluid chemical data .Geochim. Cosmochim. Acta, 74, pp. 6996–7007

Shi J.Q., Xue Z., Durucan S., Supercritical CO_2 core flooding and imbibition in Tako sandstone: Influence of sub-core scale heterogeneity Inter. J. Greenh. Gas Contro, 2011, 5, pp 75–87

127

Spycher N , Pruess, K and Ennis-King, J. CO_2-H_2O mixtures in geological sequestration of CO 2 , I: Assessment and calculation of mutual solubilities from 12 to 100 ° C and up to 600 bar . Geochim. Cosmochim. Acta, 2003, 67 pp.3015-3031

Steefel C. I. and MacQuarrie K. T. B., Approaches to modeling of reactive transport in porous media. Reviews in Mineralogy. Mineralogical Society of America. Washington D.C. 1996, 34.pp. 83–129.

Sundquist ET , Ackerman , KV , Parker , L and Huntzinger , DN., An Introduction to Global carbon Cycle . In: BJ McPherson and ET Sundquist (eds.). Carbon Sequestration and Its Role in the Global Carbon Cycle . American Geophysical Union, Geophysical Monograph, Washington, D.C. 2009, 183, pp.1-23 .

Van der Meer L.G.H., The condition limiting CO_2 storage in aquifers. Energy Conver. Mgmt, 1993, 34, pp 959-966

Velbel, M.A., 1984. Weathering processes of rock-forming minerals. Mineral. Assoc. of Canada Short Course Handbook, vol. 10, pp. 67–111.

Velbel, M.A., 1986. Influence of surface area, surface characteristics, and solution composition on feldspar weathering rates. In: Davis, J.A., Hayes, K.F. (Eds.), Geochemical Processes at Mineral surfaces. ACS Symposium Series, vol. 323.

White A.F., Blum A.E., Bullen T.D., Vivit D.V., Schulz M., Fitzpatrick J. The effect of temperature on experimental and natural chemical weathering rates of granitoid rocks Geochimica et Cosmochimica Acta, 1999, 63, pp 3277-3291

White A.F., Determining mineral weathering rates based on solid and solute weathering gradients and velocities: application to biotite weathering in saprolites Chemical Geology 2002, 190, r 2002, pp 69-89

White A.F., Bullen T.D., S. Schulz M.S., Blum A.E., Huntington T.G., Peters N.E. Differential rates of feldspar weathering in granitic regoliths, Geochimica et Cosmochimica Acta, 2001, 65, pp 847-869

White A. F. and Brantley S. L. Chemical weathering rates of silicate minerals: an overview. In Reviews in Mineralogy, vol. 31 (eds. A. F. White and S. L. Brantley). Mineralogical Society of America, 1995 Washington DC.

Wilson, M.J., Chemical weathering of some primary rock forming minerals. Soil Science, 1975, 119, 349–355.

Wilkinson M, Hazeldine RS, Fralick AE, Odling N, Stoker SJ, Gatliff RW. CO2 - mineral reaction in a natural analogue for CO_2 storage: implications for modeling . J. Sed. Res., 2009, 79 pp. 486- 94

Wolery T.J., EQ3/6, A Software Package for Geochemical Modeling of Aqueous Systems, Lawrence Livermore National Laboratory, 1992

Scislewski A.. Zuddas P., Estimation of reactive mineral surface area during water–rock interaction using fluid chemical data .Geochim. Cosmochim. Acta, 2010, 74, 6996–7007

Schecher W.D., Mac Avoy D.C., MINEQL+: A chemical equilibrium program for personal computer, 1994

Schrag DP. Storage of carbon dioxide in offshore sediments. Science, 2009, 325 pp 1658-1659

Steefel C.I. Software for Modeling Multicomponent Reactive Flow and Transport, 2011, Earth Sciences division Lawrence Berkeley National Laboratory Berkeley, CA 94720 USA

Stumm, W., Morgan, J.J., Aquatic Chemistry, Chemical Equilibria and Rates in Natural Waters, 3rd ed. John Wiley & Sons, Inc., 1996, 1022p.

Stumm W., Lee, G. F., Oxygenation of Ferrous Iron, 1961 Ind. Eng. Chem. 53, pp.143-146

Stumm W., Wollast R., Coordination chemistry of weathering: Kinetics of the Surface-Controlled Dissolutidn of Oxide Mineral, 1990, Reviews of Geophysics, 28, pp. 53- 69

Taylor H.E., Shiller A.H., Trace metal budgets for a forested watershed in hte New Jersey pine barrens, Water Resources Research, 1995, 16, pp. 373-376

Van der Lee, J., Thermodynamic and mathematical concepts of CHESS. Technical Report LHM/RD/98/39,CIG, Ecole des Mines de Paris, Fontainebleau, France, 1998, 99pp.

Velbel, M.A., Weathering processes of rock-forming minerals. Mineral. Assoc. of Canada Short Course Handbook, 1984, vol. 10, pp. 67–111.

Velbel, M.A., Influence of surface area, surface characteristics, and solution composition on feldspar weathering rates. In: Davis, J.A., Hayes, K.F. (Eds.), Geochemical Processes at Mineral surfaces. ACS Symposium Series, 1986, vol. 323.

Wilson, M.J., Chemical weathering of some primary rock forming minerals. Soil Science 1975, 119, 349–355.

Window H.L., Byrol J.T., Smith R.G, Huan F., Inadequacy of NASQAN data for assessing metal trends in the nation's rivers, Environmental Sciences and Technology, 1995, 25, pp 1137-1142

Yeskis D., Zavala B., Ground-Water Sampling Guidelines for Superfund and RCRA Project Managers, Ground Water Forum Issue Paper, 2002

Xu T., Apps J. A., Pruess K. and Yamamoto H. Numerical modeling of injection and mineral trapping of CO2 with H2Sand SO2 in a sandstone formation. Chem. Geol., 2007, 242, pp. 319–346.